NORTHWESTERN UNIVERSITY

Synaptic and Spiking Activity of Cerebellar Neurons During Learning and Swimming in Larval Zebrafish

A DISSERTATION

SUBMITTED TO THE GRADUATE SCHOOL
IN PARTIAL FULFILLMENT OF THE REQUIREMENTS

for the degree

DOCTOR OF PHILOSOPHY

Field of Neuroscience

By

Thomas Curtis Harmon

EVANSTON, ILLINOIS

September 2018

Abstract

The cerebellum contributes to movement initiation, execution, and adaptation. Principal cerebellar neurons receive synaptic inputs related to sensory stimuli and motor commands, leading to modulation of their firing. Furthermore, synaptic input differs substantially between cerebellum-dependent behaviors. I have made voltage- and current-clamp recordings from Purkinje and eurydendroid neurons in the larval zebrafish cerebellum while simultaneously recording fictive swimming from the ventral root in the tail to describe the synaptic inputs and spiking activity of these cells while the fish was at rest, during visual sensory stimulation, spontaneous swimming, and sensory-evoked reflexive swimming. For Purkinje cells, I have tested how plasticity manifests in individual neurons during associative motor learning by following synaptic activity and spiking from when the fish is naïve to when it reliably performs learned swimming. I discovered differences in Purkinje cell spiking during learned swimming that reflected different forms of plasticity, were partially predicted by basal synaptic properties, and related to the position of the cell. Using optogenetics to manipulate Purkinje cell activity, I found that Purkinje simple spikes can play a transient, instructive role during learning. For eurydendroid neurons, I found that inhibition from Purkinje complex spikes is similar to that from simple spikes, and that 2-7 Purkinje cells converge onto each cell. Spiking is differentially modulated during cerebellar behaviors. Acute excitation makes spiking more likely during visual stimuli. During swimming, spiking is anticorrelated with inhibitory drive, which is rhythmic during volitional but not reflexive swimming. Overall, my experiments demonstrate differential responses of cerebellar neurons to movements, diversity among neurons in the types of synaptic

drive they receive, and multiple forms of plasticity that support different aspects of cerebellar learning. Many of my findings match those from experiments on the cerebellum of mammals, revealing properties of this circuit that are likely conserved across all vertebrates.

Acknowledgements and Funding Sources

This work was funded by the following sources: NIH R37-NS39395 (IMR), Brain Research Foundation (IMR, DLM), NIH T32-MH067564 (TCH), NIH F31-NS095476 (TCH). Thank you for your generosity.

This thesis is not only a document of my own efforts, but also the support, knowledge, and hard work of many others.

I am firstly grateful to Jenna Harmon. Thank you for being my partner in this and all else. Thank you for acting as a sounding board for my ideas and frustrations, for correcting my grammar, for challenging me and for not challenging me, for doing all the things I couldn't do myself. As you know, periodically, graduate school has taken long hours, divided my attention, and left me frayed – but you've supported me through all of it. I know you are proud of me, and that makes me feel very good.

I would also like to thank my parents, Ann and Bob Harmon. Thank you for taking me to every zoo within a 4-hr drive when I was a child; for the animal husbandry lessons you gave so that I could care for pet toads, fish, worms, lizards, hermit crabs, hamsters, dogs, and cats that you kept in our home; for sending me to science camp; for supervising my first experiments; for indulging my curiosity; for lessons on hard work and perseverance; for always asking about how things are going in the lab; for your unqualified support. I remember it all, it has all counted.

I would like to thank my science teachers: Jeff Hepburn, Larry Jones, David Mahler, Scott Schoenberg, Karen Sievers, and Susan Stroope. Your instruction was enriching, formative, and

essential. I would like to thank Dr. Grazyna Kochanska, who was exceedingly kind and nurturing to me when she hired me to work in her lab as a teenager, and Dr. Jelena Radulovic, who mentored me as a rotating graduate student and has encouraged me throughout my time in graduate school.

I would especially like to thank my first mentor in neuroscience, Dr. John Freeman. Taking your behavioral neuroscience class as an undergraduate at the University of Iowa changed my life, and working in your lab has led to all the professional success I have experienced. You were the one to advise me to go to graduate school and what schools to apply to, and to work with Indira Raman at Northwestern. Thank you for teaching me, for training me, and for championing my work. I'll always consider you a friend and mentor of the highest caliber.

I have received institutional support from many members of the NUIN community: Conor Calam, Andrea Edwards, Alana Lackore, Dr. Sally McIver, Dr. David Schneeweis, Chernise Turner, Dr. Cassandra van Dunk, as well as many faculty members who support the program. Thank you all.

My graduate school experience has been made special by my fellow neuroscience students. To Nick Bush, Jessica Creery, James Ellis, Dominic Frank, Natalie Frederick, Josh Glaser, Carmen Lin, Dan Ohm, Dan O'Young, Nelly Papalambros, Brad Radvansky, Eanna Ryan, and Laura Shanahan, thank you for your fellowship, scientific and otherwise. I will miss you all and I look forward to what you all will do.

I would also like to thank members of the Raman lab: Spencer Brown, Dr. Amanda Lewis, Dr. Audrey Mercer, Dr. Marion Najac, Kristen Palarz, Dr. Rashmi Sarnaik, Dr. Chris Vaaga, Hayley

White, and Dr. Yeechan Wu. I would especially like to thank Uri Magaram, who trained me when I joined the lab. I have so much respect for all of you and I'm tremendously proud to be associated with you. Thank you for the camaraderie, constructive criticism, and general support and pleasantness. I have many memories in Cook 2-117 – you all have blunted the bad and sweetened the good.

I also thank all the members of the McLean lab: Moneeza Agha, Priscilla Ambrosi, Dr. Martha Bagnall, Dr. Cindy Chiu, Ana Istrate, Dr. Mike Jay, Dr. Sandeep Kishore, Dr. Evi Menelaou, Dr. Brad Patterson, Saul Rojas, Dr. Cassandra van Dunk, and Dr. Wei-Chun Wang. I especially thank Elissa Szuter as well as Matt Chiarelli for taking care of the fish. You all have been generous and open, socially and scientifically, and I have learned much from all of you.

I would like to thank my committee members, firstly for reading this far into my thesis. Sincerely, thank you to Drs. Dan Dombeck. Malcolm McIver, and Catherine Woolley as well as JC Cang for serving on my committee and providing constructive feedback. My project has been stronger for it. I reiterate my thanks to Dr. Catherine Woolley, for chairing my committee, but also for serving as a mentor to me when I was a rotating student, during my teaching assistantship, during my time on the information storage training grant, and during my time in the neurobiology department more broadly. I have learned much about teaching, writing, scientific rigor, professionalism, and service, from lessons you've offer me directly as well as from your example. Your influence on me was early and formative, and I can't imagine my training without your contributions.

I offer special thanks to Dr. Dave McLean, who has served as a second advisor to me. Of course, I've learned much about motor control, electrophysiology, scientific and aesthetic rigor, and zebrafish from Dave. Additionally, from his example, I've learned about professional generosity and service, and about the importance of contributing to scientific communities, in the lab, the department, and across the field. Above all, thank you for your enthusiasm and friendship.

Finally, I offer special thanks to my advisor, Dr. Indira Raman. Early in graduate school, I learned many facts about the brain that seemed to emerge from expressions of scientific genius. I felt certain that my own efforts would never live up to the examples set by Ramon y Cajal, Hubel and Weisel, Levi-Montalchini, and Hodgkin and Huxley. The mythology around these people was dissolved somewhat during the great experiments course that you lead (I remember being particularly affected and amused by the observation that so many of these scientists were conducting experiments on the neuromuscular junction with cigarettes hanging from their mouths). But ultimately, you provided me a more wholistic view of scientific endeavor, through your example and readily-offered lessons.

In my experiments, thank you for training me, and demonstrating the importance of being thoughtful, deliberate, careful, and persistent. In my studies and writing, thank you for teaching me how to edit critically, to argue affirmatively, and how to walk the line between cynicism and skepticism. In addition, you have shown me that ethics, compassion, and empathy are as essential for every scientist. What I've learned from you is that science isn't about expression of genius. Instead, it's summarized as a simple imperative: work hard and be kind. The rest will take care of itself. Thank you for everything.

List of Abbreviations

Arch – Archaerhodopsin-3

cf – climbing fiber

CR – conditional response

CS – conditional stimulus

dpf – days postfertilization

EN – eurydendroid neuron

LTD – long-term depression

LTP – long-term potentiation

MAI – Marrs-Albus-Ito theory

mf – mossy fiber

mGluR – metabotropic glutamate receptor

MCS – multiple complex spiking cell

nMLF – nucleus of the medial longitudinal fasiculus

pf – parallel fiber

pfEPSP – parallel fiber excitatory postsynaptic potentials

Pkj – Purkinje cell

SCS – single complex spiking cell

UR – unconditional response

US – unconditional stimulus

ZCS – zero complex spiking cell

Table of Contents

Abstract……....3

Acknowledgements and Funding Sources...……5

List of Abbreviations……..……..9

Figures…….……...15

1 Introduction……..16

1.1 Comparative cerebellar anatomy……..18

1.1.1 Gross anatomy…….……18

1.1.2 Cerebellar circuit anatomy……19

1.1.2.1 Mossy fibers and granule cells: mammals…….....19

1.1.2.2 Mossy fibers and granule cells: fish…….....21

1.1.2.3 Purkinje cells and climbing fibers……22

1.1.2.4 Cerebellar nuclei…….....22

1.1.2.5 Eurydendroid neurons…….....23

1.2 Functional organization and regional heterogeneity in the cerebellum……24

1.2.1 Functional organization of the cerebellum……...25

1.2.2 Regional heterogeneity…….....26

1.3 Physiological characteristics of principal cerebellar neurons……...……28

1.3.1 Purkinje cells…….28

1.3.1.1 Purkinje cells: intrinsic properties…….28

1.3.1.2 Purkinje cell: parallel fiber excitation…….....30

1.3.1.3 Purkinje cells: climbing fiber excitation……30

1.3.2 Cerebellar nuclear cells…….31

1.3.2.1 Cerebellar nuclear cells: intrinsic properties…….....32

1.3.2.2 Cerebellar nuclear cells: inhibition from Pkjs……...32

1.3.2.3 Cerebellar nuclear cells: Mossy fiber drive…….....33

1.3.2.4 Cerebellar nuclear cells: Inhibition by complex spikes……..…...34

1.3.2.5 Eurydendroid recordings……35
1.4 Responses of precerebellar and cerebellar neurons to sensory stimuli…….35
1.4.1 Sensory modulation of Pkjs…….....36
1.4.2 Sensory modulation of cerebellar nuclear cells……37
1.4.3 Synaptic drive to interconnected Pkjs and nuclear cells……...38
1.5 The contribution of cerebellar neurons to movement……...39
1.5.1 Mossy fiber and parallel fiber activity during movement…….....41
1.5.2 Purkinje cell activity…….....42
1.5.3 Cerebellar nuclear cell activity…….44
1.5.4 Movement initiation versus execution…….....46
1.6 Initiation and adaptation of movements supported by cerebellar learning……...47
1.6.1 Plasticity in Pkjs……48
1.6.2 Plasticity in cerebellar nuclear cells……..49
1.6.3 Cerebellum-dependent associative learning: eyelid conditioning……50
1.7 Swimming and learning in larval zebrafish……..52
1.7.1 Sensory-evoked swimming……...53
1.7.2 Learning-dependent adaptation of sensorimotor behaviors……...…...55
1.8 My experiments……....56

2 Distinct responses of Purkinje neurons and roles of simple spikes during associative motor learning in larval zebrafish……..58
2.1 Abstract……58
2.2 Introduction……..…….59
2.3 Results…….……..61
2.3.1 Purkinje cell recordings……...……61
2.3.2 Identification of events…….....63
2.3.3 Heterogeneity of Purkinje cell responses during motor behavior and sensory stimulation……65

2.3.4 A cerebellar learning task in the zebrafish…….....69
2.3.5 Purkinje cell activity during learning…….....73
2.3.6 Multiple complex spike cells……76
2.3.7 Single complex spike cells……79
2.3.8 Zero complex spiking cells……...81
2.3.9 Suppressing Purkinje cell simple spikes…….....81
2.3.10 Simple spike suppression during acquisition…….....86
2.3.11 Simple spike suppression following CR acquisition……88
2.4 Discussion…….…92
2.4.1 Pre-training responses of Purkinje cells…….....92
2.4.2 Topographical organization of the zebrafish cerebellum……..93
2.4.3 Relating naïve and learned responses of Purkinje cells……95
2.4.4 Complex spike plasticity in Purkinje cells……96
2.4.5 A changing role for simple spikes during cerebellar learning……..97
2.5 Materials and Methods……....100
2.5.1 Zebrafish…….100
2.5.2 Electrophysiological recordings……..100
2.5.3 Behavior……..103
2.5.4 Analysis of electrophysiological events…….....104
2.5.5 Statistical analysis……...107

3 Alternative modes of synaptic integration in cerebellar output neurons induced by sensory stimulation and fictive swimming……..108
3.1 Abstract……...108
3.2 Introduction…….....109
3.3 Results…….……112
3.3.1 Anatomy and spiking properties olig2+ eurydendroid neurons……..112
3.3.2 Basal properties of synaptic inputs…….115

3.3.3 IPSCs from presynaptic complex spikes……118
3.3.4 Estimating Purkinje-eurydendroid convergence……120
3.3.5 Synaptic responses and spiking to visual stimulation……125
3.3.6 Spiking and synaptic drive during spontaneous and evoked fictive swimming……127
3.3.7 Activity related to the motor burst cycle during spontaneous and evoked swimming……131
3.4 Discussion……136
3.4.1 Possible ontogeny of EN firing……136
3.4.2 Features of parallel fiber inputs……137
3.4.3 Inhibition from complex spikes……139
3.4.4 Purkinje-eurydendroid convergence……140
3.4.5 Spiking to visual sensory stimulation……142
3.4.6 Spiking during spontaneous swimming……143
3.4.7 Synaptic contributions to spontaneous swimming……146
3.4.8 Purkinje drive during evoked swimming……147
3.5 Materials and Methods……149
3.5.1 Zebrafish……149
3.5.2 Electrophysiology……149
3.5.3 Targeting fluorescent cells……151
3.5.4 Analysis of electrophysiological events……152
3.5.5 IPSC simulations……154
3.5.6 Statistical analysis……155
4 Discussion and future directions……156
4.1 Comparison of learning and expression of conditional responses……157
4.1.1 Individual differences in learning ability……157
4.1.2 Possible mechanism for CR acquisition and expression……158
4.1.3 Divergent signals and targets of ENs……161
4.2 Cerebellar involvement in volitional movement……162

4.2.1 Studying movement initiation…….162
4.2.2 Possible internal forward models in larval zebrafish cerebellum……...164
4.3 Interspecies differences in the mossy fiber-parallel fiber pathway……...166
4.3.1 Feedforward excitation and integration at pf-granule cell synapse……166
4.3.2 Sparse coding at the pf-Pkj synapse in larval zebrafish……..167
4.4 Synaptic plasticity that supports cerebellar learning…….169
4.4.1 Divergent complex spike properties……...169
4.4.2 Parallel fiber-Purkinje cell plasticity during associative learning…….....171
4.4.3 Possible plasticity at pf-EN synapses…….172

References…….……..175

Figures

Figure 1.1 Schematic of the cerebellum……20

Figure 2.1 Spontaneous activity during dual recordings of Purkinje cells and ventral roots…...62

Figure 2.2 Purkinje cell responses during sensory stimuli and motor commands associated with fictive swimming……...67

Figure 2.3 Cerebellar associative learning…….……72

Figure 2.4 Three classes of Purkinje cell activity during learned swimming…….……...74

Figure 2.5 MCS Purkinje cell responses over the course of cerebellar learning…….…..77

Figure 2.6 SCS Purkinje cell responses over the course of cerebellar learning……80

Figure 2.7 ZCS Purkinje cell responses over the course of cerebellar learning…….…...82

Figure 2.8 Effects of Arch-mediated simple spike suppression on acquisition of learned responses……84

Figure 2.9 Effects of Arch-mediated simple spike suppression on expression and maintenance of learned responses……...89

Figure 3.1 EN cellular anatomy and spiking…….....113

Figure 3.2 Features of spontaneous EPSCs and IPSCs…….116

Figure 3.3 Properties of IPSCs attributable to complex spikes…….119

Figure 3.4 Simulations of IPSCs from converging Pkjs……...122

Figure 3.5 Synaptic and spiking responses to a visual stimulus……126

Figure 3.6 Spiking and synaptic responses to spontaneous and evoked swimming……..128

Figure 3.7 Synaptic and spiking activity in relation to the burst cycle……..134

Chapter 1: Introduction

The cerebellum contributes to the initiation, execution, and adaptation of movements through the firing patterns of its principal neurons – Purkinje cells (Pkj) and cerebellar output neurons. Both cell types receive excitatory synaptic drive which conveys information related to sensory stimuli and motor commands generated by neurons involved in movement elsewhere in the brain. These neurons also interact with each other, with Pkjs making inhibitory synapses with cerebellar output neurons that further alters their firing. Many cerebellar output neurons project to brain areas involved in movement, and changes in the firing of these neurons can affect movements in real time.

Without the cerebellum, a given movement may not be attempted or it may not be completed successfully. In other words, the cerebellum influences movements by affecting *movement initiation* and *movement execution*. The cerebellum's contribution to most movements is not innate, but instead emerges after some learning process, and some movements are more sensitive to cerebellar learning and influence than others. The motor circuits necessary for reflexive movements (i.e. sensory-evoked movements initiated in an unlearned, stereotyped manner) are different from those which support learned, cued movements (i.e. sensory-evoked movements that emerge after some learning process) and volitional movements (i.e. movements that cannot be attributed to an external event, but instead reflect some internally sourced signal). Because of these circuit-level differences, and because some movements are triggered by a specific sensory

stimulus, afferent synaptic drive provided to the cerebellum will differ across these movements, and resultant spiking of cerebellar output will have differential effects.

Addressing whether the cerebellum contributes to initiation and execution of different kinds of movements requires a preparation in which the synaptic drive and spiking related to the movement can be recorded. Additionally, testing how the cerebellum responds and influences different kinds of movements requires a preparation in which the animal will perform volitional, reflexive, and learned movements. In my thesis project, I have addressed these issues using the larval zebrafish. I have recorded from Pkj and eurydendroid neurons (ENs) while simultaneously monitoring fictive swimming. I have described the synaptic inputs and firing of both cell types while the fish was at rest, as well as during spontaneous and reflexive swimming. I have also described and manipulated Pkj firing during the acquisition and expression of a learned movement.

In this introductory chapter, I have organized a review of the cerebellum to emphasize the different forms of synaptic drive presented to the cerebellum, some attributable to sensory stimuli and other to motor commands. I address how these forms of synaptic drive interact with the intrinsic properties of principal cerebellar neurons. I review evidence for the cerebellum's involvement in movements, and movement-related activity and forms of plasticity that support cerebellum-dependent learned movements, comparing findings from mammalian and fish cerebellum when prudent. My experiments and findings on Pkj synaptic activity and spiking during swimming have been published previously (Harmon et al., 2017) and are reported in chapter 2. My findings concerning the synaptic and spiking activity of ENs during swimming are

reported in chapter 3. A broader discussion of my findings and future directions are addressed in chapter 4.

1.1 Comparative cerebellar anatomy

The general appearance of the teleost cerebellum differs greatly from the cerebellum of a rodent or a human. Nevertheless, the functional and circuit organization of the cerebellum is largely conserved. In this section, I review the lobular anatomy of the mammalian and teleost cerebellum, sources of cerebellar input, synaptic connections made by neurons within the cerebellum, and postsynaptic targets of cerebellar output neurons.

1.1.1 Gross anatomy

In both mammals and fish, the cerebellum is a bilateral structure divided into multiple anatomical regions. In mammals, these regions are organized along the mediolateral axis. The cerebellar cortex consists of the lateral hemispheres, the medially-located vermis, and the flocculus (Figure 1.1A, B). Each region is foliated, forming multiple lobules with their own name and functional specialty. Multiple regions are also apparent in the cerebellar nuclei, which contains the lateral, interposed, and fastigial nucleus (nomenclature for the rodent cerebellum). Pkjs in the flocculus project to the vestibular nucleus, rather than the cerebellar nuclei, where they regulate eye movements.

The larval zebrafish cerebellum consists of three regions: the valvula cerebelli, corpus cerebelli, and the caudal-lateral lobe (Knogler et al., 2017; Figure 1.1C, D). The valvular cerebelli is

relatively small and found at the most rostral-medial extent of the cerebellum. Pkjs in the valvula project out of the cerebellum to the octaval nucleus, indicating that this structure is likely homologous to the mammalian flocculus (Matsui et al., 2014a). The corpus cerebelli extends caudally from edge of the valvula and covers the entire mediolateral extent of the hemisphere, making it the largest lobe of the zebrafish cerebellum. ENs in the caudal-lateral lobe also innervate the octaval nucleus, hypothalamus, and the midbrain, whereas ENs in the corpus project to the thalamus, midbrain, red nucleus, and nucleus of the medial longitudinal fasiculus (nMLF). While the exact functional and anatomical homologs to these structures need to be confirmed, the available evidence suggests that the caudal-lateral cerebellar lobe is homologous to the vermis, while the corpus cerebelli is homologous to the lateral lobes (Matsui et al., 2014a).

1.1.2 Cerebellar circuit anatomy

1.1.2.1 Mossy fibers and granule cells: mammals

The mammalian cerebellum is divided into the cerebellar cortex and the cerebellar nuclei, whereas the fish cerebellum only has the equivalent of the cerebellar cortex. In mammals and fish alike, the cerebellar cortex is a layered structure, consisting of the granule cell layer most ventrally, the molecular layer most dorsally, and a thin somatic layer in between. Axons of granule cells (i.e. parallel fibers, pfs) extend dorsally from the granule cell layer into the molecular layer, where make glutamatergic synapses with Pkjs and molecular layer interneurons (stellate and basket cells).

Granule cells receive excitatory synaptic inputs from mossy fibers (mf). In mammals, mfs most prominently but not exclusively come from the pontine nucleus, lateral reticular nucleus, the

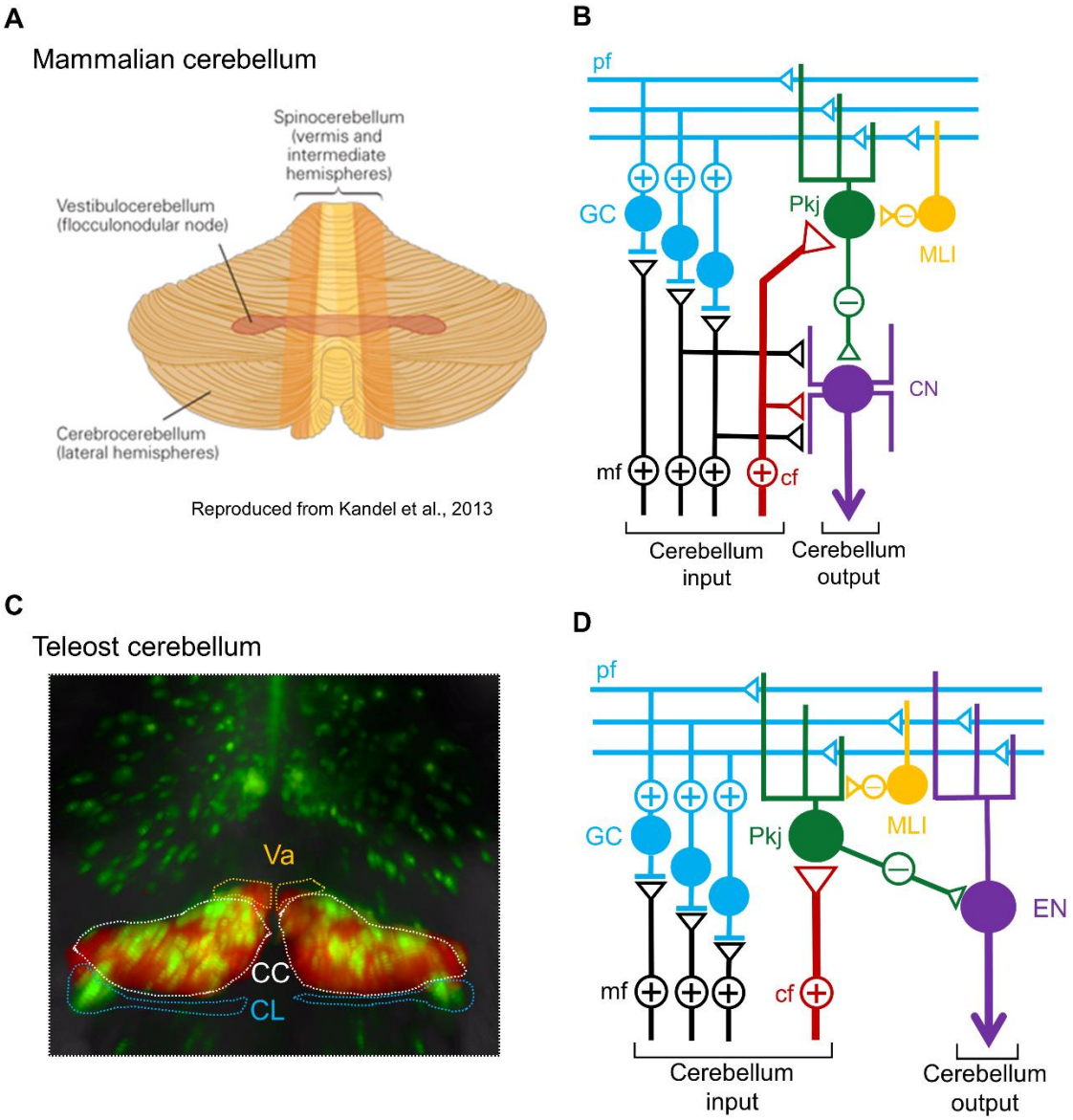

Figure 1.1 Schematic of the cerebellum circuit. (**A**) Illustration of mammalian cerebellar cortex, reproduced from Kandel et al., 2013. (**B**) Circuit diagram of mammalian cerebellum. cf: climbing fiber, mf: mossy fiber, pf: parallel fiber, CN: cerebellar nuclear cell, GC: granule cellsMLI: molecular layer interneuron, Pkj: Purkinje cell. (**C**) Left, image of olig2+ (green) and Pkj (red) cells from a PTU-treated *olig2:GFP/Arch-tagRFP-T:car8:GCamp5* fish. Approximate dimensions of teleost cerebellar lobes. CC: corpus cerebelli, CL: caudolateral lobe, Va: valvular cerebellum. (**D**) Circuit diagram of the fish cerebellum. EN: eurydendroid neuron.

nucleus reticularis tegmenti pontis, and spinocerebellar system (Holdefer et al., 2005; Arshavsky et al., 1972a,b). The pontine nucleus receives inputs from many brain areas, and transmits signals related to both sensory stimuli and motor commands. Neurons in the lateral reticular nucleus preferentially receive and transmit signals related to motor commands (Esposito et al., 2014; Azim et al., 2014). The nucleus reticularis tegmenti pontis likely transmits visual, vestibular, and motor command signals related to eye movements (Gerrits et al., 1984). Mfs from the spinocerebellar tract communicate proprioceptive sensory information to the cerebellum (Arshavsky et al., 1972). Granule cells receive feedback inhibitory input from Golgi cells, which are excited by pfs. The cerebellum also receives neuromodulatory inputs from the raphe nuclei, locus coeruleus, and ventral tegmental area.

1.1.2.2 Mossy fibers and granule cells: fish

In teleost fish, the structure that may be homologous to the pontine nucleus (i.e. the nucleus of the isthmic level) is relatively small (Finger, 1978), and known mf sources are distributed widely throughout the brain. Researchers have reported homologous precerebellar nuclei, like the lateral reticular nucleus, raphe nuclei, locus coeruleus, and vestibular nuclei (Finger, 1978; McLean and Fetcho, 2004). Neurons in the periventricular pretectal nucleus receive input from the visual system and provide excitatory inputs to the cerebellum and the inferior olive (Xue et al., 2006). Additionally, neurons in the lateral valvular nucleus receive input from pretectum, telencephalon, and hypothalamus, and are likely well-suited for transmitting integrated sensory signals to the cerebellum (Yang et al., 2004). Several other nuclei with no known mammalian homolog or

function have also been identified in the pretectum and reticular formation, and sparse labeling of neurons in the spinal cord has been reported as well (Finger, 1978; Folgueira et al., 2006).

1.1.2.3 Purkinje cells and climbing fibers

The principal neurons of the cerebellar cortex are Pkjs. The dendrite of Pkjs extends into the molecular layer, where it receives excitatory synaptic inputs from pfs and a climbing fiber (cf) from a neuron in the inferior olive. Pfs transverse the Pkj dendrite, making single synapses as they pass. In total, an individual Pkj receives ~150,000 unique pf inputs (Isope and Barbour, 2002). While it is unknown how many pfs synapse with Pkjs in the larval zebrafish, granule cells outnumber Pkjs by a factor of 20 (6000 vs 300 cells, respectively), indicating convergence between these cell types (Knogler et al., 2017). Pkjs also receive inhibitory inputs from basket cells (which receive pf inputs and make synapses on the Pkj soma and axon initial segment; Blot and Barbour, 2014) and stellate cells (which synapses on the Pkj dendrite). While these specific cell types have not been identified in zebrafish, $GAD2^{+}$ molecular layer interneurons have been reported (Bae et al, 2009), and Golgi and stellate cells have been identified in the cerebellum of mormyrid fish (Han and Bell, 2003).

1.1.2.4 Cerebellar nuclei

In mammals, Pkjs axons leave the cerebellar cortex and extend ventrally to make inhibitory synapses on neurons in the cerebellar nuclei. Each nuclear cell receives converging inputs from many Pkjs. Estimates of the convergence ratio differ between species and studies. Researchers using cats have made estimates ranging from 26:1 (Palkovits et al., 1977) to 600:1 (Bengtsson et al., 2011), whereas ratios from mice range from 11:1 (Caddy and Biscoe, 1979) to 40:1 (Person

and Raman, 2011). Nuclear cells also receive excitatory inputs from mfs and cf collaterals. Two populations of projecting nuclear cells have been described. Projections from large, glutamatergic neurons go to the red nucleus, ventrolateral nucleus of the thalamus, and various nuclei in the reticulospinal system, while those from small, GABAergic neurons go to the inferior olive. Large and small cells are intermingled within each of the nuclei.

1.1.2.5 Eurydendroid neurons

In teleosts, cerebellar output neurons are called eurydendroid neurons (ENs). EN cell bodies are not organized into nuclei but are instead located in the somatic layer of the cerebellar cortex where they mingle with Pkj bodies (Meek et al., 1992; Bae et al., 2009). ENs do not receive synaptic inputs from mfs. Instead, these neurons have multiple dendritic branches which extend into the molecular layer and make excitatory synapses with pfs (Meek et al., 1992). Cf collaterals in the zebrafish cerebellum have not been reported. ENs receive somatic inhibitory synaptic input from neighboring Pkjs, whose axons have been reported to be ~5 μm long (approximately the diameter of the cell body; Matsui et al., 2014a). Despite their proximity, ENs likely receive inputs from multiple Pkjs (Alonso et al., 1992), though the convergence ratio has not been estimated.

Two non-overlapping populations of ENs have been reported – those that express the transcription factor *olig2*, and those that express *calretinin* (Castro et al., 2006; McFarland et al, 2008). The target of EN axons relates to the position of the cell along the mediolateral axis (Heap et al., 2013). Cells located laterally project to the ipsilateral tectum, whereas medially-located cells project laterally then rostrally through the tectal neuropil to the diencephalon. Additionally,

some axons project rostrally through the medial longitudinal fasciculus and terminate in the reticular formation, nMLF, red nucleus, and various pretectal nuclei, whereas others project caudally to the inferior olive (Ikenaga et al., 2006; Matsui et al., 2014a). The olivary projection raises the possibility that some ENs provide inhibitory feedback, in a manner homologous to small GABAergic cerebellar nuclear cells. However, neither group of ENs is GABAergic, suggesting that inhibitory feedback may require recruitment of local inhibitory olivary interneurons.

1.2 Functional organization and regional heterogeneity in the cerebellum

Subsections of the cerebellum contribute differentially to cerebellum-dependent behaviors. The functional specialty of a subsection is a consequence of its afferent/efferent connections, which are evidenced by correlated spiking during ongoing behaviors, as well as initiation or interruption of movements by manipulations of neuronal activity. The functional organization overlaps with anatomical modules along the mediolateral axis (reviewed by Cerminara et al., 2015). While modules are in part defined by shared synaptic input, neurons within a module also have a molecular and physiological phenotype that differs from neurons in other modules. The specific properties of neurons within a module likely has consequences for the behaviors to which those neurons contribute. In this section, I will describe the functional organization of the cerebellum and regional heterogeneity of cerebellar neurons, relating the two subjects when possible.

1.2.1 Functional organization of the cerebellum

The functional specialty of individual neurons or subsections of the cerebellum can be inferred from neuronal responses to sensory stimuli as well as specific movements. Pkjs and nuclear cells show a range of responses to sensory stimuli, some more selectively than others, which may reflect the origin of the subjacent mfs (Shambes et al., 1978; Bower and Woolston, 1983; Lee and Bulluck, 1984; Fushiki and Barmack, 1997; Ekerot and Jorntell, 2001). Manipulating cerebellar output reveals regionalized contributions to movements. Stimulation of the subsections of the cerebellar nuclei can elicit movements localized to specific body parts (e.g. Schultz et al., 1979) and spike modulation of individual nuclear cells varies across movements (e.g. Thach et al., 1993). Regional optogenetic manipulation of Pkj spiking can elicit or interupt movements localized to the face/eyelid (Heiney et al., 2014; ten Brinke et al., 2017), forelimbs (Lee et al., 2015), hindlimbs (Witter et al., 2013; Sarnaik and Raman, 2018), tail (Witter et al., 2013), and whiskers (Proville et al., 2014; Brown and Raman, 2018). These results support the hypothesis that the mammalian cerebellum is roughly somatotopically organized, with different cerebellar regions contributing to movements of different parts of the body. However, many cerebellar nuclear cells project to areas not directly implicated in movement generation, like the inferior olive and thalamus (e.g. Medina et al., 2002; Halverson et al., 2010). While these neurons might indirectly contribute to movements, it is likely that these parts of the cerebellum are involved in non-motor neural processes instead.

Subsections of the fish cerebellum project to different parts of the brain and likely support different neural processes, with medial ENs of the corpus projecting to the thalamus, and lateral

ENs to the tectum (Heap et al., 2013). Representations of sensory stimuli are non-randomly distributed as well, with medially-located Pkjs and granule cells responding robustly to visual stimuli (Lee and Bulluck, 1984; Knogler et al., 2017). In addition, optogenetic manipulation of medially- or laterally-located Pkjs differentially effects the reflexive movements of the tail and eye, respectfully (Matsui et al., 2014a). Divergent body types make direct application of organizational principles of the mammalian cerebellum difficult, however.

1.2.2 Regional heterogeneity

The mammalian cerebellar cortex is divided into modules of Pkjs that share synaptic inputs and molecular phenotype. Progressing medial to lateral, modules are sagittally demarcated by the absence or expression of glycolytic enzyme aldolase-C (also known as zebrin II) in Pkjs (Ahn et al., 1994). Aldolase-C levels predict expression of proteins related to synaptic transmission (i.e. EAAT4) and intracellular signaling (i.e. PLCβ3; Wadiche and Jahr, 2005; Cerinara et al, 2015). Generally, Pkjs within the same module receive cf input from the same part of the olive, and their axons project to the same region of the cerebellar nuclei (Voogd and Ruigrok, 2004; Sugihara and Shinoda, 2007). Also, although individual pfs synapse with cells in modules, Pkjs within a module share common pf inputs with one another and with molecular layer interneurons (Valera et al., 2016). Thus, the mammalian cerebellum is anatomically modular, which likely relates to the functional contributions of cerebellar subsections.

While heterogeneity among mammalian Pkjs can be indexed with aldolase-C expression, all teleost Pkjs are aldolase-C positive (Bae et al., 2009). However, examination of other candidate markers has revealed differential expression along the mediolateral axis (Takeuchi et al., 2016).

Pkj structure differs along the mediolateral axis as well: laterally-located cells have planar dendritic arbors while medially-locates cells are bushy (Tanabe et al., 2003). Regional differences in Pkj structure are observable in the mammalian cerebellum as well. Cell bodies of Pkjs located in the vermis are larger and contain more organelles than those of Pkjs in the lateral lobes (Muller and Heisen, 1984). Pkj dendritic morphologies differ between cells located in the sulcus and those located in at the apex of the cortical folia (Nedelescu and Abdelhack, 2013). These morphological properties likely affect computations made by Pkjs that are reflected in their spiking and synaptic input.

Some researchers have reported spatially organized heterogeneity in the intrinsic properties of Pkjs. For instance, simple spike rates are lower and more irregular for aldolase-C^- Pkjs, while aldolase-C^+ cells show greater rebound firing (Xiao et al., 2014; Zhou et al., 2014; Tang et al., 2017). Also, in the vermis, a subset of Pkjs in lobule X display more modes of firing in response to direct current injection compared to Pkjs in lobules III-V (Kim et al., 2012). Likewise, comparisons between Pkjs in different lobes of the mormyrid electric fish cerebellum have revealed physiological differences between neurons in the caudal lobe, which show only sodium-dependent simple spikes and complex spikes, and those in the central and valvular lobes, which show mixed sodium- and calcium-dependent spikes in addition to complex spikes (Han and Bell, 2003; Zhang and Han, 2007). Mixed sodium and calcium spikes have been observed in larval zebrafish Pkjs as well (Sengupta and Thirumalai, 2015). These results suggest that Pkjs contributions to cerebellar behaviors is in part determined by their basal firing properties.

1.3 Physiological characteristics of principal cerebellar neurons

Pkjs and cerebellar output neurons produce action potentials spontaneously, but their firing is modulated by excitatory and inhibitory synaptic inputs during cerebellum-dependent behaviors. In this section, I review the spiking and synaptic properties of Pkjs and cerebellar nuclear cells.

1.3.1 Purkinje cells

Pkjs produce two types of action potentials – simple spikes and complex spikes – which can be distinguished by their waveform (Eccles et al., 1965). Simple spikes have a canonical action potential waveform, with a monotonic rising phase and a single peak. Recordings made in vivo, in slice, and in isolated Pkjs reveal spontaneous simple spiking at a rate of ~50 spikes/s (Thach 1968; Llinás and Sugimori, 1980; Raman and Bean, 1997a), but rates can reach ~250 spikes/s with sufficient synaptic drive (Dezeeuw et al., 2011). The rate of simple spikes recorded from larval zebrafish range from 5-10 spikes/s (Hsieh et al. 2014; Scalise et al., 2016; Harmon et al., 2017), a level comparable to rates recorded at room temperature from mammalian Pkjs (~12 spikes/s; Wulff et al., 2009). In addition, simple spikes are modulated by weak and numerous pf inputs that provide a sparse, combinatorial code to precisely alter spiking. These features make simple spikes well suited for influencing cerebellar output neuron firing in real time.

1.3.1.1 Purkinje cells: intrinsic properties

In response to current injections, most Pkjs produce trains of simple spikes that follow a tonic firing pattern (i.e. firing at a regular rate that persists for the entire step). High rates of tonic firing are promoted through fast K_v3-mediated potassium conductance (Gähwiler and Llano,

1989; Akemann and Knöpfel, 2006) as well as an additional state of the $Na_v1.6$ channel in which the channel is activated but nonconducting (Raman et al., 1997; Raman and Bean, 2001; Khaliq et al., 2003; reviewed by Lewis and Raman, 2014). This state (channel block) competes with channel inactivation, limits the refractory period, and is evidenced by voltage protocols that reveal resurgent sodium current (Raman and Bean, 1997a). Larval zebrafish Pkjs also display tonic firing that emerges developmentally along with $K_v3.3$ and $Na_v1.6$ expression (Hsieh et al., 2014), and Pkjs in mormyrid fish display resurgent current (de Ruiter et al., 2006), indicating that similar membrane components underlie Pkj tonic firing in fish and mammals.

While simple spiking occurs spontaneously, Pkjs can transition into extended periods of quiescence that last for seconds. A proposed mechanism for toggling from high to low firing is negative regulation by serotonin of I_H current, which contributes to depolarization of the membrane during tonic firing, combined with phasic inhibitory synaptic input (Williams et al., 2002). In larval zebrafish, the cerebellum receives serotonergic inputs (McLean and Fetcho, 2004), and bistable simple spiking has been reported (Sengupta and Thirumalai, 2015).

In addition to tonic firing, a subset of Pkjs display a complex bursting pattern in response to current injections, which reflects activation of big- and small-conductance K(Ca) channels by calcium, which enters the cells through P-type Ca channels (Edgerton and Reinhart, 2003). In a subset of larval zebrafish Pkjs, wide, TTX-insensitive spikes attributable to voltage-gated calcium conductances have been reported (Sengupta and Thirumalai, 2015). Thus, Pkjs in larval zebrafish display many of the same intrinsic properties as mammalian Pkjs.

1.3.1.2 Purkinje cell: parallel fiber excitation

Simple spiking is modulated by excitatory input from pfs and inhibitory input from stellate and basket cells. *In vivo* recordings of granule cells from anaesthetized mice have revealed spontaneous firing rates of ~0.5 spikes/s, though rates of individual cells vary considerably, and spikes can be driven at 250 spikes/s by direct current injection (D'Angelo et al., 1998; Chadderton et al., 2004). Recordings of spontaneous pf EPSCs have revealed events with modal amplitudes of 4-20 pA, though the distribution is skewed with a long rightward tail that reach values of ~40 pA (Barbour, 1993; Isope and Barbour, 2002; Valera et al., 2012; Tempia et al., 2015). Many pf synapses may be silent (Isope and Barbour, 2002; Liu and Regehr, 2014; Valera et al., 2016), with estimates of the proportion of silent synapses ranging from 50-85%. The single synapse conductance is also variable, ranging from 0.2 – 28 nS, with an average conductance of 0.7 nS (Barbour, 1993; De Schutter and Bower, 1994; Isope and Barbour, 2002). Features of the pf-Pkj synapse align with classic theories of learning and memory storage in the cerebellar cortex (Marr, 1969; Albus, 1971; Ito, 1984) in which Pkjs integrate across many coincidentally-active pf inputs, and the strength of these inputs is regulated by plasticity mechanisms across time (Liu and Regehr, 2014).

1.3.1.3 Purkinje cells: climbing fiber excitation

In contrast to simple spikes, complex spikes are generated solely in response to cf transmission, with 100% reliability (Eccles et al., 1966). Complex spikes often serve as an error or teaching signal, because they induce plasticity at coincidentally-active pf synapses (Ito, 1984). Olivary neurons that supply cf input generate spontaneous action potentials at a rate of ~1 spike/s (Llinas

et al., 1974), matching the rate of complex spikes. Cf EPSCs are much larger (0.1 – 2 nA) than pf EPSCs. These synapses show dramatic short-term depression attributable to acute depletion of ready-release vesicles (Hasimoto and Kano, 1998; Silver et al., 1998; Foster and Regehr, 2004), which can result in an altered complex spike waveform (Campbell and Hesslow, 1986). The "complexity" of the complex spike refers to secondary spikes that occur after the initial sodium spike. These secondary spikes propagate with moderate reliability (Khaliq and Raman, 2005), presumably lengthening the duration of inhibition experienced by the postsynaptic cell. Additional dendritically-sourced conductances contribute to the complex spike and are important for heterosynaptic plasticity.

No recordings of pf and cf EPSCs in zebrafish Pkjs were reported prior to my thesis work. However, slice recordings from Pkjs in the mormyrid fish cerebellum revealed AMPA-mediated, paired pulse-facilitating pf EPSPs and AMPA-mediated, paired pulse-depressing cf EPSPs (Han and Bell, 2003; Zhang and Han, 2007).

1.3.2 Cerebellar nuclear cells

The signal that leaves the cerebellum is encoded in the spiking of cerebellar output neurons. Recordings made during cerebellum-dependent behaviors have revealed increased nuclear cell firing that corresponds to the kinematics of specific movements or temporal features of the task (e.g. Thach 1968; McCormick and Thompson, 1984a). From these results, researchers have argued that nuclear cells signal using a rate and/or temporal code. Changes in rate and generation of specifically-timed spikes results from the interaction of excitatory and inhibitory synaptic inputs with intrinsic membrane properties that support spontaneous firing.

1.3.2.1 Cerebellar nuclear cells: intrinsic properties

Cerebellar nuclear cells also generate action potentials spontaneously at rates of 30-60 spikes/s (Thach 1968; Jahnsen 1986; Wu and Raman, 2017). Spontaneous firing is achieved in part by leak cation channels which depolarize the resting membrane potential (Raman et al., 2000), fast deactivation kinetics of K_v3 channels (Hurlock et al., 2009), and sodium channels which display resurgent current (Afshari et al., 2004). Additionally, nuclear cells display rebound firing following periods of inhibition or hyperpolarization, which is attributable to in part to recovery of sodium channels (Aman and Raman, 2007). These intrinsic properties promote spiking in opposition of nearly continuous inhibition from spontaneously active, converging Pkjs.

1.3.2.2 Cerebellar nuclear cells: inhibition from Pkjs

The computational potential of Pkj spiking begs questions about how inhibition from Pkjs affects cerebellar output. Recordings of spontaneous Pkj IPSCs reveal events that vary in size, with a modal amplitude of ~40 pA and larger events ranging up to ~140 pA (Momiyama and Takahashi, 1994; Anchisi et al., 2001; Telgkamp and Raman, 2002). Concerted inhibition could theoretically modulate firing by promoting rebound firing, where spike rate is elevated upon relief of inhibition. Rebound firing is attributable to activation of I_H current and low-threshold calcium channels, as well as recovery of inactivated sodium channels (Aizenman and Linden, 1999; Zhang et al., 2004; Zheng and Raman, 2009). Furthermore, optogenetic induction of rebound firing can elicit movements (Witter et al., 2013; Heiney et al., 2014), suggesting that Pkj control of cerebellar output through rebound firing can support certain cerebellum-dependent behaviors.

Inhibition is limited by the fast decay kinetics of Pkj IPSCs, however. Brief IPSCs constrain rebound firing by limiting summation of inhibitory inputs. Rather than controlling rate, concerted inhibition from Pkjs may more effectively control the timing of nuclear cell firing. In previous work from our lab (Person and Raman, 2011), this possibility was tested by simulating the synchronization of presynaptic Pkjs using dynamic clamp. Asynchronous IPSCs significantly suppressed nuclear cell firing, while synchronization of a subset IPSCs lead to less depressed rates (despite equal numbers of IPSCs), and entrainment of spike timing to the post-inhibitory window following synchronized IPSCs. These results demonstrated that synchronization is an effective means for producing specifically-timed nuclear cells spikes and help explain synchronous Pkj firing observed in behaving animals (Bell and Grimm, 1969; Heck et al., 2007; de Solages et al., 2008; Wise et al., 2010; Brown and Raman, 2018).

1.3.2.3 Cerebellar nuclear cells: Mossy fiber drive

Mf excitation interacts with Pkj inhibition and promotes nuclear cell firing. Mf synapses feature AMPAR- and NMDAR-mediated currents. In these cells, NMDARs are frequently unblocked because the cell is often depolarized, and magnesium block is incomplete (Anchisi et al., 2001; Wu and Raman, 2017). Consequently, long-term potentiation of these synapses does not follow from coincidental mf transmission and depolarization, but instead from a heterosynaptic interaction between mf and Pkj inputs (discussed in section 1.6.2).

Phasic mf drive can lead to the generation of specifically-timed action potentials. Such input generates spikes with moderate reliability, depending on the momentary excitability of the neuron (Yarden-Rabinowitz and Yarom, 2017). Additionally, mf drive can facilitate specifically-

timed spiking as well as long-lasting increases in spike rate through interactions with concerted Pkj IPSCs (Wu and Raman, 2017). Under this mechanism, mf drive need not be temporally structured: spike timing is determined by momentary synchrony of Pkj IPSCs, with tonic and phasic mf drive facilitating spiking within the disinhibitory window. Spiking is facilitated and spike rates are elevated for as long as mf drive lasts and Pkj IPSCs remain relatively synchronized. Mf drive promotes rebound firing as well through potentiation of calcium currents though L-type channels via an mGluR-mediated mechanism (Zheng and Raman, 2011). Thus, mfs can promote spiking of nuclear cells independent from or in concert with inhibition from Pkjs.

1.3.2.4 Cerebellar nuclear cells: Inhibition by complex spikes

When compared to mf collaterals, cf collaterals provide a smaller excitatory drive to nuclear cells, particularly in adult animals (Najac and Raman, 2017). Stimulation of the olive can elicit a mixed response in nuclear cells, with a short-latency increase in spike rate (attributable to collateral transmission) followed by a period of depressed spiking (attributable to simultaneous complex spikes in several Pkjs; Hoebeek et al., 2010; Biekenkemp and Lang, 2011; Tang et al., 2016). Nuclear cell spiking decreases only slight in response to single complex spikes (Bengtsson et al., 2011). Inhibition of nuclear cells is likely prolonged by spikelets, which presumably lead to secondary release events. In combination, inhibition related to the initial and subsequent spikelets is likely larger than the inhibition from a single simple spike. However, inhibitory currents related simple and complex spikes have not been isolated.

1.3.2.5 Eurydendroid recordings

Prior to this project, no recordings have been made of cerebellar output neurons in the larval zebrafish. However, slice recordings have been made from neurons in the cerebellum of mormyrid fish (Han and Bell, 2003). In some recordings, stimulation of pfs generates mixed EPSPs and IPSPs that are consistent with monosynaptic inputs from pfs and disynaptic inputs from Pkjs. EPSCs show pair-pulse facilitation, a common feature of pf-Pkj synapses that is observed at some mf-nuclear cell synapses. Thus, although physiological data is lacking, synaptic connections made onto ENs seem to share some characteristics with cerebellar nuclear cells.

1.4 Responses of precerebellar and cerebellar neurons to sensory stimuli

All synaptic input to the cerebellum comes from mfs and cfs. As a population, mfs represent multiple sensory modalities. For instance, recordings from either mfs directly in the middle cerebellar peduncle, which contains axons of neurons in the pons, or their granule cells targets have revealed recruitment of mfs in response to visual (Noda 1981; Charbrol et al., 2015), somatosensory (Joseph et al., 1978), and vestibular (Arenz et al, 2008; Charbrol et al., 2015) stimuli. In this section, I review how mossy and cf input related to sensory stimuli affects downstream neurons in the cerebellum, focusing on Pkjs and cerebellar nuclear cells.

1.4.1 Sensory modulation of Pkjs

Transmission in response to sensory stimulation within a mf's preferred modality leads to a burst of EPSPs and granule cell spikes (Chadderton et al., 2004; Rancz et al., 2007). These spikes lead to excitatory input to Pkj and inhibitory molecular layer interneurons. Consequently, both positive and negative modulation of Pkj firing has been reported in response to tactile, vestibular, visual, and acoustic stimuli (Freeman, 1970; Eccles et al., 1972; Ansorge and Grüsser-Cornehls, 1977; Bower and Woolston, 1983; Bosman et al., 2010). Furthermore, Lee and Bulluck (1984) recorded Pkj spikes extracellularly in adult catfish and reported increases and/or decreases in firing in response to visual, acoustic, electric, tactile, and vestibular stimuli, as well as during passive movement. Responsive Pkjs were not evenly distributed across the entire cerebellum, nor were all sensory modalities equally represented. Mechanical brushes against the side of the fish elicited responses in larger group of cells which were located throughout the corpus cerebelli, but particularly numerous in the lateral corpus. Cells responsive to visual stimuli were also relatively numerous and found in the medial corpus cerebelli. Vestibular-responsive cells were less numerous and located in the lobus caudalis. The topographical organization matches the responses of larval zebrafish granule cells to sensory stimuli and agrees with anatomical afferent and efferent connections of the zebrafish cerebellum (Matsui et al., 2014a; Knogler et al., 2017). Together, these findings demonstrate that sensory stimuli from multiple modalities are widely and non-randomly distributed across the fish cerebellum.

Cf transmission can be elicited by sensory stimuli as well. Recordings of complex spikes from Pkjs or from olivary neurons have revealed phasic, short latency responses to tactile, visual,

proprioceptive, vestibular, and auditory stimuli (Gellman et al., 1983; Bauswein et al., 1983; Winkelman et al., 2014; Ohmae and Medina, 2015), though sensory responses were not detected in some cells, and others showed responses to multiple stimuli. It is likely that cf collaterals modulate nuclear cell firing in response to sensory stimuli. However, modulation by these inputs is difficult to detect because it is obscured by predominating mf drive. These data demonstrate that cf transmission is well-suited to communicate the onset of sensory stimuli, a signal which may be useful in driving synaptic plasticity.

1.4.2 Sensory modulation of cerebellar nuclear cells

Increased nuclear cell firing can be elicited by proprioceptive, vestibular, auditory, and visual stimuli (Favilla et al., 1978; Boyle and Pompeiano, 1979; Berthier and Moore, 1990; Halverson et al., 2010; Luan et al., 2013; Ohmae et al., 2013; Ten Brinke et al., 2017). These responses are likely attributable to increased mf drive. While all these studies found increases in rate, responses differed across sensory modalities. For example, studies on proprioceptive and vestibular modulation which have used sinusoidally modulated stimuli (i.e. passive, continuous rotation of the head 5º to the left and right of rest position; Boyle and Pompeiano, 1978) report rhythmic rate modulation throughout the cycle. In contrast, studies with auditory pure tone stimuli have reported brief increases in firing rate that occur at short latencies from stimulus onset. These results suggest that systems for different sensory modalities send qualitatively different signals to the cerebellum via mfs (Halverson et al., 2010), depending on the features of stimulus.

1.4.3 Synaptic drive to interconnected Pkjs and nuclear cells

Mfs provide excitatory drive to nuclear cells and Pkjs concomitantly. If interconnected cells both receive increased mf drive, recruitment of mfs may not lead to increased nuclear cell spiking. An example of this complexity comes from ten Brinke and colleagues (2017), who found that in response to flashes of light, the firing of some cerebellar nuclear cells transiently decreases, then increases to an elevated level for the remainder of the stimulus. These authors argued that the pause was caused by inhibition by presynaptic Pkj complex spikes, while the subsequent facilitation of the nuclear cell spiking was caused by rebound firing, paused Pkj simple spiking, and mf drive. Because mf transmission to the visual stimulus is a prerequisite for increased mf-dependent spiking, these results suggest that facilitation of spiking by mfs was initially cancelled out by Pkj inhibition.

Another study from Luan and colleagues (2013) reported a variety of responses to whole-body rotation (i.e. vestibular stimulus) and head rotation (i.e. proprioceptive and vestibular stimulus) among cerebellar nuclear cells, with one group of cells displaying increased firing to both stimuli and another showing dampened modulation during head rotations. The authors argued that, for the latter group of neurons, mf excitation related to vestibular stimulation had been cancelled out by increased inhibition from Pkjs, which had increased their firing in response to proprioceptive stimulation. These results suggest that mf sources to Pkjs and the nuclear cells they target overlap nonrandomly so as to facilitate nuclear cell responses to some stimuli and dampen the response to others.

Synchronization of Pkj spiking can also result in increased rates. Previous work from our lab (Brown and Raman, 2018) reported synchronization of Pkj spikes, increased mf drive, and increased nuclear cell spiking in response to a tactile airpuff, indicating that in response to some stimuli both inputs integrate to facilitate spiking. Thus, the response of cerebellar output neurons to sensory stimuli depends interactions between excitatory drive and Pkj inhibition. This interaction is central to how nuclear cells elicit learned, cerebellum-dependent cued movements.

1.5 The contribution of cerebellar neurons to movement

The cerebellum is involved in volitional, well-established movements, as first suggested in case studies on patients will injuries to the cerebellum (Babinski, 1899; Kandel et al., 2013). Such patients exhibit various forms of ataxia, have trouble with repetitive motions, show delayed reaction times, and struggle to perform movements smoothly. However, discerning the cerebellum's role is complicated because multiple parts of the brain contribute to volitional movement. Furthermore, attempted movements may trigger plasticity within the cerebellum, affecting how the cerebellum contributes during subsequent attempts. To confirm that the movement being studied requires the cerebellum, and to control for the history of movement performance, some researchers have focused on movements generated within cerebellum-dependent learning tasks.

To study the role of cerebellar neurons during movement execution, researchers have made recordings of spiking during various kinds of movements. Spiking of cerebellar neurons is modulated by reafferent sensory feedback, such as proprioceptive and mechanoreceptive

responses to movement, as well as synaptic drive related to motor commands. Motor commands refer to signals sent from other motor areas involved in movement execution. To decouple these signals researchers have attempted to isolate reafferent signals by comparing active movement with passive movement, isolate motor commands by studying fictive movements, isolate motor commands by silencing signals arriving from reafferent circuits, or compared movements initiated by different motor systems.

In this section, I will review the findings from these experiments. Because my experiments relate neuronal and synaptic activity to fictive swimming, this review focuses on activity which corresponds with locomotion, either in awake or decerebrated animals. Briefly, locomotion in terrestrial mammals depends on various nuclei in the midbrain and brainstem (e.g. the mesencephalic locomotor region, lateral paragigantocellular nucleus, for example; reviewed by Armstrong, 1988; Esposito et al., 2014; Capelli et al., 2017) which integrate inputs from multiple motor areas (including the cerebellum) and send signals via the reticulospinal tract to central pattern generators in the spinal cord which execute movements. Firing of reticulospinal neurons that normally aligns with the step cycle becomes arrhythmic when the cerebellum is removed (Orlovsky, 1970), and manipulating neuronal activity in the cerebellum can interrupt ongoing locomotion (Sarnaik and Raman, 2018), demonstrating that the cerebellum is an important element in the circuit for generating locomotion.

In this section, I address mf and granule cell, and cf responses to during movement, followed by Pkj and cerebellar nuclear cell spiking. When possible, I attempt to distinguish between motor command signals and reafferent sensory signals. Along with execution of ongoing movement,

the cerebellum's role in movement initiation requires additional considerations, particularly when comparing volitional to reflexive movements. Thus, in the final section, I contrast neural correlates reflexive and sensory-evoked movements, particularly during movement initiation.

1.5.1 Mossy fiber and parallel fiber activity during movement

Many mfs increase their firing during movement. For example, during wrist movements, mfs fire between 50-300 spikes/s (van Kan et al., 1993). Mfs from various sources (including inputs from the dorsal spinocerebellar tract, ventral spinocerebellar tract and lateral reticular nucleus, and neurons in the pons) display tonic increases in firing rate and/or rhythmic activity that matches the step cycle during locomotion (reviewed by Armstrong, 1985). Dorsal spinocerebellar neurons carry proprioceptive sensory input and entrain to the step cycle during passive and active locomotion, (Arshvasky et al., 1972). Lateral reticular neurons show rhythmic bursts of spiking during locomotion, conveying ascending motor command input from propriospinal neurons that arrives via the ventral spinocerebellar tract (Archvasky et al., 1978; Azim et al., 2014). Neurons in the pons show tonically-elevated spiking or cyclic activity during spontaneous bouts of decorticated locomotion (Zangger and Schultz, 1977). Thus, mfs convey either cyclic or tonic excitatory input to the cerebellum during locomotion.

In vivo intracellular recordings of mf EPSCs and granule cell spikes during walking have revealed mf drive and bursts of spikes that align with the step cycle (Powell et al., 2015). Increases in firing were observed in most neurons, which is consistent with evidence from calcium imaging studies that found large scale recruitment of granule cells during spontaneous walking suggests that tonic excitatory drive from mfs translates to large scale recruitment of

granule cells (Ozden et al., 2012). Similar recruitment has been observed during fictive swimming in larval zebrafish (Knogler et al., 2017). Together, these results suggest that both Pkj and cerebellar output neurons receive some combination of tonic and rhythmic excitatory input from presynaptic neurons during locomotion.

Rhythmic modulation of Pkjs and cerebellum nuclear cells is determined in part by rhythmic mf (and pf) drive. Both cell types respond to passive movement of the limbs and show rhythmic firing during decerebrated locomotion (Orlovsky, 1972a). Under these conditions, the averaged response across all nuclear cells showed firing which peaks at the transition between the stance and swing phase (i.e. when the paw leaves the ground), whereas Pkjs peaked soon early in the stance phase. Synaptic drive available to the cerebellum is presumably limited to peripherally-sourced motor commands from propriospinal neurons (e.g. Azim et al., 2014) and proprioceptive reafferent feedback.

1.5.2 Purkinje cell activity

Pkj simple spiking is positively and/or negatively modulated during a variety of movements (e.g. Thach 1968; Jirenhed et al., 2007; Yang and Lisberger, 2013; Brown and Raman, 2018). During locomotion, Pkj simple spike rates correlate with the kinematics of the step cycle. Not all cells respond the same, however. Cell-by-cell analyses show that maximum spike rates can correspond to different timepoints in the step cycle (Armstrong and Edgley, 1984), while some cells show multiple peaks within the step cycle (Sarnaik and Raman; 2018). Furthermore, stride-to-stride variations expose correlations to different kinematic parameters, with spiking of some Pkjs covarying with speed and others with head roll, for example. Also, neighboring Pkjs cells

which likely share synaptic inputs and project to similar areas of the cerebellar nuclei are more likely to covary their firing (Sauerbrei et al., 2015). Together, these results suggest that groups of Pkjs represent kinematic parameters across multiple body parts during locomotion. The average spike rate among all Pkjs shows a sigmoidal oscillation that aligns with the step cycle such that spiking begins to ramp up just before the ipsilateral forelimb is lifted (Armstrong and Edgley, 1984) or just before the hindlimb is set down (Sarnaik and Raman, 2018). Correlated firing is not incidental, but instead locomotion relies on certain patterns of Pkj firing. Transgenic mice with abnormal granule cell and Pkj synaptic transmission and plasticity show abnormal speed, accuracy and consistency of limb placement, and multi-joint coordination (Vinueza Veloz et al., 2014). Also, optogenetic stimulation of Pkjs can disrupt limb movements during locomotion (Sarnaik and Raman, 2018). Thus, rhythmic Pkj simple spiking is at least permissive, if not a controller, for ongoing locomotion.

Cf transmission during active movements has also been reported. During wrist flexion and extension, complex spikes were reported either just prior to or just after movement onset, but at overall lower rates when compared to passive movement (Bauswein et al., 1983). Increased complex spiking has been reported during decerebrated walking, with some Pkjs producing complex spikes at the onset of the stance phase as well as initiation of locomotion, while other respond during the swing phase (Kim et al., 1987). In contrast, during volitional locomotion in awake animals, complex spike rates remain constant and timing is not entrained to the step cycle, though complex spikes are more likely in response to slips (Armstrong et al., 1988; Sauerbrei et al., 2015). Together, these data suggest that during locomotion olivary neurons are readily

recruited by proprioceptive sensory input that communicates perturbations in the step cycle. When motor command input is available during volitional movement, recruitment of olivary neurons is dampened, suggesting an antagonistic interaction between sensory and motor drive.

Pkjs of larval zebrafish show significant, variable modulation during locomotion, with most cells showing combinations of increased simple and complex spiking, and a minority of cells producing fewer spikes (Sengupta and Thirumalai, 2015; Scalise et al., 2016). While spiking is elevated, only a small proportion of cells show rhythmic firing. These results indicate that Pkjs receive synaptic drive and modulate their firing significantly during swimming, though cells that fire in relation to the structure of the swim bout are sparse.

1.5.3 Cerebellar nuclear cell activity

Much like in Pkjs, individual cerebellar nuclear cells show varied rhythmic modulation of firing during the step cycle. Spiking of many cells peaks at transitions in the step cycle, just before paw lift or paw placement (Sarnaik and Raman, 2018). Across all cells, the population average oscillates and peaks just before the ipsilateral paw is lifted. Comparisons with the forelimb show rates that begin to ramp up prior to paw lift, with maximum rates in the middle of the swing (Armstrong and Edgley, 1984). When compared to activity during walking of decerebrate animals (e.g. Orlovsky, 1972a), these results indicate that while proprioceptive sensory input and spinally-sourced motor commands are sufficient for producing rhythmic movement, cerebellar nuclear cells fire at timepoints which can affect initiation of the swing phase when the rest of the nervous system is intact. Comparisons with the hindlimb movement show rates that increase gradually during stance and peak just before the paw is lifted (Sarnaik and Raman, 2018). Firing

was confirmed to be related to hindlimb movement with optogenetic stimulation of proximal Pkjs to elicit locomotor arrest and extensions of the hindlimb. Nevertheless, because clusters of Pkjs fire in correspondence with different kinematic parameters of locomotion, similar variability is likely encoded in nuclear cell firing as well.

That spiking of both Pkjs and nuclear cells is rhythmically modulated raises the possibility that inhibition from Pkjs controls nuclear cell firing during locomotion. One possibility is that elevated Pkj spiking leads to more inhibition and less nuclear cell firing. This hypothesis is supported by recordings made during decerebrate locomotion, during which the firing of Pkj and nuclear cells is anticorrelated (Orlovsky, 1972a; Armstrong, 1988). However, recordings made from awake, walking cats revealed phase-matched rhythmic firing, with the average response for both cell types peaking just before the paw is lifted (Armstrong and Edgley, 1984). Similar results were reported during volitional walking in mice, though in this case, Pkj firing rates peaked slightly earlier in the step cycle than nuclear cells (Sarnaik and Raman, 2018). These data support an alternative to inverse coding in which the pattern of Pkj firing is permissive for nuclear cell spiking. One mechanism through which more nuclear cell spikes are permitted is through synchronization of converging Pkjs (Raman and Person, 2011). In support of this possibility, excitation which synchronizes Pkj spiking is less likely to interrupt ongoing locomotion than excitation which does not (Sarnaik and Raman, 2018). Thus, during locomotion, concerted Pkj spiking may permit spiking of nuclear cells which becomes cyclical through rhythmic excitatory drive.

1.5.4 Movement initiation versus execution

While the cerebellum likely participates in the execution of ongoing movements, its role in the initiation of movements is more difficult to determine for a variety of reasons. One reason is that movement initiation is difficult to experimentally control or define. Sensory-evoked movements are useful for controlling when an animal produces a movement during an experiment. However, these movements often evoke different responses in cerebellar neurons. For instance, initiation of decerebrated treadmill walking corresponds with an acute increase in complex spiking (Kim et al., 1987). Similar responses are observed during isometric movement tasks when the direction of the applied torque is switched (Gilbert and Thach, 1977), and during unconditional eyelid closure elicited by a puff of air (ten Brinke et al., 2017). Complex spikes are likely not essential for real-time modulation of cerebellar output, but instead support plasticity that alters spiking on subsequent trials. Furthermore, treadmill walking and unconditioned eyelid closure persist without the cerebellum (Shik and Orlovsky, 1976; McCormick et al., 1982), raising the possibility that the activity of cerebellar nuclear cells may simply be permissive for movement initiation and execution in these contexts.

Another reason is that the cerebellum likely works in concert with other motor areas for initiation of many movements. For instance, animals will still attempt cued movements after inactivation of the cerebellar nuclei, though the reaction time is lengthened and execution is disrupted (Mason et al., 1998; Goodkin and Thach, 2003). In contrast, cerebellar output is essential for initiating conditional responses in eyelid conditioning (McCormick et al., 1982) and learning persists even in the decerebrated animal, when the cerebellum is isolated from forebrain motor

areas (e.g. Jirenhed et al., 2007). However, in this paradigm, recruitment of cerebellar neurons depends on input related to the conditional stimulus. For a behaving animal outside of the experimental context, it is unknown how often sensory signals capable of eliciting a response that is sufficient for initiating movement are delivered to the cerebellum.

Using spontaneously generated movements is perhaps the most ethologically valid approach to studying the cerebellum's role in movement initiation. By definition, these movements are not attributable to acute sensory signals, and synaptic drive provided to the cerebellum should relate to motor commands. Models of cerebellar learning and processing (such as internal forward models; Miall and Wolpert, 1996) have posited that this input is crucial for priming the cerebellar circuit to undergo plasticity in the event of a motor error, while also modulating signals from the cerebellar to alter descending motor commands. Cerebellar output neurons can evoke EPSPs in motor neurons within 1-3 ms through a multisynaptic circuit (Azim et al., 2014), suggesting that signals from the cerebellum can add to other motor commands with minimal delays. Thus, the cerebellum may be contributing to initiation of spontaneous movements if synaptic input arrives and modulates spiking prior to the onset of the movement.

1.6 Initiation and adaptation of movements supported by cerebellar learning

The cerebellum can use synaptic drive related to motor commands to alter ongoing movements in real time, as well as transforming synaptic drive related to sensory stimuli into a signal which can generate movement. In both contexts, the cerebellum's contribution is not automatic, but instead emerges following plasticity within the cerebellar circuit that takes place during

behavioral training and learning. For *in vitro* and *ex vivo* slice experiments, plasticity is often tested by determining if some physiological parameter (i.e. EPSC amplitude, input resistance) deviates from basal measurements following an induction protocol. Translating this definition to *in vivo* experiments, plasticity can be defined as a deviation from the initial synaptic response when the animal was naïve to the response once the animal has been trained. Depending on the task in which the movement is produced, the initial synaptic drive may relate to motor commands, sensory stimulation, or both.

In this section, I will review forms of plasticity identified in Pkjs and cerebellar nuclear cells. Because my experiments focus on movements learned within a cerebellum-dependent associative learning task, I will then discuss delay eyelid conditioning, focusing on task-related activity of Pkjs and cerebellar nuclear cells, and the forms of plasticity that may support that activity.

1.6.1 Plasticity in Pkjs

Forms of plasticity that decrease Pkj simple spiking lead to less inhibition of output neurons, thereby permitting greater influence of the cerebellum on behavior. While multiple forms of plasticity have been described in Pkjs, much focus has been placed on long-term depression (LTD) at pf synapses, which occurs when transmission immediately precedes a complex spike (Ito and Kano, 1982; Ito et al., 2014). Cf transmission frequently occurs in response to aversive stimuli and motor errors. By depressing the amount of drive provided by coincidentally-active pf inputs, this mechanism decreases the likelihood that Pkjs will contribute to subsequent motor errors (Ito, 1984).

However, depression is sensitive to the temporal relationship between pf and cf transmission. In fact, pf inputs are not depressed but instead potentiated if they follow the complex spike or significantly precede it (Chen and Thompson, 1995; Safo and Regehr, 2008). In some case, the temporal relationship between pfs and cfs is calibrated to match the behavior to which a Pkj preferentially contributes. For instance, among Pkjs in the mouse flocculus that regulate eye movements, latencies that most effectively induce depression match the latencies expected between pf drive that contributes to movement execution and complex spiking related to retinal slip (Suvrathan et al., 2016). Together, these findings suggest that temporally-specific heterosynaptic interactions between pf and cf inputs are central to regulating Pkj simple spiking.

1.6.2 Plasticity in cerebellar nuclear cells

Researchers have focused on forms of plasticity that promote spiking of cerebellar output neurons, such as long-term potentiation (LTP) of mf inputs, which is induced when mf transmission coincides with a period of post-inhibitory rebound spiking. In other words, LTP is the result of sequential but overlapping transmission from mfs and Pkjs (Aizenman et al., 1998; Pugh and Raman, 2006; McElvain et al., 2010; Pugh and Raman, 2008). Intracellularly, coincidental activity is detected through two acute influxes of calcium that activate calcineurin and CaMKII, which leads to potentiation (Person and Raman, 2010). Additionally, nuclear cell spiking can be promoted by increasing intrinsic excitability, which can be induced by calcium entry at mf synapses or during rebound spiking (Aizenman and Linden, 2000; Zhang et al., 2004).

1.6.3 Cerebellum-dependent associative learning: eyelid conditioning

Associative learning tasks, in which an animal learns to produce a conditional behavioral response (CR) to a neutral conditional stimulus (CS) that predicts a disruptive or aversive unconditioned stimulus (US), have been used to study how the cerebellum produces learned movements. The associative task most frequently used to study cerebellar learning is eyelid conditioning, during which a neutral CS is paired with a US that elicits reflexive closure of the eyelid. Conceptually, plasticity that supports learning proceeds when the neural traces related to the CS and US converge within the cerebellar circuit, leading to a modified cellular response to the CS on subsequent trials. In a well-trained animal, the cerebellar circuit will transform synaptic drive related to the CS into a pattern of firing by cerebellar nuclear cells that can lead to initiation and execution of CR. Thus, the CR is a learned, cued movement that depends on the cerebellum

Stimulation studies have suggested that the CS neural trace enters the cerebellum through mfs, whereas the US neural trace arrives through cfs (Steinmetz et al., 1986; Mauk et al., 1986). The sequential, overlapping transmission of these inputs likely leads to heterosynaptic plasticity that alters the firing pattern of Pkjs and nuclear cells. Researchers have generated hypotheses about forms of plasticity that support learning after recording from the eyeblink zone of the cerebellum in extensively-trained animals. While Pkjs show different forms of task-related activity, some cells display depressed simple spiking during the CR that matches the inverse of CR kinematics on a trial-by-trial basis (Jirenhed et al., 2007; Wetmore et al., 2014; Halverson et al., 2015; Ohmae et al., 2015; ten Brinke et al., 2015). In addition, lesions of the cerebellar cortex in well-

trained animals do not prevent CR execution, but instead alter the timing of the CR (Perrett et al., 1993). These observations support a model in which the timing and amplitude of the CR is set by the removal of inhibition provided by Pkjs to nuclear cells.

Possible forms of plasticity that explain Pkj pauses are decreased pf drive related to the CS, as well as increased CS-related inhibition of Pkjs from inhibitory interneurons. Decreased pf drive can be achieved by LTD at these synapses, although transgenic animals in which pf LTD is prevented show normal eyelid conditioning (Schonewille et al., 2011). Molecular layer interneurons show spiking that inversely correlates to simple spike pauses in nearby Pkjs during CRs (ten Brinke et al., 2015). Moreover, Pkj pauses are disrupted when inhibition in the molecular layer is blocked (Johansson et al., 2014). Together, these results indicate that increased inhibition rather than decreased excitation is the primary factor in Pkj pausing. In addition, a subset of Pkjs respond to training by producing complex spikes in response to the CS (Ohmae and Medina, 2015; ten Brinke et al., 2015). This form of plasticity may reflect decreased CS-related inhibition of olivary neurons by cerebellar nuclear cells. Decreased complex spiking in response to the US has also been reported (Sears and Steinmetz, 1991; Hesslow and Ivarsson, 1996). Both forms of plasticity provide evidence for the regulation of cf transmission during learning (Medina et al., 2002).

Signals from the cerebellar nuclei are essential for learning and executing the CR. Lesions and reversible inactivations of cerebellar nuclear cells abolish the CR when applied after learning and prevent acquisition of the CR when applied prior to training (McCormick and Thompson, 1984b; Clark et al., 1992; ten Brinke et al., 2015). Furthermore, lesions and reversible inactivations of

cerebellar cortex in trained animals do not prevent CR expression, but instead alter timing (Perrett et al., 1993; Ohyama et al., 2006), demonstrating that plasticity within the nuclei is sufficient for expressing the CR. Furthermore, multiunit recordings have revealed that as a population nuclear cells show increases in firing that both slightly preceded and match the kinematics of the eyelid-closure CR (McCormick and Thompson, 1984a). Individual cells show a variety of responses, however. While most nuclear cells within the eyeblink zone of the interpositus nucleus show no response during the CS, a subset shows increased firing or decreased firing that matches the time course of the CR. These firing rate changes are acquired gradually across the multiple training session and preceded the emergence of CRs (ten Brinke et al., 2015). While multiple forms of plasticity (i.e. increased excitability, synchronization of Pkj spiking) could explain increases in rate, increased mf drive has been supported most directly. Firstly, stimulation protocols modeled after the pattern of synaptic input that nuclear cells were predicted to receive during associative learning induced LTP at mf-nuclear cell synapses (Pugh and Raman, 2006). Furthermore, eliminating Pkj modulation in trained animals leads to short-latency CRs which match the timing of mf drive (Perrett et al., 1993; Ohyama et al., 2006), suggesting that well-timed CRs result from an interaction between mf drive, which is potentiated, and Pkj inhibition, which determine the specific timing by pausing.

1.7 Swimming and learning in larval zebrafish

Despite their immaturity, larval zebrafish are capable of many different behaviors, many of which must require an operational cerebellum. Nevertheless, the capabilities of the cerebellum at

this age (~7 days postfertilization, dpf) are likely limited. Principal neurons of the cerebellum are first observed 2-2.5 dpf and continue to divide for several months as the fish develops (McFarland et al., 2008; Volkmann et al., 2007; Hamling et al., 2015; Knogler et al., 2017). By 7 dpf, their numbers are relatively modest (~300 Pkjs, ~6000 granule cells). Cerebellar neurons show changes in excitability, synaptic pruning, and elaboration of their dendritic arbors across the first week of life, evidencing dramatic changes in cerebellar physiology that correspond with the emergence of many behaviors (Hsieh et al., 2014). In this section, I review evidence for the involvement of the cerebellum in the execution and adaptation of swim movements, focusing on various forms of sensory-evoked swimming and sensorimotor learning displayed by larval zebrafish.

1.7.1 Sensory-evoked swimming

Larval zebrafish display various kinds of sensory-evoked swim movements that relate to recruitment of different central circuits. Abrupt stimuli, such as a tap or loud acoustic stimulus, can elicit short-latency escape responses that are driven by Mauthner cells, which are large, spinal-projecting neurons located bilaterally in the hindbrain (Zottoli, 1977; Liu and Fetcho, 1999; Burgess and Granato, 2009; Mu et al., 2012). Tactile stimuli are communicated to Mauthner cells after detection by spiral fiber neurons in the head and Rohon-Beard neurons in the tail (Knogler and Drapeau, 2014; Lacoste et al., 2015). Flashes of light can also elicit swim responses, though at longer latencies. This form of reflexive swimming is driven by spinally-projecting neurons in the nMLF, which drive contraction of ipsilateral tail muscles (Severi et al., 2014; Wang and McLean, 2014; Thiele et al., 2014).

Fish also display optomotor swimming in response to moving visual gradients (Brockerhoff et al., 1995; Portugues and Engert, 2011; Ahrens et al., 2012). The response is likely useful for maintaining position against surrounding water currents, as right-left gradient progression induces turning behavior while back-front progression induces forward swimming. Optomotor swimming relies on a sensorimotor circuit that begins with direction-sensitive retinal ganglion cells, which synapse with neurons in the optic tectum. Gradients that evoke turning lead to an asymmetrical signal to the spinal-projecting neurons in the mid- and hindbrain, whereas those that favor forward motion generate a symmetrical signal (Orger et al., 2008; Naumann et al., 2016). Independent of learning, execution of the optomotor response is at least permitted by real-time signaling of cerebellar neurons. Pkjs in the rostromedial corpus cerebelli are active during optomotor swimming, and unilateral inhibition of these neurons biases tail movements toward the contralateral side (Matsui et al., 2014a). Thus, input from the cerebellum likely converges with input from the tectum to control spiking of spinal-projecting neurons during optomotor swimming.

Left-right gradients can also evoke the optokinetic reflex in which the eyes move to stabilize the visual field (Brockerhoff et al., 1995). Pkjs in the caudolateral lobe of the cerebellum are active during optokinetic eye movements (Matsui et al., 2014a), suggesting that the cerebellum is involved in smooth pursuit eye movements, as it is in mammals (reviewed by Lisberger 2010). This action likely contributes to more sophisticated behaviors, like the smooth pursuit eye movements involved in prey capture behaviors (Portugues and Engert, 2009; Patterson et al., 2014).

1.7.2 Learning-dependent adaptation of sensorimotor behaviors

Larval zebrafish show a variety of learned swimming behaviors that resemble behaviors learned by mammals in commonly-used behavioral paradigms. For instance, these fish show a non-associative form of learning in which the escape response to an acoustic stimulus is potentiated (Mu et al., 2012) or inhibited (Burgess and Granato, 2009) by a preceding stimulus. Called paired-pulse facilitation or inhibition, this form of learning occurs when the preceding stimulus triggers release of neuromodulators by hypothalamic neurons, which leads to changes in excitability of Mauthner cells. Larval zebrafish also show place avoidance behavior when given electrical shocks while investigating part of their tank. The association between place and shock likely forms within the habenula, which exerts it effects on downstream motor circuits through recruitment of serotonergic neurons in the raphe nuclei (Amo et al., 2014).

Larval zebrafish display cerebellum-dependent learning as well. One form of learning is adaptation of optomotor swimming in response to visual feedback, which is similar to adaptation of the vestibular-ocular reflex (Portugues and Engert, 2011). In this paradigm, researchers provide optic flow visual feedback that is yoked to the fish's swim commands. Changing the gain of the feedback induces increases or decreases in the strength of swimming, with complete adaptation evident after a few bouts. Changes in gain correspond with increased activity in cerebellar neurons, and lesions to the inferior olive prevent adaptation, suggesting that learning depends on the cerebellum (Ahrens et al., 2012). Cerebellum-dependent associative learning has also been reported. For instance, conditioned bradycardia, a paradigm in which omission of an expected electrical shock results in a skipped heartbeat, correlates with activity in cerebellar

neurons and is impaired in transgenic fish with mutations that affect granule cells (Matsuda et al., 2017). Also, in response to pairing a visual stimulus that elicits phototaxic swimming with a tactile stimulus, zebrafish will increase the amplitude of their tail bends. Training corresponds with task-related activity in cerebellar neurons, and learning is blocked if the cerebellum is ablated (Aizenberg and Schumann, 2011). Thus, larval zebrafish show multiple forms of sensorimotor adaptation that depend on the cerebellum.

My experiments

Emphasized in this introduction are the multiple modes of cerebellar processing. The cerebellum receives afferent synaptic input attributable to sensory stimuli and motor commands. Differences in the amount and timing of synaptic drive determine how cerebellar neurons respond and contribute to volitional, reflexive, and cued movements. Furthermore, interactions between synaptic inputs and between cerebellar neurons induce plasticity, leading to changes in how these neurons respond to synaptic drive, and altering how and whether movements are generated. Despite their immaturity, larval zebrafish offer a means through which cerebellar contributions to movement can be studied. These animals also display cerebellum-dependent learning, meaning plasticity that supports expression of learned movements can be studied as well. In chapters 2 and 3, I report my findings from experiments in which I have made intracellular recordings from Pkjs and ENs in the larval zebrafish while simultaneously recording fictive swimming from the ventral root in the tail. For both neuron types, I examine the synaptic responses to visual sensory stimuli, as well as during spontaneous and evoked fictive swimming.

I also developed an associative learning task that depends on the cerebellum and followed changes in the activity of Pkjs that emerged during training. I related Pkj spiking patterns observed during learned swimming to responses when the fish was naïve and to activity during spontaneous and evoked swimming. Also, I manipulated Pkj activity during training to test how these neurons contributed to learned swimming. Findings from these experiments reveal homologies between the cerebellum of teleost fish and mammals, and provide evidence for differences in cerebellar processing during volitional, reflexive, and learned movements.

Chapter 2: Distinct responses of Purkinje neurons and roles of simple spikes during associative motor learning in larval zebrafish

2.1 Abstract

To study cerebellar activity during learning, we made whole-cell recordings from larval zebrafish Pkjs while monitoring fictive swimming during associative conditioning. Fish learned to swim in response to visual stimulation preceding tactile stimulation of the tail. Learning was abolished by cerebellar ablation. All Pkjs showed task-related behavior. Based on how many complex spikes emerged during learned swimming, they were classified as multiple, single, or zero complex spike (MCS, SCS, ZCS) cells. With learning, MCS and ZCS cells developed increased climbing fiber (MCS) or parallel fiber (ZCS) input during visual stimulation; SCS cells fired complex spikes associated with learned swimming episodes. The categories correlated with location. Optogenetically suppressing simple spikes only during visual stimulation demonstrated that simple spikes are required for acquisition and early stages of expression of learned responses, but not their maintenance, consistent with a transient, instructive role for simple spikes during cerebellar learning in larval zebrafish.

2.2 Introduction

The activity of cerebellar Pkjs regulates both practiced and new movements (Thach 1968; McCormick and Thompson, 1984; Medina et al., 2000; Mauk et al. 2014). In vertebrates from fish to mammals, Pkjs influence motor behavior via both simple and complex spikes (Eccles, Llinás, and Sasaki, 1966; Monsivais et al. 2005; Khaliq and Raman 2005; Han and Bell 2003). Simple spikes occur spontaneously and are modulated by synaptic input from granule cells and inhibitory interneurons; the resulting activity alters firing patterns of Pkj target neurons, whose output generates movements (Thach, 1968; McDevitt et al., 1987; Witter et al., 2013; Heiney et al. 2014; Lee et al. 2015). Complex spikes arise from synaptic input from climbing fibers and can induce plasticity of other afferents to Pkjs, thereby serving as teaching and/or error signals during motor learning (Gilbert and Thach, 1977; Mauk et al., 1986; Medina et al. 2002; Ohmae and Medina 2015).

Despite their shared modes of action potential firing, Pkjs in different cerebellar regions contribute differentially to behaviors, owing to distinct innervation patterns by mossy fiber-granule cell pathways (Bower et al. 1981; Bower and Woolston 1983; Garwicz et al. 1998) and inferior olivary modules (Voogd and Glickstein 1998; Sugihara and Shinoda 2005; Ruigrok 2011; Cerminara and Apps 2011). Among Pkjs engaged by a particular action, learning often correlates with the emergence of new patterns of activity. In primates, ferrets, rabbits, and mice, the rate and timing of simple spikes and/or complex spikes can change as animals acquire novel motor behaviors (Gilbert and Thach 1977; Jirenhed et al. 2007; Halverson et al. 2015; Ohmae and Medina 2015; ten Brinke et al, 2015). *In vitro* studies have demonstrated many forms of

synaptic plasticity that may underlie these changes (Hansel et al. 2001; Ito et al., 2014). Few *in vivo* preparations are available, however, in which synaptic changes and the resultant spikes can be monitored and manipulated over the full time course of learning.

Here, we explored whether larval zebrafish might offer such a preparation. At 6-8 days post-fertilization (dpf), the zebrafish cerebellum has a relatively simple structure, containing ~300 Pkjs (Hamling et al., 2015). Zebrafish larvae swim and learn to alter their movements in response to sensory stimulation (Portugues and Engert, 2011; Mu et al., 2012; Amo et al., 2014; Matsui et al., 2014a; Pantoja et al., 2016), and they display some forms of motor learning that depend on the cerebellum (Aizenberg and Schuman, 2011; Ahrens et al., 2012). Additionally, larval zebrafish Pkjs generate both simple and complex spikes (Hsieh et al., 2014; Sengupta and Thirumalai, 2015), providing a potentially useful system to examine how these conserved signals may contribute to cerebellar learning in different species (Scalise et al., 2016).

We therefore developed a cerebellar associative learning task for immobilized larval zebrafish, and made whole-cell recordings of Pkj activity (1) in response to visual and tactile sensory stimuli, (2) during episodes of spontaneous, reflex, and learned swimming and (3) before, during, and after training. Three populations of Pkjs could be distinguished by their complex spike responses after conditioning, as well as by their topographical location in the cerebellum. Optogenetically suppressing simple spikes in all Pkjs during training further showed that the role of simple spikes changes as learned movements emerge, such that learning can be abolished and/or altered depending on when simple spikes are disrupted.

2.3 Results

2.3.1 Purkinje cell recordings.

With the goal of testing how Pkj neurons contribute to associative learning in larval zebrafish, we first investigated whether they displayed consistent synaptic responses and firing patterns during sensory stimuli and/or fictive swimming. In immobilized fish, whole cell recordings from Pkjs and extracellular recordings from ventral roots in the tail were made simultaneously (Figure 2.1A, 2.1B). Pkjs were located in the most superficial cell body layer of the corpus cerebelli (Bae et al., 2009) and were identified by their single apical dendrite in the molecular layer (Figure 2.1A, 2.1C). Under voltage-clamp, spontaneous synaptic activity was evident as large-amplitude EPSCs (-253 ± 29 pA, N=39 cells), likely from climbing fibers, and small-amplitude EPSCs, generally < 20 pA, likely from parallel fibers (Figure 2.1D, 2.1E). Current-clamp recordings from these cells revealed large-amplitude complex spikes and small-amplitude simple spikes (Figure 2.1F, *top,* 2.1G), further confirming their identity as Pkjs (Hsieh et al., 2014; Sengupta and Thirumalai, 2015; Scalise et al., 2016). As expected, basal firing rates were lower for complex spikes than for simple spikes (0.3 ± 0.03 *vs.* 6.4 ± 1.2 spikes/s, N=42 cells; $p<0.001$, paired t-test). These values are in good agreement with previous studies in larval zebrafish (Scalise et al. 2016). Subthreshold EPSPs, likely arising from parallel fibers, were also evident (Figure 2.1F, *bottom*). In some records, increased parallel fiber activity correlated with episodes of fictive swimming that occurred spontaneously. In voltage clamp, this activity was evident as clusters of EPSCs (Figure 2.1E, 2.1H); in current clamp these events could summate to produce long-lasting depolarizations, typically with simple spikes riding on top (Figure 2.1I).

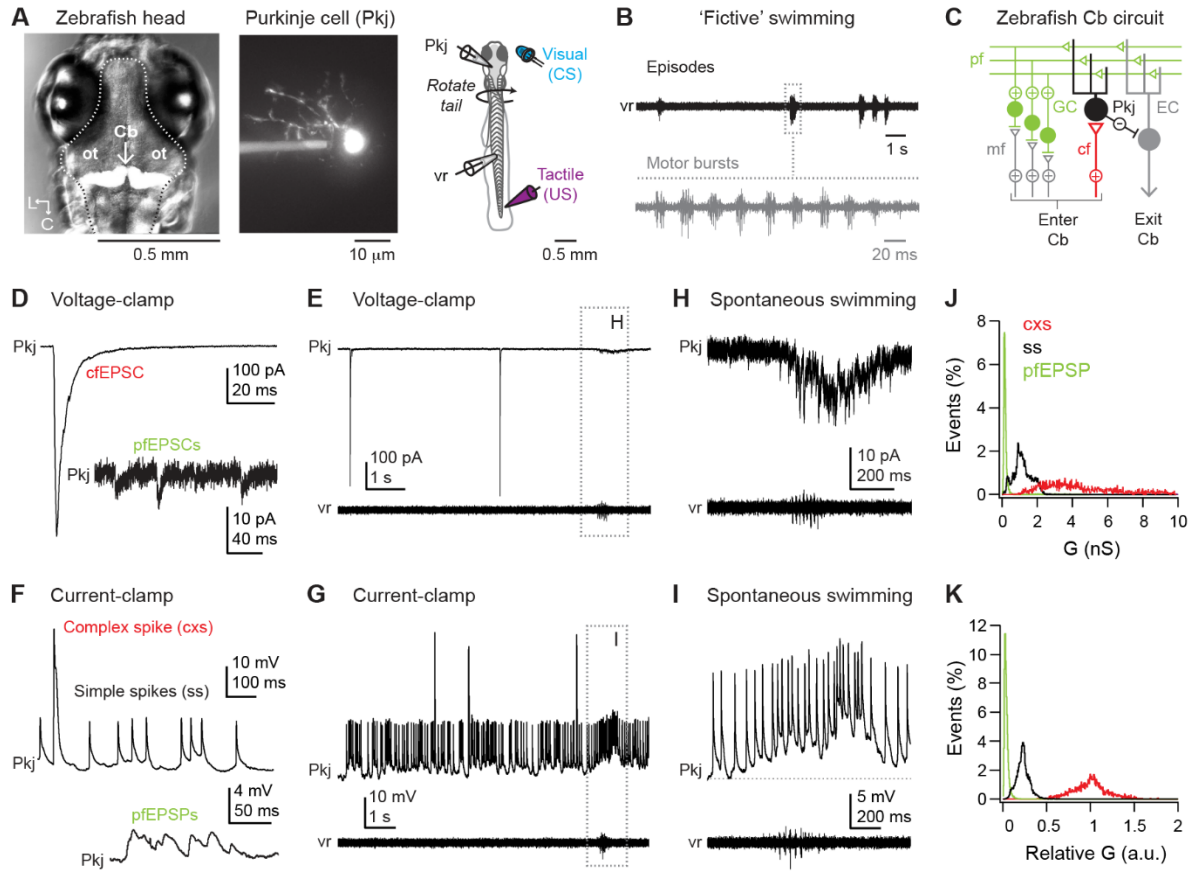

Figure 2.1. Spontaneous activity during dual recordings of Purkinje cells and ventral roots. **(A)** Left, dorsal view of larval zebrafish head illustrating the location of the cerebellum (Cb, arrow). In this image, cerebellar Purkinje cells are fluorescently labeled by Archaerhodopsin-3 (white). Dotted line, outline of brain. ot: optic tectum. L, lateral; C, caudal. Middle, a Purkinje cell filled with Alexa Fluor 488. Right, schematic of the preparation. **(B)** Sample ventral root (vr) recording showing episodic bouts of fictive swimming (compressed time base, black) and cyclical motor bursts (expanded time base, grey). **(C)** Schematic of the zebrafish cerebellum. Pkj: Purkinje cell. EC: eurydendroid cell; GC: granule cell; cf: climbing fiber; mf: mossy fibers; pf: parallel fibers; Cb: cerebellum. **(D)** Sample voltage-clamp recording (holding potential = -60 mV, all voltage-clamp records) of cfEPSC and pfEPSCs (inset). **(E)** Sample voltage-clamp recording (top) and simultaneous vr recording (bottom). Box, episode of spontaneous swimming, expanded in **(H)**. **(F)** Sample current-clamp recording of complex and simple spikes (top) and pfEPSPs (bottom).**(G)** Sample current-clamp recording of Purkinje cell spikes and simultaneous vr recording. Box, episode of spontaneous swimming, expanded in **(I)**. Recordings in **(E)** and **(G)** are from the same cell. **(H)** Higher gain voltage-clamp and vr recording from **(E)** of clustered parallel fiber EPSCs during spontaneous swimming. Legend continued on next page.

Figure 2.1 continued. (I) Higher gain current-clamp and vr recording from **(G)** of a parallel fiber driven long-lasting depolarization and simple spikes during spontaneous swimming. Dotted line, inter-spike potential (-56 mV) to illustrate depolarization. **(J)** Distribution of conductances associated with all complex spikes (cxs), simple spikes (ss), and parallel fiber EPSPs (pfEPSPs) included in the study. Absolute conductances (bin width, cxs and ss = 0.02 nS; pfEPSP = 0.01 nS).**(K)** As in **(J)** but conductances normalized to the mean cxs conductance in each cell (bin width = 0.005).

2.3.2 Identification of events

In each cell, complex spikes were larger in amplitude and rose faster than simple spikes. Their absolute amplitudes and rise times varied from event to event, however, since variations in membrane potential (e.g., from summating EPSPs or hyperpolarization) could alter driving force on synaptic currents or inactivate/recover voltage-gated channels. Amplitudes and rise times were also influenced by the magnitude of the underlying synaptic conductances, which varied from cell to cell. Since subsequent analyses relied on distinguishing climbing-fiber-driven and parallel-fiber-driven events, we (1) identified complex spikes based on rate of rise, (2) confirmed by inspection that they were large events rising directly from the baseline (as expected for synaptic currents exceeding intrinsic currents), and (3) verified their identity as climbing-fiber-dependent by estimating the conductance underlying the upstroke of the event. With complex spikes extracted from the record, we identified simple spikes based on rise rate, visually confirmed that they had an inflection on the upstroke, consistent with activation of voltage-gated channels, and estimated the underlying conductance. Lastly, with simple spikes extracted, we identified EPSPs based on rise rate, confirmed them by inspection, and calculated the conductance (see *Materials and Methods*).

In the complete study, we identified 1,930 complex spikes, 16,763 simple spikes, and 21,096 EPSPs. The mean conductance (± S.D.) associated with complex spikes was 4.86 ± 0.25 nS; with simple spikes, 1.17 ± 0.5 nS; and with EPSPs, 0.17 ± 0.08 nS. These values correspond to about -300 pA at -60 mV for the climbing fiber EPSC and -10 pA at -60 mV for parallel fiber EPSCs, consistent with voltage-clamp recordings. They also predict about -100 pA of Na current around -30 mV on the upstroke of the simple spike. The complete distribution of all conductances in all cells (Figure 2.1J) showed that the overlap of the complex and simple spike distributions was 15.2%. This overlap does not reflect the likelihood of misidentification, however, because complex and simple spikes were distinguishable within each record, by the absence (complex spike) or presence (simple spike) of an inflection as well as by the conductance normalized to the mean complex spike-associated conductance within each cell. Plotting the conductances for simple spikes relative to those for complex spikes in the same cells gave an overlap of 0.66% with all cells pooled (Figure 2.1K). When these normalized measurements were made on a cell-by-cell basis, the overlap fell to 0.082 ± 0.058%. A subset of cells showed EPSPs but were too depolarized to fire simple spikes (*Materials and Methods*); in these cells the conductance associated with the complex spike was ≥2 S.D. from the mean conductance of the simple spike distribution. Thus, simple and complex spikes could be distinguished with little error.

Similar analyses gave a simple spike-EPSP overlap of 9.8% for the non-normalized distribution across all cells (Figure 2.1J), 5.2% for the normalized distribution across all cells (Figure 2.1K), and 2.1 ± 0.6% within cells. EPSPs and simple spikes could thus be distinguished; however, our primary interest in these events was to identify parallel-fiber-dependent, synaptically driven

spikes, rather than spontaneous spikes, during cerebellar learning. Therefore, we focused subsequent analyses on parallel-fiber EPSPs (pfEPSPs) that led to simple spikes rather than on simple spikes directly.

2.3.3 Heterogeneity of Purkinje cell responses during motor behavior and sensory stimulation.

To begin to examine task-related Pkj activity, we first assessed responses during spontaneous motor behavior. During 39 of 49 Pkj recordings, spontaneous fictive swimming occurred. All 39 Pkjs modulated their activity during spontaneous swimming, but not all cells responded in the same way. The variety of responses is catalogued here to provide the context for the studies of motor learning described below.

Many cells generated complex spikes during spontaneous swimming (N=29/39; Figure 2.2A); in 11 of these cells, complex spikes occurred on every swimming episode, while the others produced complex spikes on 53.4 ± 4.8% of episodes. Most Pkjs also showed EPSPs with long-lasting depolarizations (>200 ms) that evoked simple spikes, which could outlast swimming (N=26/39; Figure 2.2A, *top three panels*), while others showed long-lasting hyperpolarizations of 5- to 10-mV (N=9/39 cells; Figure 2.2A, *bottom*). These observations are consistent with previous descriptions of spontaneous, motor-related Pkj responses in larval zebrafish (Sengupta and Thirumalai, 2015).

Next, to examine Pkj responses to sensory input, we presented fish with a high-contrast blue light (the “visual” stimulus, 2 s) or a brief, mild electrical stimulus to the tip of the tail (the “tactile” stimulus, 5 ms). With repeated presentations, each sensory stimulus evoked a consistent

response in each Pkj. As in the case of spontaneous swimming, however, responses varied across the population of Pkjs. With high-contrast visual stimuli, both parallel and climbing fiber responses were observed in 12 of 49 cells, while other cells showed only climbing fiber responses (N=16/49), only parallel fiber responses (N=10/49), or no detectable change in activity (N=11/49) (Figure 2.2B, *top to bottom*).

Next, to examine Pkj responses to sensory input, we presented fish with a high-contrast blue light (the "visual" stimulus, 2 s) or a brief, mild electrical stimulus to the tip of the tail (the "tactile" stimulus, 5 ms). With repeated presentations, each sensory stimulus evoked a consistent response in each Pkj. As in the case of spontaneous swimming, however, responses varied across the population of Pkjs. With high-contrast visual stimuli, both parallel and climbing fiber responses were observed in 12 of 49 cells, while other cells showed only climbing fiber responses (N=16/49), only parallel fiber responses (N=10/49), or no detectable change in activity (N=11/49) (Figure 2.2B, *top to bottom*).

In 82% of recordings (N=40/49), high-contrast visual stimulation also evoked fictive swimming (Figure 2.2C). In some fish, swimming occurred a few hundred ms after light onset, with or without another episode of swimming after light offset (N=22/40); other fish swam only at the offset of the light (N=18/40). The swimming latencies are consistent with the relatively long delays reported for visuomotor behavioral responses in zebrafish (Brockerhoff et al., 1995; Wang and McLean, 2014; Portugues et al., 2015).

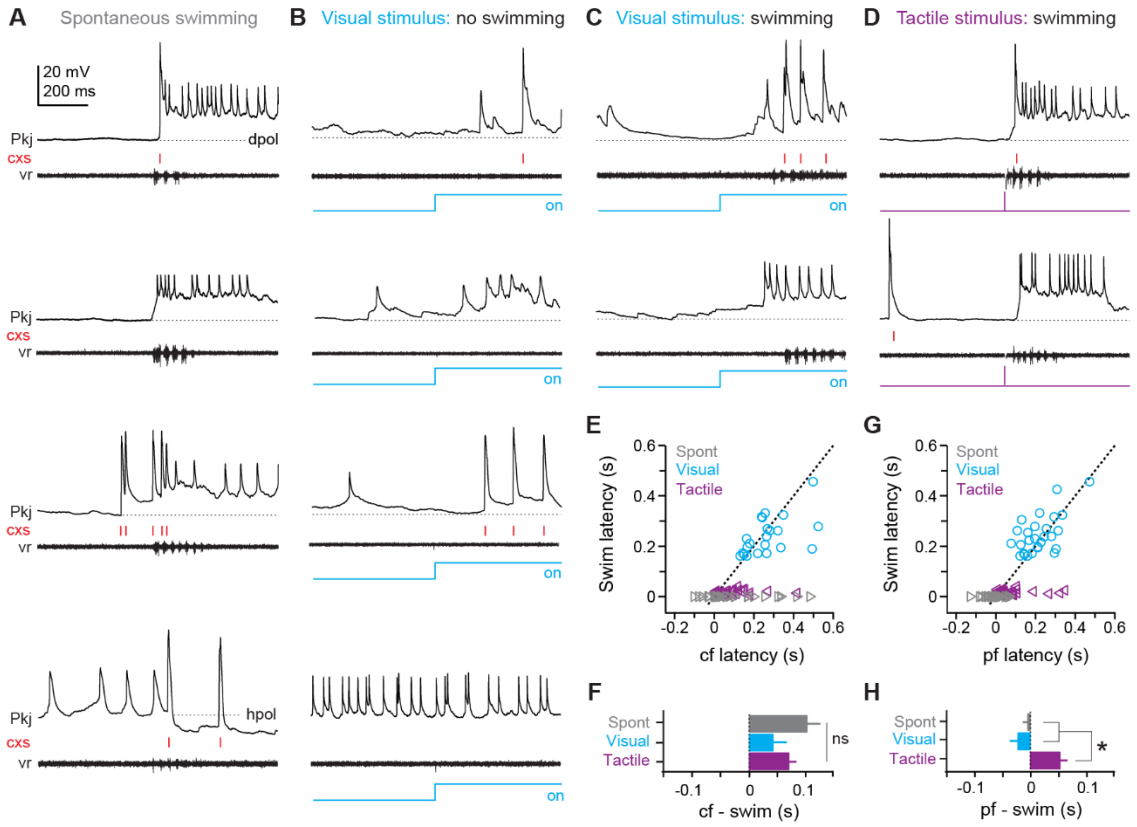

Figure 2.2. Purkinje cell responses during sensory stimuli and motor commands associated with fictive swimming. **(A)** Responses of four different Purkinje cells (top to bottom) during spontaneous swimming, showing different combinations of climbing fiber, parallel fiber, and putative inhibitory input, resulting in complex spikes, simple spikes with long-lasting depolarizations, and/or hyperpolarization. In all panels, complex spikes (cxs) are indicated with red tick marks and the corresponding ventral root recording is included. Dotted lines at inter-spike potentials (top to bottom, -59 mV, -61 mV, -55 mV, -57 mV) illustrate depolarization (dpol) and hyperpolarization (hpol). **(B)** Responses of four different Purkinje cells to a visual stimulus (blue step, all panels) that did not evoke swimming. Dotted lines, top to bottom, -57 mV, -54 mV, -55 mV, -50 mV. **(C)** Responses of two different Purkinje cells to a visual stimulus that elicited swimming, either with (top) or without (bottom) complex spikes during the swimming episode. Dotted lines, top and bottom, -63 mV, -66 mV. **(D)** Responses of two different Purkinje cells to tactile stimulus (purple step, all panels), either with (top) or without (bottom) complex spikes during the swimming episode. V, ventral; C, caudal. Dotted lines, top and bottom, -60 mV, -66 mV. Legend continued on next page.

Figure 2.2 continued. (E) Swim latency vs. climbing fiber response (complex spike) latency relative to stimulus onset for visual (blue), and tactile (purple) evoked swimming for all cells. Data for spontaneous (grey) swimming is included at a latency of 0. Dotted line, unity. **(F)** Mean latency of first climbing fiber response (complex spike) relative to swimming onset calculated from difference between x and y values in **(E)**. Zero indicates coincidence. $F_{(2,80)}$=1.84. **(G)** As in **(E)** but for latency of long-lasting (>200 ms) pfEPSP-initiated depolarizations. **(H)** As in **(F)** but for long-lasting depolarizations. $F_{(2,88)}$=16.54. In all figures, data are plotted as mean ± SEM, and asterisks on plots indicate $p<0.05$.

With tactile stimuli, fictive swimming was evoked with a short latency (16.9 ± 1.3 ms after stimulation) and with 100% reliability (N=49/49 fish; Figure 2.2D). This invariant response is consistent with the involvement of reflexive brainstem pathways responsible for evasive swimming maneuvers in larval zebrafish (Bhatt et al., 2007; Lacoste et al., 2015; Koyama et al., 2016), and validates the tactile stimulus for use as an unconditional stimulus in later associative learning experiments. Additionally, 86% of Pkjs responded to the first tactile stimulus with at least one complex spike (N=42/49 cells).

Next, we measured the latency of Pkj responses relative to the onset of swimming. On average, climbing fiber responses lagged the onset of spontaneous and sensory-evoked swimming (Figure 2.2E, 2.2F; spontaneous: 102 ± 31 ms, N=109 episodes/29 cells; visual: 40.1 ± 23.4 ms, N=23 episodes/23 cells; tactile: 70.3 ± 13.6 ms, N=42 episodes/42 cells; $p=0.17$). The timing of complex spikes, however, had relatively high variance (spontaneous, coefficient of variation =1.1; visual, CV=1.1; tactile, CV=1.1), such that complex spikes in some cells preceded swimming. This observation helps exclude the possibility that complex spikes simply report a visuomotor mismatch; if so, they would always lag swimming onset, and would be equally probable during all forms of swimming, neither of which was the case.

Because pfEPSPs were numerous and probably undersampled (see *Materials and Methods*), we estimated the latency of substantial parallel-fiver drive by measuring the onset of long-lasting (>200 ms) depolarizations initiated by pfEPSPs, which drove simple spikes (Figure 2.1I). In contrast to climbing fiber responses, the timing of these events nearly coincided with spontaneous and visually evoked swimming onset (Figure 2.2G; lag for spontaneous: -6.3 ± 8.3 ms, N=91 episodes/26 cells; visual: -23.4 ± 13.0 ms, N=28 episodes/28 cells). With tactile stimulation, however, pfEPSPs significantly lagged swimming onset, by 52.9 ± 14.2 ms (Figure 2.2H, N=35 episodes/35 cells, $p<0.001$). The high variance of response latencies suggests that Pkjs may play heterogeneous roles in spontaneous and sensory-evoked swimming, possibly ranging from triggering to reporting these motor responses (but see ablation studies below). These observations are consistent with those reported for Pkjs during the optomotor response (Scalise, et al. 2016). More generally, the data demonstrate that individual Pkjs respond to a variety of sensory modalities, as well as to motor commands.

A cerebellar learning task in the zebrafish

Next, to prepare to study Pkj activity during associative learning, we tested whether larval zebrafish could be conditioned to produce fictive swimming in response to a visual cue. In these experiments, the ventral root signal was recorded without concurrent recording from Pkjs. A 2-sec blue light that was low enough contrast not to evoke fictive swimming served as a conditional stimulus (CS) (see *Materials and Methods*). The CS was immediately followed by the tactile unconditional stimulus (US), which elicited the unconditional response (UR) of fictive swimming (Figure 2.3A). Because the start-to-start interval between individual trials was 40-55

seconds, the number of trials roughly corresponded to the number of minutes of training. With repeated presentations of the paired CS and US, a subset of fish developed a conditional response (CR) of fictive swimming to the low-contrast light (Figure 2.3A, 2.3B).

In mammalian studies of cerebellar associative learning, particularly eyelid conditioning, a 2-s CS is relatively long (e.g., García and Mauk, 1998). We therefore tested briefer CS-US intervals. Fish trained with a 2-s CS produced CRs on 32.0 ± 5.0% of trials (N=22). With a 1-s CS, performance was similar (29.1 ± 6.6%, N= 15). With a 0.5-s CS, fish produced CRs on about half as many trials as with a 2-s CS (17.8 ± 4.4%, N=15), but performance was statistically indistinguishable with all intervals ($p=0.39$, Figure 2.3B). All subsequent experiments used a 2-s CS, which gave the largest number of fish producing a high fraction of CRs and which had the additional benefit of providing the longest window to detect changes in Pkj and ventral root activity during the CS.

Because different fish varied considerably in the percentage of CRs they performed (Figure 2.3B), for analyses of response properties and of manipulations of learning, fish were separated into “learners” which performed CRs on >20% of trials in a 70-trial experiment (N=10/22 fish; 45%), and “non-learners” (N=12/22; 55%), which did not. While non-learners performed CRs on only 4 ± 1% of trials, learners generated CRs on 44 ± 2% of trials ($p<0.001$). In addition, learners performed consecutive CRs (i.e., they “acquired” CRs) after 27.5 ± 5 trials and reached a plateau of 59 ± 5% CRs after 40 trials (Figure 2.3C).

The CRs that emerged over training likely reflected associative learning rather than sensitization of visually evoked swimming, since unpaired presentations of the CS and US (pseudoconditioning) did not lead to the emergence of CRs (Figure 2.3C; N=10 fish, $p<0.001$). To test whether CRs extinguished, seven additional fish received up to 30 paired presentations of the CS and US. Six fish achieved a criterion of 3-5 consecutive CRs in 16 ± 3 trials. Subsequent presentations of the CS alone extinguished CRs in all six fish after 5 ± 1 trials, providing further evidence that the swimming episodes during the visual stimulus after training were indeed associatively learned CRs.

To test whether the behavior reflected cerebellar learning, we ablated the cerebellum before training (N=10). Without an intact cerebellum, fish still displayed fictive swimming both in response to the tactile stimulus and to high-contrast light (Figure 2.3D), indicating that the loss of the cerebellum did not disrupt sensory or motor pathways required for URs, nor did it abolish the ability to generate motor output to drive swimming. The fish did not acquire CRs, however (Figure 2.3C; $p<0.001$), confirming that the cerebellum is required for this form of learning. In intact fish, the properties of CRs changed over repeated trials, with respect to the latency to the initiation of swimming, the number of motor "bursts" within swimming episodes, and the frequency of these bursts. The initial CR occurred in the middle of the CS and was relatively brief and slow (latency, 1.1 ± 0.19 s; bursts/episode, 7.2 ± 1.6; burst frequency, 23 ± 1.4 Hz). Across subsequent trials, the changes in swimming properties reached a plateau by approximately the fifth CR trial; the latency decreased ($p<0.001$); the number of bursts increased

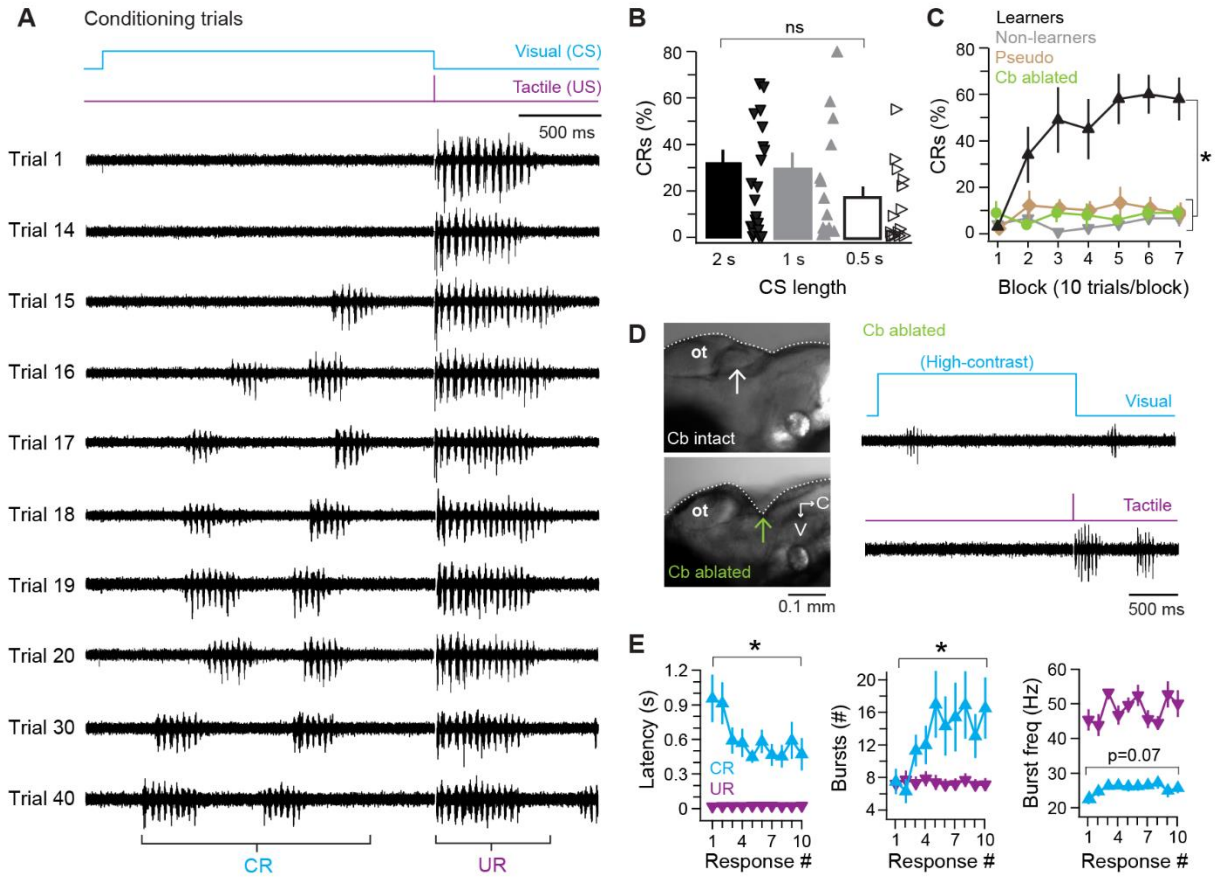

Figure 2.3. Cerebellar associative learning. **(A)** Sample ventral root recordings during training, illustrating the emergence and persistence of conditional responses (CRs) over time, as well as unconditional responses (UR). Trial numbers as indicated. Blue step, conditional stimulus (CS); purple step, unconditional stimulus (US). **(B)** Percentage of trials with a CR over all 70 trials. Bars are means; markers are data from individual fish; ns, not significant. $F_{(2,49)}$=0.97. **(C)** Percentage of trials with a CR per 10-trial block for learner and non-learner groups from fish in (B) trained with 2-s CS. $F_{(6,18)}$=4.92. (**D**) Left side view of exposed zebrafish brain before (top) and after (bottom) ablation of the cerebellum (arrow). Right, sample ventral root recordings of swimming evoked by a high-contrast visual stimulus (top) or tactile stimulus (bottom) after cerebellar ablation. **(E)** Changes in CR properties from first 10 CR trials in learner fish. UR data plotted for comparison. Left, swimming latency (relative to CS or US onset), CR: $F_{(9,81)}$=3.80, UR: $F_{(3.98,81)}$=0.78, *p=0.5*. Middle, number of bursts per swim response, CR: $F_{(9,81)}$=2.8, UR: $F_{(9,81)}$=1.60, *p=0.13*. Right, frequency of bursts, CR: $F_{(9,81)}$=2.84, UR: $F_{(3.47,81)}$=1.82, *p=0.16*.

(*p=0.006*); and swimming frequency increased slightly (*p=0.07*; Figure 2.3E; UR data overlaid for comparison). The observation that multiple parameters of learned swimming change during acquisition of the CR suggests that cerebellar circuits influence premotor regions that not only control the initiation of swimming but also its patterning (e.g., duration and frequency). In addition, the gradual approach of CR parameters to plateau values indicates that this form of learning is not all-or-none, but stabilizes over time.

2.3.5 Purkinje cell activity during learning

To test whether and how Pkj firing was modified during learning, we recorded from Pkjs during training in 31 fish. In these fish, CRs were acquired in 12.4 ± 1.6 trials, and experiments lasted 20.7 ± 1.8 trials. The activity of all Pkjs changed over training, but the responses were heterogeneous across the population. Inspection of climbing fiber and parallel fiber responses that developed over the course of training suggested that Pkjs might be distinguished according to their patterns of complex spiking *after* learning had taken place. Specifically, they could be categorized as firing 0, 1, or >1 complex spike in association with each CR. It is worth emphasizing, however, that alternate or additional classification schemes are not ruled out by this approach. We considered the possibility of classifying Pkjs on the basis of parallel fiber drive (pfEPSP-driven spiking), but the data did not fall into self-evident categories, and most criteria seemed arbitrary. We therefore proceeded with the preliminary classification of Pkj responses based on complex spikes fired during the CR, which placed every cell unequivocally into one of three groups (“classes”), and tested its validity by further analysis. Figure 2.4A-C illustrates

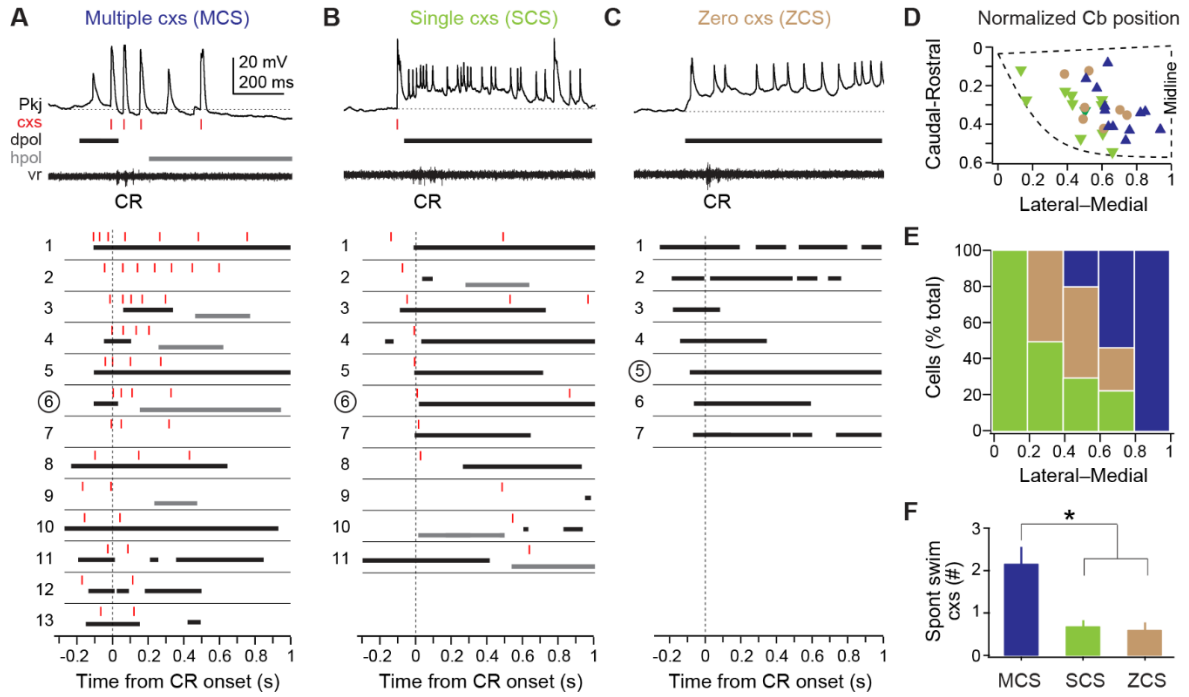

Figure 2.4. Three classes of Purkinje cell activity during learned swimming. **(A)** Sample recording from a multiple complex spike (MCS) cell, top, during the conditional response (CR) late in training. Horizontal dotted line, -55 mV. Schematized responses from MCS cells, below, aligned to the CR onset (vertical dotted line). For (A), (B), and (C): red ticks, complex spikes; black bars, pfEPSP-initiated depolarizations (dpol); grey bars, hyperpolarizations (hpol). MCS cells are ordered by the number of complex spikes within the CR. The number corresponding to the sample recording is circled. **(B)** As in (A) but for single complex spike (SCS) cells. Horizontal dotted line, -59 mV. SCS cell schematized responses are ordered by the latency of CR-related complex spikes. **(C)** As in (A) but for zero complex spike (ZCS) cells. Horizontal dotted line, -56 mV. ZCS cell schematized responses are ordered by the latency of CR-related pfEPSPs **(D)** Topographical distribution of MCS, SCS, and ZCS cells in the cerebellum. The position of the rostrolateral, rostromedial, and caudomedial corners are plotted (dashed line) to approximate the edges of the hemisphere, and relative positions of cells were calculated accordingly. **(E)** Ratios of each class of Purkinje cells along the mediolateral cerebellar axis. **(F)** Number of complex spikes in each class of Purkinje cells during episodes of spontaneous swimming. $F_{(2,22)}=7.78$.

sample traces of Pkj responses, followed by schematics illustrating the responses of every cell in each group, from trials after fish produced at least 2 consecutive CRs. The first group, multiple complex spike cells (MCS, N=13/31), produced two or more complex spikes during the CR (Figure 2.4A). In these cells, complex spikes were evident on every trial that included a CR. pfEPSPs with simple spikes and/or hyperpolarization were present, but variable. The second group, single complex spike cells (SCS, N=11/31), generated one complex spike during the CR on most trials (Figure 2.4B). This complex spike tended to be temporally associated with the swim episode, and could also be accompanied by pfEPSPs with simple spikes or by hyperpolarization. The third group, zero complex spike cells (ZCS, N=7/31), produced no complex spikes during the CR on all CR trials, instead displaying summating parallel fiber pfEPSPs and simple spikes (Figure 2.4C). All ZCS cells did, however, fire complex spikes to the US (on 35 ± 10% of trials), so they were indeed Pkjs innervated by climbing fibers with task-related activity. By comparison, all MCS cells also produced complex spikes to the US before training (on 67 ± 7% of trials), while 9 of 11 SCS cells produced complex spikes to the US before training (on 46 ± 7% of trials).

We then tested whether this categorization provided a reasonable classification of distinct groups of Pkjs for this associative learning task. Plotting the location of cells coded by group revealed that these neurons were topographically ordered along the mediolateral axis of the cerebellar hemisphere. MCS cells predominated most medially and were absent from the most lateral zone, SCS cells predominated most laterally and were absent from the most medial zone, and ZCS cells lay only between these extremes (Figure 2.4D, 2.4E). Next, we examined the activity of

these cells during spontaneous swimming, before learning had occurred. This analysis showed that the probability and number of complex spikes that occurred during spontaneous swimming was partially predictive of the classification of Pkjs after learning; specifically, of the 10 cells that fired at least one complex spike on every episode, 8 became MCS cells, resulting in a larger mean number of complex spikes during spontaneous swimming for this group (Figure 2.4F; $p<0.02$). Because all these analyses taken together provided reasonable anatomical and physiological support for the initial classification scheme, we next analyzed each group separately for changes in Pkj activity over the course of training.

2.3.6 Multiple complex spike cells

For MCS cells, we examined complex spikes during (1) spontaneous swimming, (2) UR swimming, and (3) the CS over repeated trials until CR swimming emerged (Figure 2.5A, 2.5B). MCS cells produced more complex spikes during CRs than during either spontaneous swimming or URs ($p<0.02$; Figure 2.5C, *top*). Also, the initial complex spike associated with each event approximately coincided with spontaneous swimming onset and consistently lagged the UR, but *preceded* the CR ($p<0.02$; Figure 2.5C, *bottom*, 2.5D). In addition to firing complex spikes, most MCS cells (N=9/13) showed pfEPSPs and simple spikes during CRs, while the remainder produced hyperpolarizations (N=4/13; Figure 2.5B).

In MCS cells, the quantity and timing of complex spikes throughout the visual stimulus (i.e., not only during the CR) was plastic over successive trials (Figure 2.5B). Over the course of training, the number of complex spikes increased in MCS cells ($p<0.001$). Most of these events occurred

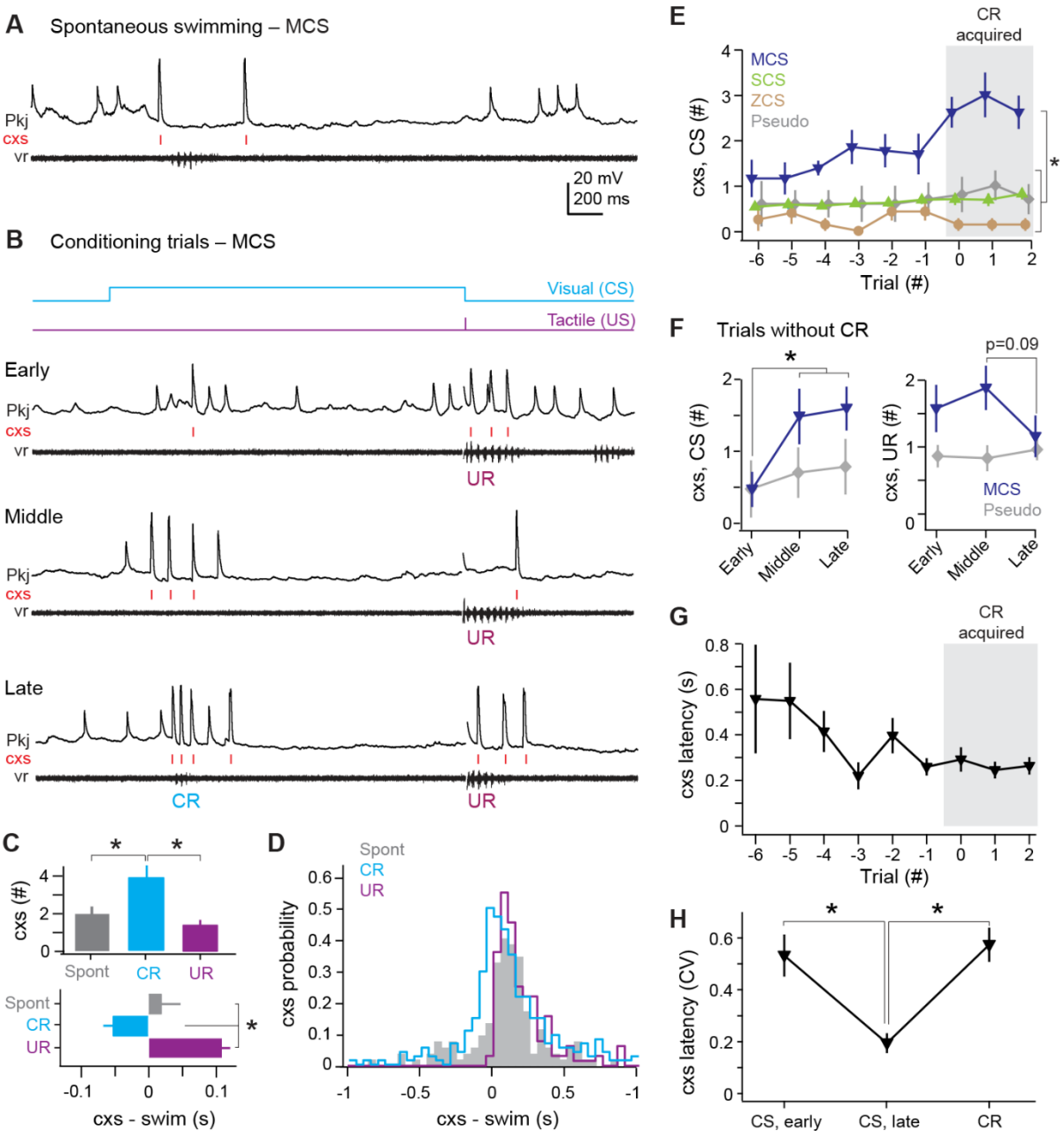

Figure 2.5. MCS Purkinje cell responses over the course of cerebellar learning. **(A)** Sample recording from a multiple complex spike (MCS) cell during spontaneous swimming. **(B)** Sample recording from the same MCS cell in (A), at the beginning of training (early), just before acquisition of the conditional response (CR; middle), and after CR acquisition (late). **(C)** Top, number of complex spikes during three forms of swimming: spontaneous, the CR, and the unconditional response (UR). $F_{(2,35)}$=9.20. Bottom, mean latency of the first complex spike in all cells. $F_{(2,35)}$=23.69. **(D)** Distribution of the latency of all complex spikes during swimming in all MCS cells (bin width = 50 ms). Legend continued on next page.

Figure 2.5 continued. (E) The number of complex spikes during the first 500 ms of the conditional stimulus (CS). MCS, SCS (single complex spike), and ZCS (zero complex spike) cells, and cells from pseudoconditioned fish are shown for comparison. $F_{(24,248)}$=1.95. For all similar plots, trial 0 is the first of consecutive trials with CRs for trained fish, or the tenth trial for pseudoconditioned fish (i.e., the median acquisition trial for trained fish). **(F)** The number of complex spikes during three trials *without* a CR for early, mid, and late training, for the first 500 ms of the CS (left; $F_{(1.76,32)}$=6.47) and 500 ms after the US (right). Cells from pseudoconditioned fish are shown for comparison. **(G)** Mean complex spike latency relative to CS onset for MCS cells. $F_{(8,40)}$=2.01. **(H)** CV of complex spike timing relative to CS onset early in training, late in training, and relative to the CR onset for MCS cells. The CV was calculated across trials for each cell, and the mean CV for all cells is plotted. CS points include trials regardless of whether a CR was produced. CR points represent the latency of the first complex spike.

in the first 500 ms of the CS, and their number increased gradually over training in MCS cells ($p<0.03$). No such change occurred in SCS cells, ZCS cells, or cells from pseudoconditioned fish (Figure 2.5E).

To investigate whether the learning-associated complex spikes in MCS cells were related to the motor command for the CR or the sensory input of the CS, we took advantage of the trial-to-trial variability in performance and analyzed *only* those trials that lacked CRs. The trials were grouped into *early* (three trials at the beginning of training), *middle* (three trials just before expression of consecutive CRs), and *late* (three trials just after expression of consecutive CRs).

Notably, even when learned swimming responses were absent, MCS cells fired more complex spikes during the first 500 ms of the CS on middle and late trials than during early trials ($p<0.04$; Figure 2.5F, *left*). In contrast, the number of complex spikes fired during URs tended to stay constant or decrease in MCS cells ($p=0.09$, *middle vs*. *late*; Figure 2.5F, *right*).

Examining the temporal relationship between the CS and complex spikes further indicated that complex spikes were generated in response to sensory input. Trial-by-trial analysis revealed that the latency of the first complex spike tended to decrease over training (*p=0.07*; Figure 2.5G) and became more precisely timed to the CS onset (Figure 2.5H; CV, *early:* 0.54 ± 0.08; CV, *late:* 0.19 ± 0.04, *p<0.001*). The complex spike in late trials was better timed to the CS than to the CR (CV, *CR:* 0.57 ± 0.06; *p<0.002*). These results suggest that, during learning, climbing fibers that are responsive to the sensory CS undergo changes, which preferentially affect MCS Pkjs.

2.3.7 Single complex spike cells

All 11 SCS showed changes in activity associated with spontaneous swimming, URs, and CRs (Figure 2.6A, 2.6B). Eight SCS cells responded with increases in simple and complex spikes, one cell hyperpolarized, and two cells showed both excitatory and inhibitory responses. Complex spikes during spontaneous swimming and URs followed swimming onset with lags of 96.3 ± 42 ms and 98.5 ± 33 ms (Figure 2.6C). In contrast, complex spikes occurred either just before CR onset (latency = -74 ± 17 ms; N=40/53 CRs) or after CRs ended (223 ± 28 ms, N=13/53 CRs), suggesting an association with the learned motor response (Figure 2.6B, 2.6C). A number of observations appear consistent with this idea. First, in SCS cells, unlike MCS cells, the complex spike latency was more precisely timed to either CR onset (CV=0.49 ± 0.08) or offset (CV=0.35 ± 0.13) than to the CS (CV=0.71 ± 0.08; *p=0.012, paired t-test;* Figure 2.6D). Also, the probability of a complex spike was relatively high near CR onset, while the probability of complex spikes occurring within 300 ms of the end of the CR transiently increased on the third and fourth CR trials (Figure 2.6E). Additionally, a disproportionate number of SCS cells did not

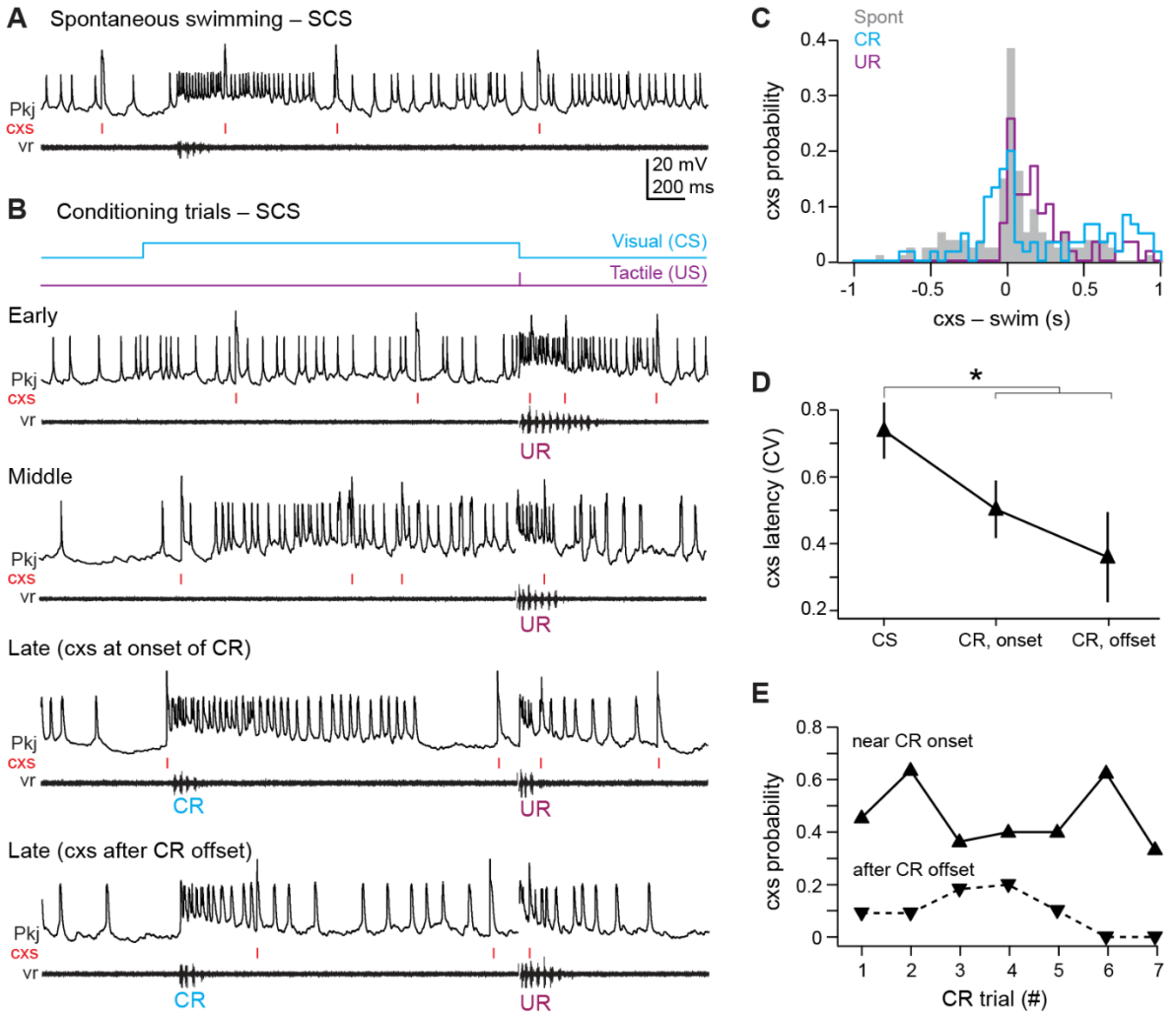

Figure 2.6. SCS Purkinje cell responses over the course of cerebellar learning. **(A)** Sample recording from a single complex spike (SCS) cell during spontaneous swimming. **(B)** Sample recording from the same SCS cell in (A) at the beginning of training (early), just before acquisition of the conditional response (CR; middle), and on two trials after CR acquisition with complex spike activity either near CR onset or after CR offset within 300 ms of the CR. **(C)** The distribution of the latency of all complex spikes in SCS cells relative to spontaneous, CR, and unconditional response (UR) swimming onset. **(D)** The coefficient of variation (CV) of complex spike (cxs) latency relative to the conditional stimulus (CS) onset, the CR onset, and the CR offset for all SCS cells. The CV for each cell was calculated across trials, and the mean CV for all cells is plotted.

respond to the visual stimulus before training (46% of SCS cells *vs.* 23% of all 49 cells tested, including those from pseudoconditioned and untrained fish), and the number of CS-related complex spikes in SCS cells did not change consistently over training (Figure 2.5E). Together, these data support the idea that climbing fiber input to SCS cells is more directly related to the motor command for the CR than the sensory input of the CS.

2.3.8 Zero complex spiking cells

All 7 ZCS cells showed many pfEPSPs, which frequently elicited long-lasting depolarizations with simple spikes. These events were associated with spontaneous swimming, the CS on non-CR trials, and CRs (Figure 2.7A, 2.7B). Over the course of training, the total number of pfEPSPs and cells from pseudoconditioned fish (Figure 2.7C). The onset of long-lasting (>200 ms) depolarizations nearly coincided with spontaneous swimming (latency, 2 ± 36 ms) and lagged tactile-evoked swimming (59 ± 19 ms). Long-lasting depolarizations, however, significantly preceded learned swimming (lag, -171 ± 15 ms, $p<0.001$ Figure 2.7B, 2.7D). Together, these observations suggest that the CS-associated parallel fiber drive to ZCS cells increases over training.

2.3.9 Suppressing Purkinje cell simple spikes

The three categories of Pkjs showed distinct responses, but together they provided evidence that both parallel fiber EPSP-driven simple spikes and climbing fiber-mediated complex spikes are systematically modified during associative learning. In addition, since some changes precede learning whereas other changes continue to develop after CRs emerged, different components of

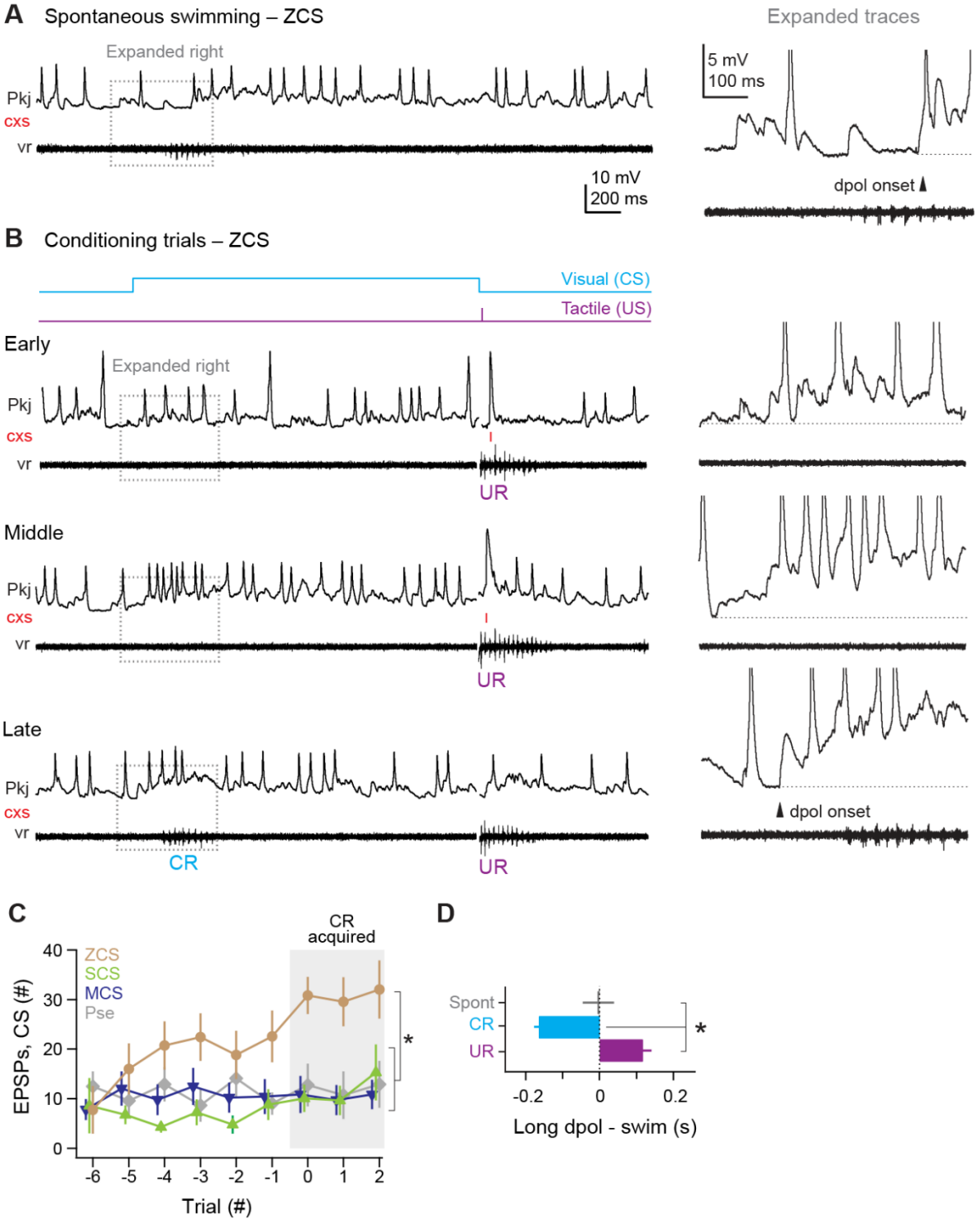
A
Spontaneous swimming – ZCS
Expanded right
Pkj
cxs
vr
10 mV
200 ms
Expanded traces
5 mV
100 ms
dpol onset
B
Conditioning trials – ZCS
Visual (CS)
Tactile (US)
Early
Expanded right
Pkj
cxs
vr
UR
Middle
Pkj
cxs
vr
UR
Late
Pkj
cxs
vr
CR
UR
dpol onset
C
CR
acquired
ZCS
SCS
MCS
Pse
EPSPs, CS (#)
40
30
20
10
0
-6
-5
-4
-3
-2
-1
0
1
2
Trial (#)
*
D
Spont
CR
UR
*
-0.2
0
0.2
Long dpol - swim (s)

Figure 2.7. ZCS Purkinje cell responses over the course of cerebellar learning. **(A)** Left, sample recording from a zero complex spike (ZCS) cell during spontaneous swimming. Right, magnification of boxed region at left. Arrow: onset of long-lasting depolarization. Dotted line, -51 mV. **(B)** Sample recording from the same ZCS cell in (A) at the beginning of training (early), just before acquisition of the conditional response (CR; middle), and after CR acquisition (late). Dotted lines, top to bottom, -51 mV, -54 mV, and -54 mV. **(C)** The number of parallel-fiber EPSPs (pfEPSPs) during the 2-s conditional stimulus (CS) for ZCS cells, as well as MCS, SCS cells and cells from pseudoconditioned fish. $F_{(11.16,198)}$=2.18. **(D)** Latency of pfEPSP-initiated long-lasting depolarization relative to the onset of spontaneous swimming, the CR, and the unconditional response (UR). $F_{(2,18)}$=22.33.

Pkj activity likely contribute differentially to acquisition (learning the association of paired stimuli during training), expression (generation of learned motor responses), and maintenance (retaining the learned association and continuing to produce learned movements). Although at present we have no reliable method to control the activity of only one group of Pkjs at a time, we reasoned that we could begin to dissect the roles of simple and complex spikes, and possibly infer roles of the cell classes, by optogenetically interfering with activity of all Pkjs.

To do so, we used a transgenic fish line in which Archaerhodopsin-3 ("Arch") was expressed only in Pkjs (Matsui et al., 2014a; see also Figure 2.1A). Arch-activating light, which was of higher intensity and different wavelength than the light used as a CS (see *Materials and Methods*), was directed onto the cerebellum through the microscope objective and constrained to the minimal diameter necessary to illuminate the cerebellum fully. Voltage-clamp recordings from Pkjs showed that Arch activation evoked an outward current of 18.6 ± 2.7 pA (N=5; Figure 2.8A, *top*) that reached a maximum within 5 ms. This current hyperpolarized current-clamped Pkjs by 27.1 ± 3.4 mV and greatly suppressed simple spikes, from 6.0 ± 1.8 spikes/s to 0.4 ± 0.3 spikes/s (*p=0.008*; Figure 2.8A *bottom,* 2.8B). Consistent with the large amplitude of climbing

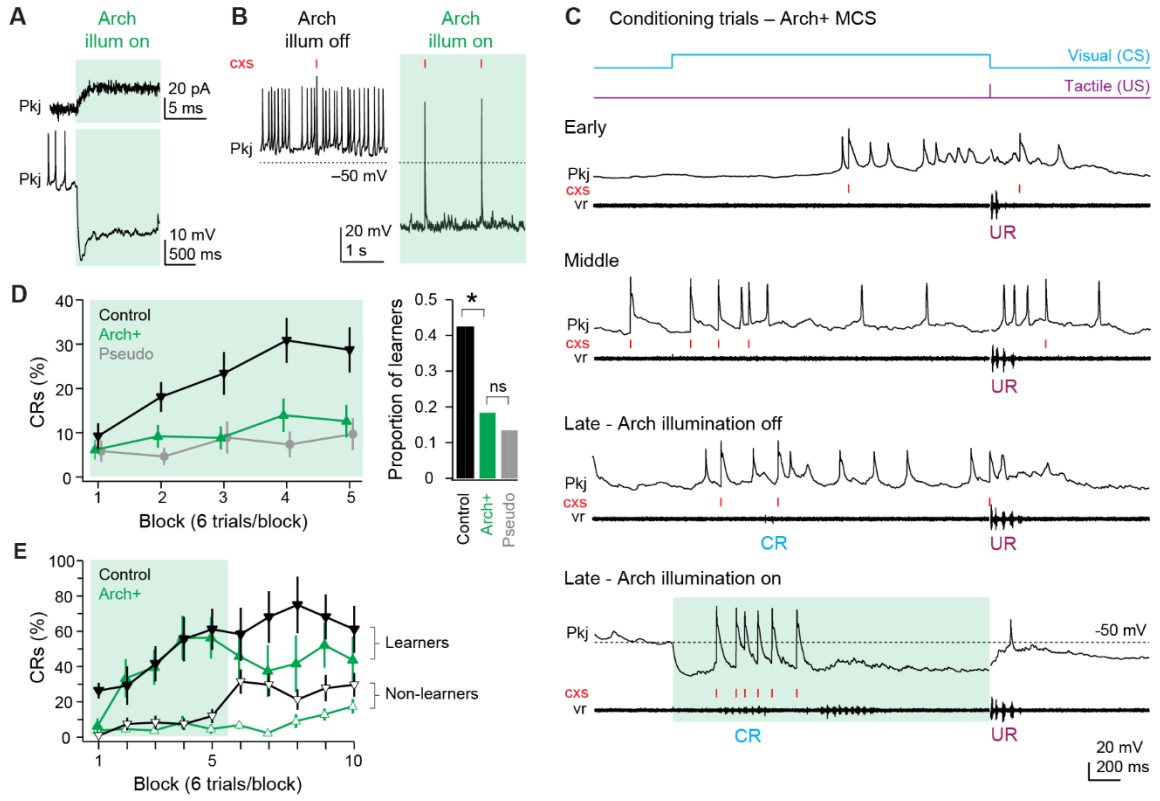

Figure 2.8. Effects of Arch-mediated simple spike suppression on acquisition of learned responses. **(A)** Sample voltage-clamp (top), holding potential = -60 mV, and current-clamp (bottom) recordings from an Arch^{+} Purkinje cell during Arch activation. Green shading in all panels in all figures indicates cerebellar illumination with Arch-activating light. **(B)** Current-clamp recording of an Arch^{+} Purkinje cell without (left) and with (right) activation of Arch. Two complex spikes (cxs) are evident during illumination. **(C)** Response of an Arch^{+} multiple complex spike (MCS) Purkinje cell at the beginning of training (early), just before acquisition of the conditional response (CR; middle), after CR acquisition without simple spike suppression (late - Arch illumination off) and after CR acquisition with simple spike suppression (late - Arch illumination on). **(D)** Left, CR percentage per 6-trial block of control, Arch^{+}, and pseudoconditioned fish that received Arch-activating cerebellar illumination during visual stimulation from the onset of training. $F_{(8,544)}$=2.14. Right, proportion of learner fish for each group. $X^2_{(1,\ N=96)}$=6.66. **(E)** CR percentage per 6-trial block for Arch^{+} (green) or control (black) fish classed as learners (closed symbols) or non-learners (open symbols) in the first 30 trials.

fiber EPSCs, however, complex spikes persisted during Arch activation (0.16 ± 0.02 spikes/s, Figure 2.8B). These rates were comparable to control (0.12 ± 0.04 spikes/s; $p=0.6$), suggesting that complex spikes were not indirectly suppressed via olivocerebellar loops (e.g., Medina et al. 2002).

To evaluate the effect of the Arch-dependent outward current during substantial excitatory drive, we recorded Pkj activity during episodes of learned swimming (N=2 MCS cells and 1 SCS cell). With Arch activation, simple spikes during swimming were largely suppressed, but summating EPSPs and complex spikes remained (Figure 2.8C). Importantly, this experiment also demonstrated that learned swimming could occur during Arch activation, indicating that the behavior did not rely solely on Pkj simple spiking (analyzed further below). We therefore concluded that Arch could reasonably be used to suppress Pkj simple spikes preferentially, without affecting complex spikes.

We therefore applied Arch-activating illumination at various points during training. In all experiments, Arch-activating light was applied *only* during the presentation of the CS, so that responses to the US and any other signals not overlapping with the CS could proceed unperturbed. Since these experiments required many trials, Pkj recordings were omitted to maximize the number of fish from which complete data sets could be obtained. Nevertheless, the previous experiments made it possible to infer the effects on different cell groups: ZCS cells, in which synaptically driven simple spikes occur throughout acquisition and expression, are expected to be most affected by such a manipulation, while the subset of MCS and SCS cells that increase their simple spiking during swimming would become affected after CRs emerge.

2.3.10 Simple spike suppression during acquisition. We first tested whether suppressing simple spikes affected the acquisition of CRs. Naïve Arch$^+$ (N=49) and control (N=47) fish were trained with paired presentations of the CS and US and pseudoconditioned fish received unpaired stimuli (N=43, of which 14 were Arch$^+$). Among control fish, conditioning with the additional Arch-activating illumination proceeded as it did with the CS light alone (Figure 2.8D, *left*). The CR percentage increased significantly, from 9.2 ± 2.9% to 28.7 ± 5.1% ($p<0.001$), and 20/47 fish (42.6%) reached the criterion of producing CRs on >20% of trials (Figure 2.8D, *right*). In contrast, in Arch$^+$ fish, the CR percentage went from 6.1 ± 2.2% only to 12.6 ± 3.7% (Figure 2.8D, *left*; $p=0.17$); this change was smaller than in control ($p=0.003$) and indistinguishable from pseudoconditioned fish ($p=0.7$). When compared to control fish, fewer than half as many Arch$^+$ fish could be classified as learners (N=9/49, 18.4%, $p=0.014$, Figure 2.8D, *right*).

This reduced CR probability may have resulted either because CRs were not acquired, owing to a disruption of plasticity, or because CRs could not be expressed, even with normal development of plasticity. To distinguish between these possibilities, we tested the effect of restoring simple spikes after training during Arch activation. For control and Arch$^+$ fish (N=30 per group), 30 trials of training with Arch activated were followed by 30 trials in which the Arch-activating light was presented but displaced from the cerebellum. We reasoned that if CRs were not acquired, then CR probability would remain depressed after restoration of simple spikes. If, however, CRs simply could not be expressed, then CR probability would increase immediately upon simple spike restoration. For this analysis, fish were classified as learners and non-learners.

We first compared the *non-learner* fish in the control (18/30) and Arch$^+$ (22/30) groups. By definition, both groups produced a low proportion of CRs at end of the first 30 trials (control, 12.0 ± 4.0%; Arch$^+$, 4.5 ± 2.7%; Figure 2.8E, *open symbols*). When the Arch-activating light was displaced to the front of the fish, however, control fish immediately produced CRs on 32 ± 7% of trials, possibly owing to an increase in the intensity of the visual cue; this result suggests that, in some control fish classed as non-learners, the association of the CS with the US may have indeed been learned but the low-contrast CS fell below detection threshold. In contrast to controls, however, non-learner Arch$^+$ fish performed CRs on only 6.8 ± 2.1% of trials immediately after displacement ($p<0.001$ *vs.* control), revealing a real failure to learn in the first 30 trials.

We next compared the control (N=12/30) and Arch$^+$ (N=8/30) *learner* fish. Although a smaller proportion of Arch$^+$ fish learned CRs, acquisition proceeded similarly between the two groups (Figure 2.8E, *filled symbols*). At the end of 30 trials with Arch activation, CR probability was indistinguishable (53 ± 12% for Arch$^+$, 58 ± 11% for control block 5; $p=0.8$). After displacement of the Arch-activating light, control fish continued to perform CRs at or above the level attained just before displacement (66 ± 6% for the last 30 trials). In contrast, with restoration of simple spikes, the CR probability in trained Arch$^+$ fish tended to decrease (Figure 2.8E, *filled symbols*) and did not improve through the rest of the session (42 ± 13% for the last 30 trials; $p=0.10$ *vs.* control). Thus, although some Arch$^+$ fish learned, the underlying cerebellar plasticity apparently adapted to the reduced level of simple spiking, such that restoring this activity generated a mild deficit in performance. Together, these results provide evidence that Pkj simple spikes participate

in the acquisition of learned responses. Specifically, reducing simple spiking alters cerebellar plasticity during learning and affects performance of this task.

2.3.11 Simple spike suppression following CR acquisition.

Next, we investigated whether simple spikes play a measurable role *after* learning has occurred normally. Because multiple parameters of learned swimming change after initial expression (Figure 2.3E), we reasoned that fish just beginning to produce CRs and fish producing CRs "reliably" (i.e., on several consecutive trials) may differ in their sensitivity to simple spike suppression. To test this idea, control and Arch$^+$ fish were trained with simple spikes unperturbed until fish reached a pre-set learning criterion of generating CRs on 1, 3, or 6 consecutive trials. Next, the Arch-activating light was applied to the cerebellum for 10 trials and the persistence of CRs was measured. Regardless of the learning criterion, the CR latency, duration, swimming frequency, and amplitude recorded from the ventral roots did not differ between control fish and Arch$^+$ fish with simple spikes suppressed (*unpaired t-tests, all p-values >0.25*), and Arch$^+$ fish with and without simple spikes suppressed (*paired t-tests, all p-values >0.30*).

In control fish, the CR probability after the first CR was stable across these 10 trials, averaging 58 ± 13% (N=20). In contrast, in the 1-CR Arch$^+$ group, which underwent simple spike suppression after a single CR (N=20), the probability of a CR fell to 41 ± 13% over the first 4 trials of Arch activation (*p=0.078 vs.* control of 63 ± 8%) before recovering to control levels

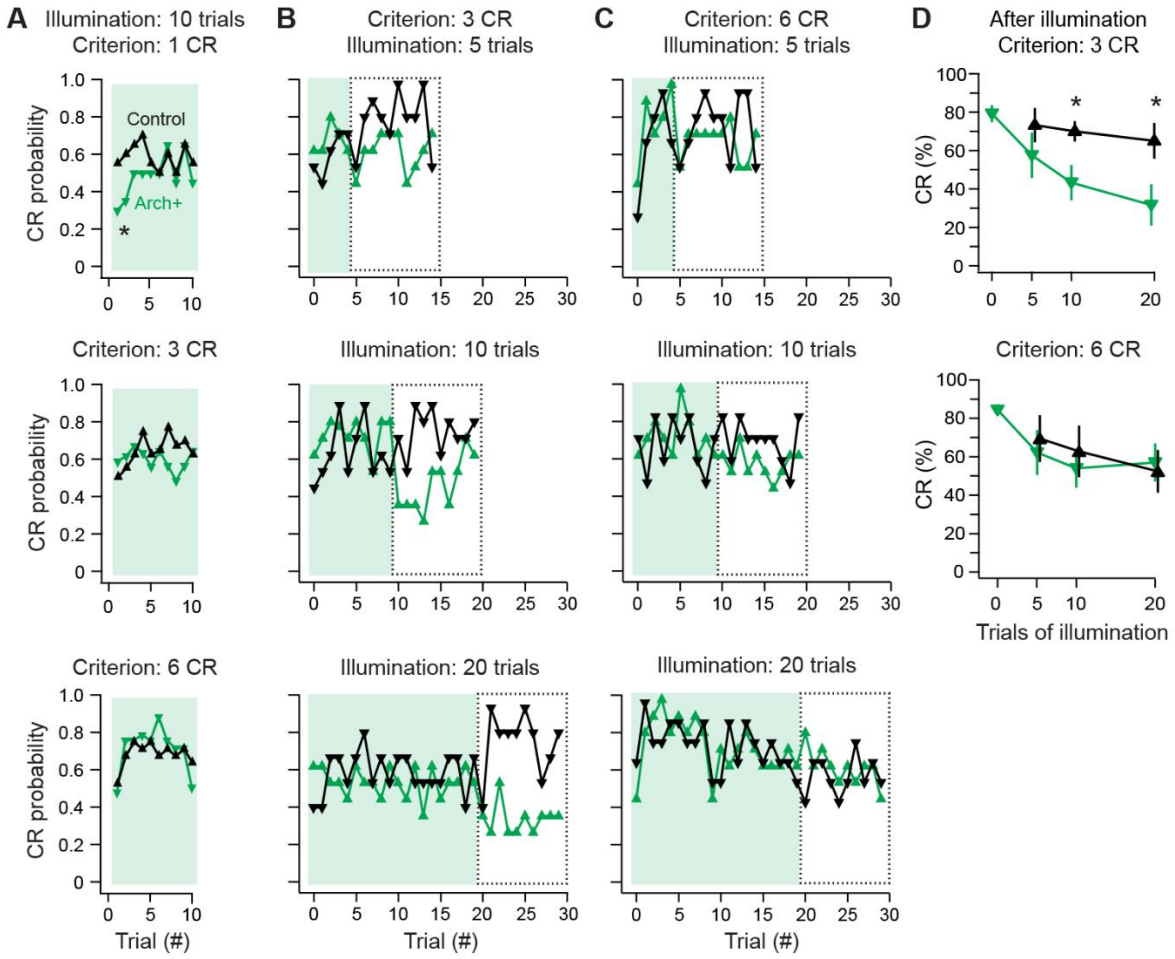

Figure 2.9. Effects of Arch-mediated simple spike suppression on expression and maintenance of learned responses. **(A)** Conditional response (CR) probability across fish during cerebellar Arch-activating illumination applied after fish reached a learning criterion of 1 (top), 3 (middle), or 6 (bottom) consecutive trials with a CR without simple spike suppression. **(B)** CR probability across fish during 5 (top), 10 (middle), or 20 (bottom) trials of Arch-activating illumination, followed by 10 trials without, for 3-CR fish. Dotted boxes, trials from which CR percentage is calculated in (D). **(C)** Same as (B) for 6-CR fish. **(D)** CR percentage calculated from trials after Arch-activating illumination for 3-CR (top) and 6-CR (bottom) fish (from dotted boxes in B and C). **(E)** The probability of a complex spike within 300 ms of the onset (solid lines) or within 300 ms after the offset (dashed lines) of the CR for all SCS cells.

(*p=0.8*; Figure 2.9A, *top*). The Arch$^+$ groups that underwent suppression after 3 or 6 consecutive CR trials, however, showed no deficits in the likelihood of CRs (N=36 in each group; Figure 2.9A, *middle and bottom*). In all cases, the mean CR probability across trials stayed near 60% (3-CR control, 60 ± 6%; 3-CR Arch$^+$, 61 ± 6%; 6-CR control, 65 ± 6%; 6-CR Arch$^+$, 70 ± 5%), consistent with the plateau of performance measured in initial behavioral experiments. Comparing the average response probabilities of the first five trials across all levels of training confirmed that simple spike suppression significantly impaired performance in the 1-CR Arch$^+$ group (*p=0.02*). Thus, only for nascent CRs do Pkj simple spikes contribute to expression.

A remaining question, however, is whether simple spikes continue to play any detectable role after CRs are acquired, i.e., in maintenance of the learned response. To explore this possibility, we tested whether a period of simple spike suppression in well-trained fish influenced performance after simple spike restoration. Fish were trained to a 3-CR or 6-CR level with simple spikes intact (N=12 in each group). Simple spikes were then suppressed during the CS for 5, 10, or 20 trials, after which they were restored for 10 more trials. In the 3-CR and 6-CR groups, learned swimming continued throughout the trials with the Arch-activating light (Figure 2.9B and 2.9C, *shaded trials*), with no difference in CR percentage between control and Arch$^+$ fish (all conditions $p > 0.3$) or between the first and second half of the Arch-activation trials (all conditions $p > 0.3$). After the Arch-activating light was displaced, the mean CR percentage also remained above 60% in control fish (Figure 2.9B, 2.9C, *unshaded trials*, 2.9D). In contrast, in Arch$^+$ fish subject to suppression trials, restoring simple spikes reduced the CR percentage in the 3-CR criterion group (Figure 2.9B, *unshaded trials*). This deficit was greater with longer periods

of reduced simple spiking. After 5, 10, or 20 suppression trials, the CR percentage fell from 58 ± 12% (*p=0.3 vs.* control), to 43 ± 9% (*p=0.02*) to 32 ± 10% (*p=0.03*; Figure 2.9D *top*).

Fish trained to the 6-CR criterion, however, showed no decrease in CR probability after simple spiking was restored, regardless of the number of trials with Arch activation (Figure 2.9C, *unshaded trials*, 2.9D *bottom*; *p>0.5,* all comparisons). These results further demonstrate that different degrees of learning, based on the reliability of CRs, have different sensitivities to simple spiking. Even fish performing with moderate reliability continue to adapt to a reduction in the level of simple spike suppression, such that when simple spiking is elevated, performance is degraded. Only in fish performing with high reliability does learned swimming persist independently of Pkj simple spiking.

Together, these results suggest that the cerebellar plasticity required for CRs relies on Pkj simple spikes during the CS, but this dependence does not segregate into straightforward categories. First, acquisition is facilitated by normal simple spiking; with simple spikes suppressed, most fish fail to learn. Those few that do acquire CRs remain particularly sensitive to changes in simple spikes. Second, expression is facilitated by normal simple spiking only for nascent CRs; once CRs are reliably produced, normal simple spikes are no longer necessary for expression. Third, maintenance of CRs is largely independent of continued simple spiking during performance; however, only robustly learned responses (6-CR criterion) are maintained consistently throughout alterations in simple spike activity, whereas moderately learned responses (3-CR criterion) remain sensitive to further changes in simple spiking.

2.4 Discussion

Here, we have made intracellular recordings from Pkjs during pre-training, acquisition, expression, and maintenance of cerebellum-dependent learned motor responses in larval zebrafish. The results indicate distinct groups of Pkjs that differ in both their location in the cerebellum and their synaptically driven electrophysiological responses through an associative learning task. During training, complex spikes from climbing fiber activity become associated with sensory input from the CS in MCS cells, but with the motor command related to the CR in SCS cells. In ZCS cells, parallel fiber input increases during learning, but complex spikes do not change. Thus, different climbing fiber afferents convey distinct information to separate populations of Pkjs that all participate in this form of cerebellar learning. The results also demonstrate that Pkj simple spikes play changing roles during different phases of this learning task. They strongly influence the acquisition of learned responses, transiently influence the expression of these responses, and become unnecessary for maintenance of well-learned behaviors.

2.4.1 Pre-training responses of Purkinje cells

Consistent with the fact that 6-8 dpf larvae are free swimming and must encode and process sensory and motor information to survive, the Pkj recordings made here from untrained fish illustrate that multimodal sensory signals are present relatively early in zebrafish development. Individual Pkjs fired simple and/or complex spikes to both light and tactile stimuli, as well as to episodes of fictive swimming, consistent with previous studies of larval zebrafish (Hsieh et al.

2014; Sengupta and Thirumalai, 2015; Scalise et al., 2016). The sources of multimodal cerebellar inputs are not yet identified in zebrafish; however, this range of responses is consistent with data from mammalian granule cells, which converge on Pkjs and respond to stimuli of different sensory modalities (Azizi and Woodward, 1990; Chabrol et al., 2015; Ishikawa et al., 2015). Likewise, mammalian inferior olivary neurons respond to sensory stimuli of different modalities and/or to movements (Bauswein et al., 1983; Gellman et al., 1983; Kim et al., 1987; Winkelman et al. 2014; Ohmae and Medina, 2015). Similar pathways likely exist in zebrafish, given the conservation of olivo-cerebellar circuitry across vertebrates (Hodos and Butler, 1997; Takeuchi et al., 2017).

2.4.2 Topographical organization of the zebrafish cerebellum.

Here, we categorized zebrafish Pkjs based on the number of complex spikes fired during learned swimming. This approach distinguishes the present study from past characterizations of Pkjs in naïve zebrafish (Hsieh et al. 2014; Sengupta and Thirumalai, 2015; Scalise et al., 2016). The classification reveals a relationship between learned activity and Pkj position along the mediolateral axis of the cerebellar hemisphere. The topographic organization of Pkjs with different learned complex spike responses suggests that the larval zebrafish cerebellum is likely to be organized into olivocerebellar modules, as in other vertebrates (Ruigrok 2011; Cerminara and Apps 2011). In the mammalian cerebellum, separate regions of the inferior olive innervate zones of Pkjs that alternate in their expression of zebrin II (aldolase C). In addition, Pkjs with

distinct intrinsic electrophysiological properties can often be distinguished by the presence or absence of zebrin II (Brochu et al., 1990; Wadiche and Jahr, 2005; Kim et al. 2012; Zhou et al., 2014; Cerminara et al., 2015). In zebrafish, however, zebrin II and other candidate biomarkers are expressed throughout the Pkj population, suggesting that other molecular signals are involved in setting up olivocerebellar modules in zebrafish (Meek et al., 1992; Bae et al., 2003; Takeuchi et al., 2017).

The present data also add to previous findings of organized anatomical and functional heterogeneity in the larval zebrafish cerebellum. Zebrafish Pkjs have short axons (~8 µm; Matsui et al. 2014) that project locally to ENs, which are analogous to neurons of the mammalian cerebellar nuclei. Thus, the medially located MCS cells described here are likely to target primarily medial ENs, while SCS cells likely contact more lateral ENs. Axons of medial and lateral ENs form zebrafish cerebellar output pathways and project to different parts of the brain. Among the targets of the medial or rostromedial cerebellum are the thalamus, rostral optic tectum, and red nucleus, while the lateral cerebellum projects to the caudal tectal neuropil; additional gradients are evident in the rostro-caudal axis (Heap et al., 2013; Matsui et al., 2014a). Pkjs in the medial and lateral cerebellum also contribute differentially to tail and eye movements evoked by optic flow (Matsui et al., 2014a). Thus, the mediolateral gradient of MCS, ZCS, and SCS cells may indicate that different learned signals are sent to distinct brain regions, including those responsible for the initiation, maintenance, speed, and termination of swimming (Brocard and Dubuc, 2003; Lambert et al., 2004; Soffe et al., 2009; Arrenberg et al., 2009; Smetana et al.,

2010; Kimura et al., 2013; Severi et al., 2014; Wang and McLean, 2014; Naumann et al., 2016; Juvin et al., 2016).

2.4.3 Relating naïve and learned responses of Purkinje cells

Given the variable nature of Pkj responses during learning, a key question is whether pre-training synaptic responses can predict Pkj activity that emerges during learning. In mammals, the absence of complex spikes to the US is predicted to limit long-term depression and possibly favor potentiation of parallel fiber responses (Jörntell and Hansel, 2006). Such plasticity rules appear consistent with those seen here in ZCS cells, which had the lowest likelihood of firing complex spikes to the US and developed greater parallel fiber responses during learning. Conversely, mammalian Pkjs that reliably generate complex spikes to a US are more likely to develop complex spike responses to a conditional stimulus (Ohmae and Medina, 2015). A similar result was seen here for MCS cells, which had the highest probability of firing complex spikes to the US. These cells also tended to produce multiple complex spikes during spontaneous swimming, suggesting that MCS cell-innervating climbing fibers are readily activated during motor commands. One possibility is that the responses of MCS cells resulted from innervation by multiple climbing fibers that had not yet been pruned over development (Hsieh et al., 2014), although the number of afferents could not be distinguished by the present experiments. Pkjs in each hemisphere differentiate in clusters, however, with a medial cluster shortly preceding a lateral cluster (Hamling et al., 2015), suggesting that the MCS cells described here may have

been born earlier than ZCS and SCS cells, and might have had more rather than less time for pruning. More importantly, the pattern of changes in MCS cells, in which complex spikes became associated with the sensory rather than the motor response, is qualitatively different from SCS cells. The response of MCS cells therefore seems more likely to arise from distinct innervation patterns than solely from the degree of climbing fiber pruning.

2.4.4 Complex spike plasticity in Purkinje cells

Much work has supported the idea that complex spikes function as instructive signals in learning, altering the production of simple spikes, often through heterosynaptic depression of parallel fiber inputs (Gilbert and Thach, 1977, Mauk et al., 1986; Raymond et al., 1996; Medina et al., 2002; Guo et al., 2014; Yang and Lisberger, 2013; Ito et al., 2014). In addition, complex spiking can itself be plastic. For instance, a learning-related reduction in complex spikes to the US has also been seen in rabbits and ferrets (Sears and Steinmetz, 1991; Hesslow and Ivarsson, 1996). Similarly, the MCS cells described here decreased their production of complex spikes during URs. A likely mechanism for such changes in mammals is an increased inhibition of inferior olivary neurons by cerebellar nucleo-olivary cells (Medina et al., 2002). Although homologous inhibitory output neurons in zebrafish have not yet been identified, the present data are suggestive of a similar pathway.

In contrast to their reduced response to the US, MCS cells increased their complex spiking to the CS. Similarly, in Pkjs of the eyeblink microzone in mice, complex spikes during the CS become

more likely after training (Ohmae and Medina, 2015); conversely, in C3 Pkjs in decerebrate ferrets, complex spikes during the CS decrease over the course of training (Rasmussen et al., 2014). Monitoring the responses of MCS cells throughout training revealed that the increase in complex spiking developed even before learned swimming episodes occurred. Possible mechanisms for this plasticity within the afferent climbing fibers include potentiation of excitatory input that relays the CS to the inferior olive, modulation of intrinsic electrical properties of olivary neurons, and/or decreased CS-evoked inhibition from nucleo-olivary-like neurons. Indeed, recent studies provide evidence for modulation and plasticity of responses in the inferior olive (Mathy et al., 2009; 2014; Lefler et al. 2014).

2.4.5 A changing role for simple spikes during cerebellar learning

Mammalian Pkjs have high intrinsic simple spike rates (~50 spikes/s, Thach 1968; Häusser and Clark 1997), which can decrease during motor learning (Gilbert and Thach, 1977; Hirata and Highstein 2001; Blazquez et al. 2003; Jirenhed et al., 2007; Halverson et al. 2015); lower simple spike rates presumably reduce the net inhibition of cerebellar output neurons and permit learned movements to occur. In zebrafish Pkjs, simple spike rates are markedly lower than in mammals (~6 Hz in the present data, ~10 Hz in Scalise, et al. 2016). Nevertheless, the experiments with Arch-activation illustrate a role for simple spiking that changes during training, depending on how reliably fish perform learned movements. In naïve fish, simple spike suppression impairs learning. In fish that have just begun expressing learned movements, suppression produces an

incomplete deficit in CR expression. In fish that perform learned swimming with moderate reliability, suppression does not affect CR expression, but restoring simple spikes impairs performance. Only in fish that perform the CR with high reliability do learned responses continue without simple spikes and remain unaffected by simple spike restoration.

These results support the conclusion that, in larval zebrafish, simple spikes influence learning before and immediately after expression of the CR, but that plasticity supporting the execution of learned movements must also take place elsewhere. For example, Pkj simple spikes could promote potentiation of excitatory synapses onto cerebellar output neurons. The idea that Pkj-mediated inhibition instructs plasticity at target neurons that drive movements has been supported by modeling and experiments in mammals, both for the vestibulo-ocular reflex and for delay eyelid conditioning (Miles and Lisberger, 1981; Medina and Mauk, 1999; Nguyen-Vu et al., 2013; Yang and Lisberger, 2014). Synaptic plasticity under the control of Pkj-mediated inhibition has also been demonstrated *in vitro* (Aizenman et al., 1998; Pugh and Raman, 2006; McElvain et al., 2007; Pugh and Raman, 2008; Person and Raman, 2010). In fact, plasticity within the zebrafish cerebellar circuit apparently adapted to a reduced level of simple spiking, since restoring simple spikes after suppression trials could decrease the likelihood of previously acquired CRs; in the simplest interpretation, the re-introduction of simple spiking effectively inhibited ENs that helped drive the first CRs. This scenario could result from submaximal potentiation of excitation of cerebellar output neurons, so that restoration of Pkj-mediated inhibition brought their responses to the CS below threshold. Thus, in the associative learning task explored here, learning is not all-or-none. Instead, plasticity in the cerebellar circuit

continues after learned swimming emerges, and only appears to stabilize after fish reliably perform learned movements.

2.5 Materials and Methods

2.5.1 Zebrafish.

All procedures conformed to NIH guidelines and were approved by the Northwestern University Institutional Animal Care and Use Committee. Wildtype zebrafish (*Danio rerio*) were obtained from an in-house facility (Aquatic Habitats, Beverly, MA). Tg(Arch-tagRFP-T:car8:GCamp5) fish ("Arch^{+}" fish), were kindly provided by Dr. Reinhard Köster (Technical University Braunschweig, Germany; Matsui et al., 2014a) and were screened for RFP fluorescence at 5 days post-fertilization (dpf). Zebrafish were housed in system water (28.5°C, pH=7.3, conductivity = 550 μS) and maintained on a 14-hour light:10-hour dark cycle. Experiments were done during the light phase (between 10 am and 7 pm), at room temperature (~22°C), on larval fish (6-8 dpf, before sexual differentiation). The time of day of the experiment did not differ between learner and non-learner fish (*p=0.32, unpaired t-test*), so data from all times of day were pooled. MCS, SCS and ZCS cells were recorded from fish of comparable ages (6.5 ± 0.2, 6.4 ± 0.2, and 6.5 ± 0.2 dpf, respectively, $F_{(2,30)}$=0.03, *p=0.98*).

2.5.2 Electrophysiological recordings.

Recordings were performed based on those described previously (Drapeau et al., 1999; Masino and Fetcho, 2005; Wang and McLean, 2014). Each fish was immobilized by 3-minute immersion in α-bungarotoxin (1 mg/ml, Tocris, Bristol, United Kingdom) in system water followed by 5 minutes in "extracellular solution" containing (mM): 134 NaCl, 2.9 KCl, 2 $MgCl_2$, 10 HEPES,

10 glucose, and 2.1 $CaCl_2$, buffered to pH 7.8 with NaOH, with final osmolarity 290 mOsm. The immobilized fish was transferred to a Sylgard-lined plastic recording chamber containing extracellular solution, with 0.01% MS-222 anesthetic added for experiments involving dissection for neuronal recordings or ablation. Blood circulation was monitored throughout the dissection. The fish was secured to the Sylgard surface with pins so the dorsal side of the head and the left side of the tail faced up. A midline incision was made and the skin was pinned to expose the brain. For recordings from peripheral motor nerves (ventral roots) along the tail, the skin was removed on the left side, from the rostral edge of the swim bladder to 3-5 segments rostral to the tail tip. For ablation experiments, the cerebellum was scored manually with a tungsten needle and aspirated through a 50-60 μm diameter micropipette positioned with a micromanipulator (MP-385, Sutter, Novato, California). Fish with damage to the tectum or brainstem or with impaired circulation were not used for experiments. After dissection, solution was exchanged for saline without MS-222 for recordings.

The brain was visualized with IR-DIC microscopy on a FS2 Axioskop (Zeiss, Oberkochen, Germany). The locations of electrophysiologically characterized Pkjs were captured with a SensiCam camera (PCO.Imaging, Kelheim, Germany) and/or from the coordinates of the Sutter MP-385 manipulator. Unpolished borosilicate patch pipettes were pulled to tip resistances of 8-12 MΩ (Model P-97 puller, Sutter; standard wall capillary glass with filament, G100F-3, Warner Instruments) and filled with intracellular solution containing (mM): 120 K-gluconate, 12 Na-gluconate, 3.2 NaCl, 2 $MgCl_2$, 0.025 $CaCl_2$, 1 EGTA, 0.3 mM Tris-GTP, 1 MgATP, 14 creatine phosphate, 10 HEPES, and 3 Alexa Fluor 488 hydroxide, buffered to pH to 7.4 with KOH.

Whole-cell recordings were made with a Multiclamp 700B and Digidata 1322A with pClamp software (Molecular Devices, Sunnyvale, California) from Pkj neurons left hemisphere of the cerebellum. Data were acquired at 50 kHz and filtered at 10 kHz. All voltage clamp recordings were made at a holding potential of -60 mV. In current clamp, the amplifier injected a constant 20-pA current even in "I=0" mode, which artificially depolarized cells in initial experiments. The depolarization could reduce the amplitude of complex spikes and inactivate voltage-gated currents required for full amplitude simple spikes, which was taken into account in the analysis. In all subsequent current-clamp recordings, an equivalent hyperpolarizing current was applied to neutralize this current. Bridge balance and capacitance neutralization were also applied.

For ventral root recordings, patch pipettes were cut to a 20-50 μm tip diameter, heat-polished, and bent to ~20° to improve contact with the body wall. The tips were cut by pressing a separate pulled pipette against the glass and pulling it orthogonally toward the tip, causing the held pipette to resonate and break. The unbent, broken pipette was then held about the filament of a microforge (Narishige MF-380, Japan) at a 20º angle and heated ~0.2 mm from the tip, forming a bend. The pipette was filled with extracellular solution and placed on the intermyotomal cleft. Recordings from the ventral root were made with an Axopatch 200B (Molecular Devices) amplifier in current clamp mode with low and high frequency cutoffs of 300 and 4000 Hz.

2.5.3 Behavior.

Presentation of sensory stimuli was controlled with a Master-8 Pulse Stimulator (A.M.P.I, Jerusalem, Israel) triggered by pClamp. The conditional stimulus (CS) was a 2-s light (unless otherwise stated) from a blue LED (470 nm, 53 lux) surrounded by a 3-cm aluminum foil disk, positioned ~5 cm above and ~30° to the right of the fish's head. The unconditional stimulus (US) was a brief electrical current (2 mA, 5 ms) applied to the tail tip by a concentric bipolar stimulating electrode (05-D, World Precision Instruments, Sarasota, Florida), which mimics a mild tactile stimulus (Kahn and Roberts, 1982). Experiments were conducted with the microscope light on (1100 lux) and the objective placed directly above the fish. The environment was homogeneous with no visual cues within the range of vision of the fish (~2 mm, Patterson et al. 2013), which minimized the possibility of behaviors driven by a visuomotor mismatch during fictive swimming.

An initial test US was applied to verify positioning of electrodes for ventral root recording and tactile stimulation. Next, a test CS was applied, and if the light evoked fictive swimming, the microscope light luminance was increased to reduce contrast with the CS light until the CS no longer elicited swimming. Six fish were discarded for persistent light-evoked or excessive spontaneous swimming. For experiments including Pkj recordings, the CS and US were each presented alone first, once in current clamp and once in voltage clamp. Training consisted of paired presentations of the CS followed immediately by the US. Trials were triggered manually, with start-to-start inter-trial interval of 40-55 sec, for a maximum of 70 trials or the duration of

the Pkj recording (15-45 trials). Pseudoconditioning consisted of equal numbers of CS and US presentations given randomly at intervals of 15-25 s.

Archaerhodopsin-3 (Arch) was activated by a green LED (565 nm; 5400 lux; Thor Labs, Newton, New Jersey). The size of the illuminated area was adjusted with an iris diaphragm. To activate Arch, green light was directed at the whole cerebellum. For control trials with illumination displaced, the green light was directed ~1 mm rostral to the head. In $Arch^+$ Pkjs, no Arch-dependent currents were evoked either by displaced illumination or by the blue CS light (N=5). Outcrossing Tg(Arch-tagRFP-T:car8:GCamp5) fish produced equal ratios of $Arch^+$ and $Arch^-$ larvae. Either wild-type or $Arch^-$ fish were used in control and pseudoconditioned groups and were counterbalanced for age.

2.5.4 Analysis of electrophysiological events.

Electrophysiological data were analyzed in IGOR-Pro (Wavemetrics, Lake Oswego, Oregon). The electrophysiological recordings from Pkjs were differentiated and dV/dt peaks were used to find putative synaptic and/or action potentials. After the identification procedure described below, every event was checked and corrected if necessary by assessing the underlying conductance extracted from the dV/dt, as described and illustrated in the *Results.*

The procedure was first optimized to identify complex spikes. We determined a reasonable starting threshold as follows: Voltage clamp recordings of climbing fiber EPSCs, which were reliably evoked by the tactile stimulus, had a mean amplitude of -280 ± 29 pA at -60 mV (N=27

EPSCs in 27 cells), and large spontaneously occurring putative climbing fiber EPSCs were -253 ± 29 pA (N=222 EPSCs in 39 cells). For Pkjs, which have a mean capacitance of 10.7 ± 0.67 pF (N=29 cells), a current of -250 pA would give a dV/dt of 25 mV/ms. In current clamp, however, cells were often more depolarized, owing to synaptic potentials (and extrinsic current from the amplifier in initial experiments, described above), such that complex spikes often arose from voltages depolarized to -60 mV. Therefore, to identify complex spikes in each differentiated record, threshold was first set at 20 mV/ms. The extracted events were then examined by eye (in the raw and the differentiated records) to assess whether large, rapid depolarizing events arising directly from the baseline were adequately selected; the membrane voltage just preceding the event was considered in this evaluation. If necessary, the threshold would be adjusted to a lower value. After events were detected with an appropriate threshold, the record was re-examined by eye to eliminate false positives, which were rare but could include secondary humps on either complex or simple spikes.

After complex spikes were extracted from the record, threshold was lowered to account for the next-most rapidly depolarizing events, which were identified as putative simple spikes. These were evident only when the membrane potential was sufficiently hyperpolarized for the recruitment of voltage-gated channels. The threshold was initially set at 8 mV/ms. After events were detected, the raw and differentiated records were once more inspected by eye to eliminate false positives, such as secondary humps on simple or complex spikes and to verify that detected events resembled action potentials with a threshold inflection. On average the dV/dt of these events was 10.5 ± 0.6 mV/ms (N=46 cells), corresponding to a current of about -114 pA (for a

~10 pF cell). Since parallel fiber EPSCs are small (<20 pA at -60 mV, i.e., <333 pS), voltage-gated Na currents likely predominated in setting this rate of rise. This factor was taken into account when the underlying conductances were calculated (see *Results*).

After extraction of simple spike events, the dV/dt threshold was lowered again to identify pfEPSPs. This value was set at 0.4 mV/ms. This corresponds to an amplitude of 40 pA, more than twice the amplitude of EPSCs visible in voltage clamp records. This threshold was then reduced by eye to capture voltage deflections with a pfEPSP-like waveform that were distinct from high-frequency fluctuations (baseline noise) throughout the trace. In addition these events were constrained to occur at voltages that were below the threshold of simple spikes. After events were detected by thresholding, the record was once more inspected by eye to eliminate false positives, including subthreshold depolarizations that did not become full-fledged simple spikes that had already been counted as a pfEPSP. These criteria were relatively stringent and were intentionally selected to bias toward rejection errors (small pfEPSPs or pfEPSPs occurring during periods of simple spikes) rather than false positives. In cells that showed pfEPSPs during swimming events, synaptic activity was often elevated for time scales that were commensurate with the duration of swimming, i.e., a few hundred ms. Therefore, for estimation of latencies of pfEPSPs relative to swimming, measurements were restricted to pfEPSPs that initiated depolarizations that lasted at least 200 ms.

During behavioral tasks, hyperpolarizations were identified as deflections below the most negative voltage during the pre-trial baseline. For ventral root signals, voltage recordings were rectified, smoothed by a moving average in a 2-ms window, and thresholded to detect individual

bursts. Fluorescent images were obtained on a confocal microscope (Zeiss LSM 710, 40x) with excitation wavelength 488 nm, and analyzed with Zen imaging software.

2.5.5 Statistical analysis.

N values for cells and fish (biological replicates) are given in the text. Data are reported as mean ± SEM, unless noted. Statistics were calculated with Microsoft Excel and SPSS (IBM), with tests as follows: Two-sided paired or unpaired t-tests, for comparisons of two groups or two measures from one group (Figures 2.5H, 2.6D [one paired CS and CR CV per cell], 2.8E, 2.9A, 2.9D); One-way ANOVA with Bonferroni *post hoc* corrections as needed, for groups of fish and/or cells (Figures 2.2F, 2.2H, 2.3B, 2.4F, 2.5C, 2.7D); repeated measures ANOVAs with Tukey *post hoc* corrections as needed, for comparisons across training (Figures 2.3C, 2.3E, 2.5E, 2.5F, 2.5G, 2.7C, 2.8D left); chi-squared tests, for the proportion of learners among $Arch^{+}$ and control fish (Figure 2.8D right). For data reported only in the text, the statistical test is indicated. F-statistics and chi-square statistics are given in legends.

Chapter 3: Alternative modes of synaptic integration in cerebellar output neurons induced by sensory stimulation and fictive swimming

3.1 Abstract

The spiking pattern of cerebellar output neurons is the signal that underlies the cerebellum's influence on movements. ENs are the output neurons of the teleost cerebellum. While their spiking activity is presumably modulated by synaptic input from pfs and Pkjs, no *in vivo* recordings from these neurons have been reported. We made voltage- and current-clamp recordings of synaptic and spiking activity of olig2^{+} ENs in the larval zebrafish while simultaneously monitoring fictive swimming. We observed spontaneous spiking, EPSCs, and IPSCs while the fish was at rest. Interrogation of Pkj IPSCs revealed that inhibition from complex spikes evokes a similar postsynaptic response as simple spikes. Based on the temporal features of IPSCs, we estimated that 2-7 Pkjs converge onto individual ENs, and simple spiking of converging Pkjs is likely not independent. Recordings during sensorimotor behaviors revealed alternative modes of activity. In response to a visual stimulus, some ENs produced a well-timed spike attributable to acute synaptic excitation. During fictive swimming, spiking was elevated and anticorrelated with inhibition from Pkjs. Both inhibition and spiking were entrained to the swim cycle during spontaneous swimming, suggesting that ENs contribute to movement execution. No entrainment was observed during sensory evoked swimming, likely reflecting combinatorial sensory and motor input. These results demonstrate alternative means through which synaptic inhibition and excitation affect the firing pattern of cerebellar output neurons.

3.2 Introduction

The cerebellum communicates with the rest of the nervous system and contributes to movement via the spiking of cerebellar output neurons. These cells fire spontaneously, but the timing and rate of spikes is affected in real time by inhibitory and excitatory synaptic drive. Output neurons as well as their presynaptic partners displayed increased firing that correlates with movement. Moreover, during repetitive, cyclical movements like locomotion, output neurons show entrained rhythmic firing (Armstrong and Edgley, 1984a; Sarnaik and Raman, 2018). Furthermore, movements can be elicited and ongoing movements can be interrupted by optogenetic manipulation of output neuron spiking (Witter et al., 2013; Heiney et al., 2014; Proville et al., 2014; Lee et al., 2015; ten Brinke et al., 2017; Sarnaik and Raman, 2018), demonstrating that correlated spiking observed in output neurons is likely affecting movement execution in real time.

While increased spike rate is consistently observed during cerebellum-dependent behaviors (e.g. Thach, 1968; Armstrong and Edgley, 1984a; McCormick and Thompson, 1984a), spike timing may also be important. Interactions between excitatory and inhibitory synaptic inputs, as well as intrinsic membrane properties which promote spiking, determine the rate and timing of output neuron spiking. Increases in rate can result from tonic excitatory drive. Relative to rates during unorganized continuous inhibition, synchronization of inhibitory inputs can also increase firing rate (Gauck and Jaeger, 2000; Person and Raman, 2011). On the other hand, specifically-timed action potentials can result from acute excitatory drive (Yarden-Rabinowitz and Yarom, 2017), as well as upon relief of acute inhibition (Person and Raman, 2011; Brown and Raman, 2018).

Coordinated synaptic drive can also produce well-timed spikes, with excitation facilitating spiking generally, and concerted inhibition controlling spike timing (Wu and Raman, 2017). While these experiments, conducted mostly in slice, have demonstrated ways that synaptic inputs can interact, few experiments have described the actual synaptic drive provided to these neurons and related it to spiking during movement.

To address this question, we have characterized the activity of cerebellar output neurons in the larval zebrafish. These neurons are called eurydendroid neurons (ENs; Meek et al., 1992). Anatomically, ENs differ somewhat from mammalian cerebellar nuclear cells. They are not organized into ventrally-located nuclei, but instead are superficially located next to Purkinje neurons (Pkjs) in the cerebellar cortex. Also, instead of receiving input from mfs, pfs form synapses on the dendrites of ENs, which extend into the molecular layer. Nevertheless, recordings from ENs in mormyrid fish suggest that the synaptic physiology of these neurons is similar to mammalian cerebellar nuclear cells (Han and Bell, 2003). However, no recordings have been made from these neurons in larval zebrafish or during swimming.

By 5 days postfertilzation, larval zebrafish are freely swimming and engaging in a variety of behaviors. Despite the age of these animals, single cell recordings and imaging techniques have demonstrated that the cerebellum is functional and actively participating in controlling movements. Pan-neuronal imaging of the cerebellum reveals changes in firing during motor learning tasks (Aizenman and Schumann, 2011; Ahrens et al., 2012), while cell-specific imaging has revealed movement-related modulation of Pkjs (Matsui et al., 2014a) and granule cells (Matsuda et al., 2017). Furthermore, Pkjs show increased pf drive and modulation of simple and

complex spiking during swimming (Sengupta and Thirumalai, 2014; Matsui et al., 2014a; Scalise et al., 2016; Harmon et al., 2017). Thus, the inhibitory and excitatory neurons immediately presynaptic to ENs are contributing to movements.

To test how ENs integrate these synaptic inputs and fire during movement, we have made intracellular current and voltage clamp recordings of ENs while simultaneously monitoring fictive swimming by recording from the ventral root in the tail. We found that while ENs fire spontaneously, they also display parallel EPSCs and Pkj IPSCs while the fish is at rest. Regarding Pkj drive, we found that IPSCs attributable to Pkj complex spikes were similar in amplitude to spontaneous IPSCs. Examination of the temporal features of IPSCs suggested that ENs receive converging input from 2-7 Pkjs. While a subset of ENs show well-timed spikes and EPSCs in response to visual stimuli, all ENs displayed increased firing and synaptic drive during spontaneous and sensory-evoked reflexive swimming. Comparison of synaptic drive and firing revealed that EN physiology differed between spontaneous and evoked swimming. During evoked swimming, firing rates were higher and inhibitory and excitatory synaptic drive was greater. During spontaneous swimming, ENs received inhibitory drive that aligned to the swim cycle, leading to production of rhythmic spiking. These data provide evidence for multiple mechanisms through which synaptic inputs control spike timing of cerebellar output neurons, and they suggest that ENs play an active role in shaping motor commands.

3.3 Results

3.3.1 Anatomy and spiking properties olig2$^+$ eurydendroid neurons

With the goal of testing how olig2$^+$ ENs signal during fictive swimming, we first examined the gross anatomy and spiking of these cells. Images from *olig2:GFP* transgenic fish (McFarland et al., 2008) revealed olig2$^+$ cells distributed throughout the brain (Figure 3.1A, 3.1B). In the cerebellum, these neurons were found throughout the corpus cerebelli (the largest lobe of the teleost cerebellum), with some packed more densely in the eminentia granularis. We counted the number of olig2$^+$ neurons and found ~200 cells per cerebellar hemisphere (148, 194, and 232 cells in 3 fish, 7 dpf). Because GFP is likely expressed in cells soon after differentiation, this value is the upperbound for the number of neurons functionally contributing to cerebellar behaviors at this point in development (6-8 days post fertilization).

We electroporated individual ENs with fluorescent dye (Alexafluor 594; N=3 cells) to better visualize their cellular anatomy. Filled ENs had multiple dendritic branches that extended into the molecular layer as well as an axon (Figure 3.1B, triangles). The cell body was approximately the size of unfilled olig2$^+$ ENs (~5 μm; Figure 3.1B). Furthermore, we noticed no difference in morphology between electroporated cells and cells filled during intracellular recording, suggesting that neither procedure damaged or significantly altered the appearance of ENs.

To examine the relative position of ENs and Pkjs, we crossed *olig2:GFP* fish with fish that expressed RFP in Pkj (*Tg(Arch-tagRFP-T:car8:GCamp5*; Matsui et al., 2014a; Figure 3.1A). Pkj cell bodies were located dorsal to EN cell bodies (Figure 3.1C). Estimates of the

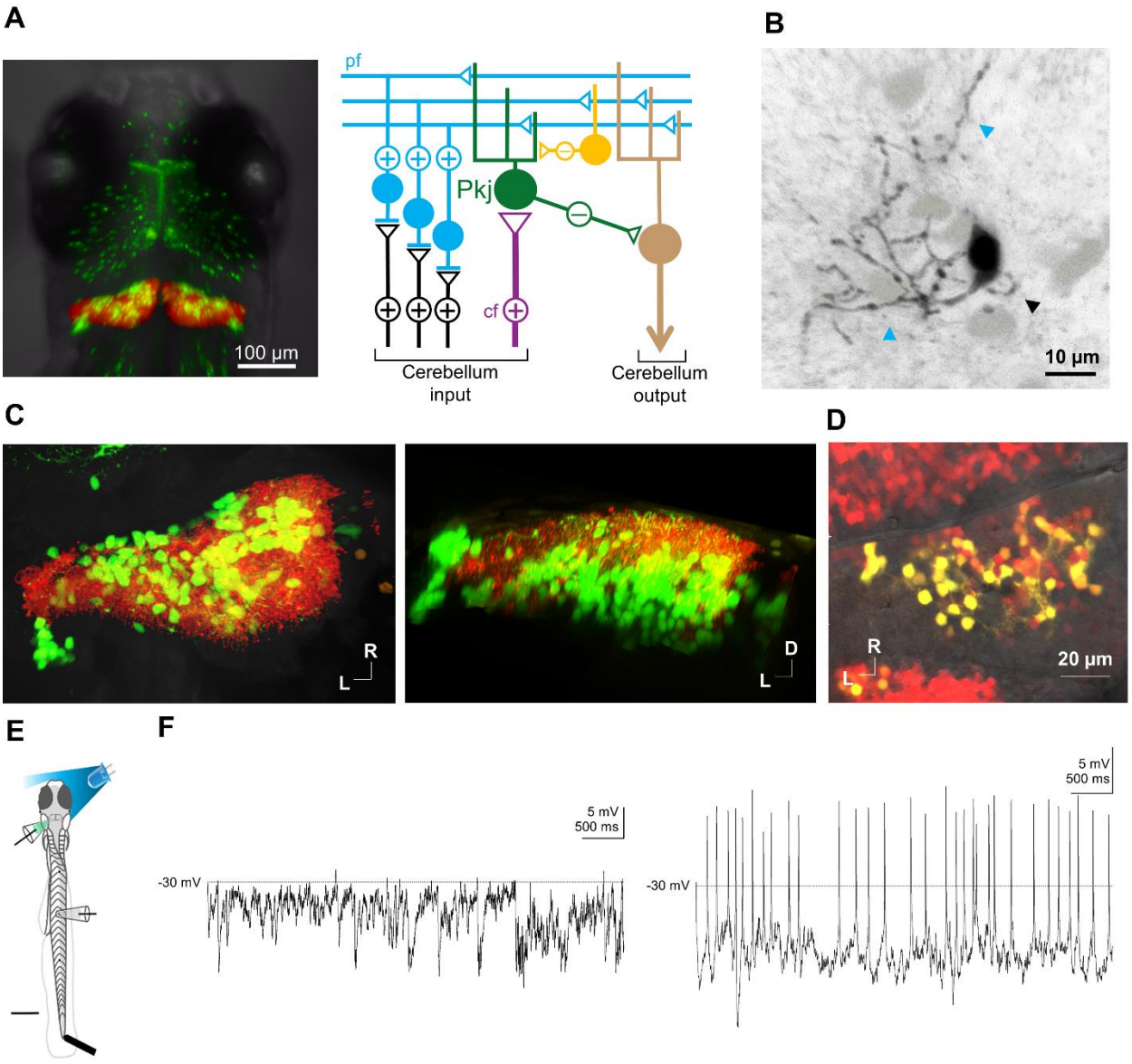

Figure 3.1. EN cellular anatomy and spiking. (**A**) Left, image of olig2^{+} (green) and Purkinje (red) cells from a PTU-treated *olig2:GFP/Arch-tagRFP-T:car8:GCamp5* fish (7 pdf). Right, schematic of the teleost cerebellum. **(B)** Filled olig2^{+} EN (black) with other olig2^{+} ENs (light grey). Blue arrows, dendritic branches. Black arrow, axon. (**C**) Image of left cerebellar hemisphere, olig2^{+} ENs (green) and Pkjs (red) viewed from above (left) and from the caudal side (right). R: rostral, L: lateral, D: dorsal. Fluorescence from Pkj confined to the cell body and dendrite. (**D**) Image of olig2^{+} ENs (green) and glutamatergic neurons (red) from *olig2:GFP/vGlut2a:RG* fish. Colabelled neurons appear yellow. (**E**) Schematic of recording preparation. (**F**) Current clamp recordings from spiking (left) and non-spiking (right) ENs.

length of the Pkj axon are between 2-8 µm (Matsui et al., 2014a), indicating that Pkjs likely contact nearby ENs. Consistent with these findings, we observed complete overlap between Pkjs and ENs in the corpus cerebelli. Moreover, Pkj cell bodies were generally dorsal to ENs, with the dendrites of both cells intermingled in the molecular layer. Crosses of *olig2:GFP* fish with *vGlut2a:RG* fish (Miyasaka et al., 2009) generated larvae in which all olig2^{+} neurons in the cerebellum were colabelled (N=2 fish; Figure 3.1D), demonstrating that these neurons release glutamate. We also observed superficially located olig2^{-} glutamatergic cells, which possibly represent a separate population of ENs.

We made whole cell patch clamp recordings from olig2^{+} neurons in immobilized larval zebrafish (Figure 3.1E). In current clamp recordings, we observed spontaneous action potentials in 16/22 cells, at a rate of 7.9 ± 1.5 spikes/s, as well as pf EPSPs and Pkj IPSPs (Figure 3.1E). Because these experiments were done soon after the beginning to eurydendroid differentiation (3-5 dpf; McFarland 2008), it is possible the absence of spikes reflects cell-by cell variation in developmental trajectory. We observed that silent cells had a higher resting membrane potential (-34.3 ± 1.5 mV) than spiking cells (-39.3 ± 1.5 mV; $p=0.036$; Figure 3.1F), but similar input resistances (2.4 ± 0.3 GΩ vs. 2.5 ± 0.2 GΩ; $p=0.86$) and Pkj IPSC rates (12.1 ± 2.2 IPSCs/s vs. 12.2 ± 4.3 IPSCs/s; $p=0.96$). Silent cells could be made to spike with hyperpolarizing current injections or in response to summating IPSPs. These results suggest that only a subset of olig2^{+} ENs spike spontaneously, and that cell-by-cell differences in spiking are not readily attributable to differences in tonic inhibitory drive or passive membrane properties.

3.3.2 Basal properties of synaptic inputs

To characterize the properties of excitatory and inhibitory synaptic inputs to ENs, we made voltage clamp recordings of pf EPSCs (N=16 cells and fish) and Pkj IPSCs (N=22 cells and fish; Figure 3.2A, 3.2B). Because these currents were small and could summate if they happened in close succession, we used rate of rise to detect individual events. The threshold for detecting events was set based on an analysis of the noise in individual recordings (see *Materials and Methods*). For EPSCs, the rate of rise across all cells was -6.1 ± 0.53 pA/ms. The mean 10-90 risetime and decay tau of EPSCs were 1.4 ± 0.3 ms and 1.9 ± 0.2 ms, respectively (Figure 3.2A, right). While the mean EPSC amplitude and charge transfer were -7.4 ± 0.7 pA and 23.5 ± 2.2 fC respectively, the modal EPSC was smaller, with an amplitude of ~ -3 pA and a charge transfer of ~15 fC (Figure 3.2C, 3.2D). EPSCs occurred at a rate of 15.2 ± 2.2 EPSCs/s (mean interval = 65.8 ± 9.5 ms). The actual rate is likely higher because some putative events were not significantly larger than background noise and may have been incorrectly excluded from analysis. The most common inter-EPSC interval was ~ 4 ms (Figure 3.2E), demonstrating that EPSCs often occurred in short succession and occasionally summed. We monitored periods of summating synaptic drive as well, which identified as timepoints in which the current deviated one standard deviation away from the baseline holding current.

Pkjs make somatic inhibitory synapses on ENs (Alonso et al., 1992; Matsui et al., 2014a). Pkj firing occurs spontaneously and is modulated by sensory stimulation and swimming (~7 spikes/s; Sengupta and Thirumalai, 2015; Scalise and Sawtell, 2016; Harmon et al., 2017), and is thus predicted to influence EN firing during cerebellum-dependent behaviors. IPSC rate of rise was

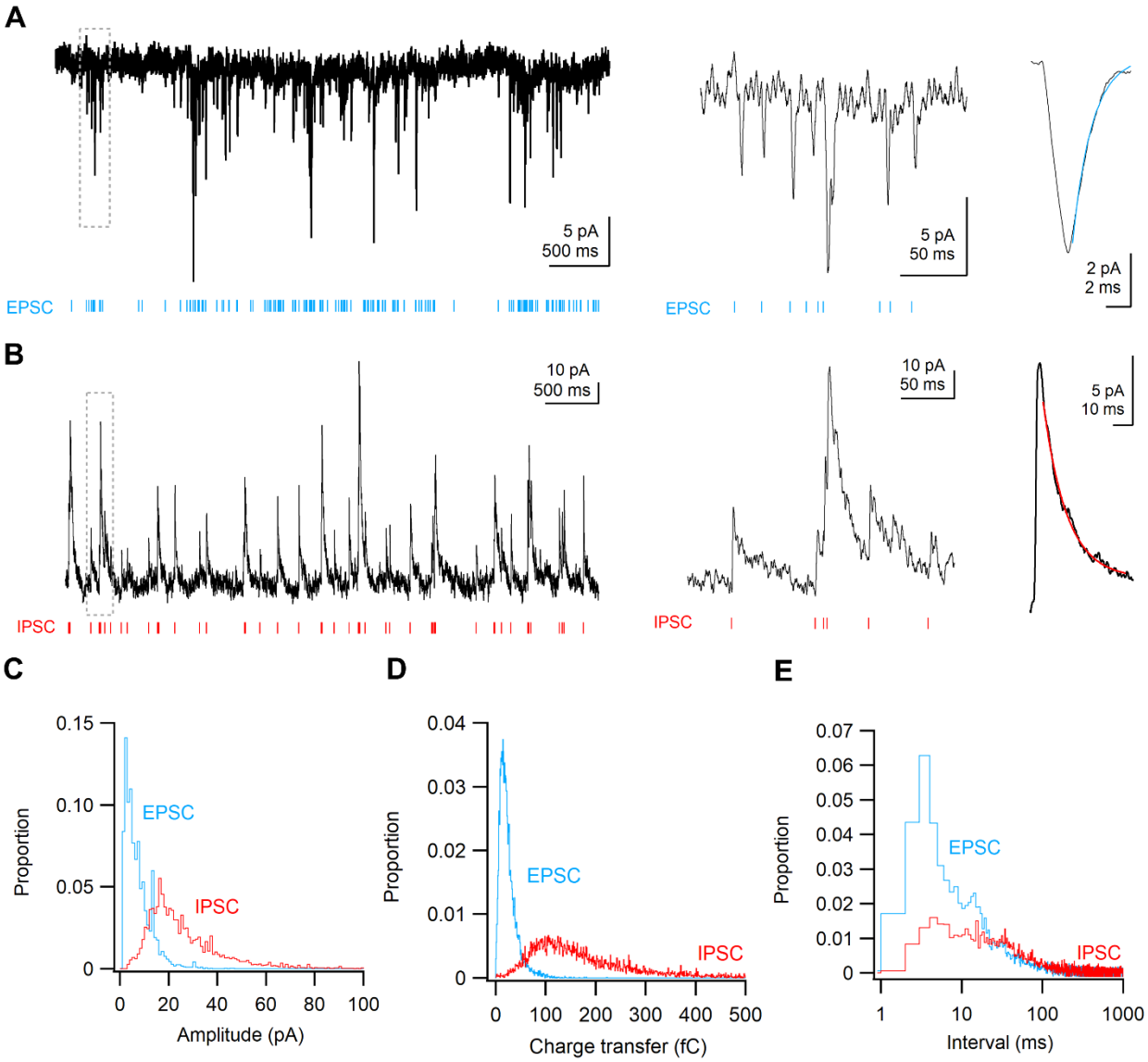

Figure 3.2. Features of spontaneous EPSCs and IPSCs. (**A**) Left, voltage clamp recording of spontaneous pf EPSCs. Middle, example of EPSCs at higher gain, from the boxed region on the left. Right, example of single EPSCs averaged across cells in the dataset. Blue line, fit line with single exponential. Average generated by selecting isolated EPSCs from each cell. Holding potential = -63 mV. (**B**) Left, voltage clamp recording of spontaneous Pkj IPSCs. Middle, example of IPSCs at higher gain, from the boxed region on the left. Right, example of single IPSCs averaged across cells in the dataset. Red line, fit line with single exponential. Holding potential = +12 mV. Legend continues on next page.

Figure 3.2 continued. (**C**) Probability histogram of absolute amplitudes of EPSCs (blue) and IPSCs (red). Bin=1 pA. Amplitude measured as absolute difference between current at onset and the peak of each event. (**D**): Probability histogram of absolute charge transfer of EPSCs (blue) and IPSCs (red). Charge transfer measurements were made from the onset to 10 ms after the onset of the event. Recordings were zeroed to the current at onset. Bin=1 fC. (**E**) Probability histogram of inter-EPSC (blue) and inter-IPSC (red) intervals. X-axis n log scale. Bin= 1 ms.

20.9 ± 1.4 pA/ms, corresponding to a risetime of 2.68 ± 0.2 ms. The decay time constant was relatively fast for inhibitory synaptic currents (7.9 ± 0.3 ms; Figure 3.2B, right). Similar values have been calculated for Pkj IPSCs in cerebellar nuclear cells (Anchisi et al., 2001; Person and Raman, 2011). IPSCs tended to occur with relatively short intervals between them. The modal interval was ~5 ms, while the mean was 84 ± 12 ms or a rate of 11.9 ± 1.7 IPSCs/s (Figure 3.2E).

We measured amplitude and charge transfer of IPSCs and found that the most common IPSC amplitude and charge transfer were ~17 pA and ~90 fC (Figure 3.2C, 3.2D; mean amplitude: 26.5 ± 1.5 pA, mean charge transfer: 182 ± 28 fC). Because the driving force on inhibitory and excitatory currents is approximately equal (~38 mV), these results indicate that the conductance of inhibitory inputs is larger than that of excitatory inputs. Like pf EPSCs, Pkj IPSCs varied in size, with skewed distributions of amplitude and charge transfer with long tails towards larger values (Figure 3.2C, 3.2D). Differences in IPSC size could be attributable to depression or potentiation of individual Pkj inputs, overlapping IPSCs from multiple Pkjs, or IPSCs related to simple and complex spikes.

3.3.3 IPSCs from presynaptic complex spikes

We next tested whether IPSCs that related to presynaptic complex spikes had different features than spontaneously-occurring IPSCs. We used a transgenic fish line in which the light-activated proton pump Archaerhopsin-3 ("Arch") was expressed in Pkjs. Activation of Arch hyperpolarizes the cells enough to suppress simple spikes, but complex spikes remain unaffected (Harmon et al., 2017). To record IPSCs attributable to complex spikes, we crossed these fish with *olig2:GFP* transgenic fish (e.g. Figure 3.1A), optimized our procedure for targeting ENs without activating Arch (Materials and Methods), and made voltage clamp recordings of IPSCs from olig2^{+} ENs with and without Arch activation (N=13 cells; Figure 3.3A). Without Arch activation, IPSCs resembled those recorded from wildtype fish. IPSC amplitudes had a mean of 23.4 ± 2.2 pA (*p=0.23 unpaired ttest*) and followed a similar distribution (Figure 3.3B).

As expected, IPSC rates decreased for all cells during Arch activation (1.4 ± 0.3 IPSCs/s during Arch; *p=0.006 paired ttest*). IPSCs that occurred during Arch activation were not larger in amplitude than spontaneous IPSCs (Figure 3.3B). On the contrary, IPSC amplitudes were significantly smaller (17.3 ± 2.5 pA; *p<0.001 paired* ttest). Remaining IPSCs still occurred with a range of amplitudes, spanning from ~3-30 pA. To test whether presynaptic Pkjs tend to produce complex spikes at similar time points, we examined the intervals between remaining IPSCs. We found that the shape of the intervals distribution was significantly changed. Except for one cell that showed IPSCs at very short intervals (modal interval ~3 ms), IPSCs occurred at both short and long intervals (Figure 3.3C). These data demonstrate that neither the large-

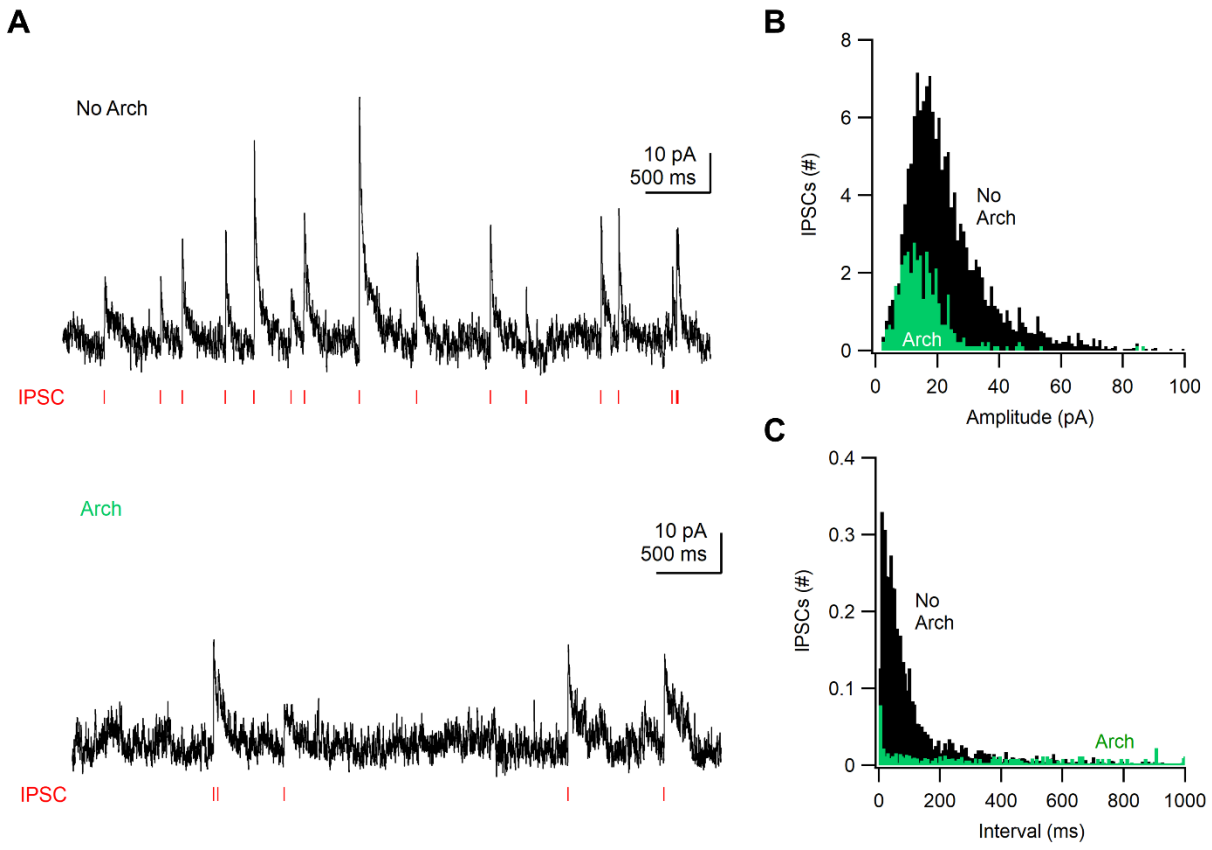

Figure 3.3. Properties of IPSCs attributable to complex spikes. (**A**) Example voltage clamp recordings of Pkj IPSCs without (top) and with (bottom) Arch activation. Remaining IPSCs are attributable to presynaptic complex spikes. (**B)** Histogram of IPSC amplitude without (black) and during (green) Arch activation. Bin = 1 pA. (**C**) Histogram of inter-IPSC intervals without (black) and during (green) Arch activation. Bin = 1 ms.

amplitude spontaneous IPSCs nor the tendency of IPSCs to occur at short intervals is attributable to complex spikes.

3.3.4 Estimating Purkinje-eurydendroid convergence

Anatomical convergence of multiple Pkjs onto individual cerebellar output neurons is an important variable for understanding information encoded in Pkj spike patterns (Person and Raman, 2012). IPSC rates provide a rough estimate of the convergence ratio. Pkjs generate simple and complex spikes spontaneously at rates of 6.4 ± 1.2 spikes/s and 0.3 ± 0.03 spikes/s, respectively (Harmon et al., 2017; Figure 3.4A). Thus, an IPSC rate of 11.9 ± 1.7 IPSCs/s suggests convergence of two Pkjs onto each EN. This method assumes similar levels of presynaptic simple spiking across EN recordings. However, simple spiking is variable across cells and across time, with individual Pkjs alternating between extended periods with few simple spikes and many simple spikes (Sengupta and Thirumalai, 2015). Complex spike rates are likely more stable because they do not depend on the real-time excitability of the Pkj and instead solely reflect cf transmission. IPSC rates with simple spiking suppressed were 1.4 ± 0.3 IPSCs/s, approximately 5-times the complex spike rate. Thus, we can estimate the Pkj-EN convergence ratio to be between 2-5 Pkj per EN.

In addition to rate, convergence is suggested by the temporal pattern of IPSCs. Intervals between IPSCs were often short, between 3-5 ms (Figure 3.2E). This corresponds to a rate of 200-333 spikes/s, too fast to be attributable to a single Pkj. To further estimate convergence and test whether convergence by itself can explain brief inter-IPSC intervals, we reconstructed the

distribution of IPSC intervals using simulations of IPSCs based on recorded spiking patterns of individual Pkjs (Figure 3.4A). We reanalyzed a subset of previously reported Pkj recordings (Harmon et al., 2017; N=27 cells; see Materials and Methods) to measure the intervals between all spikes, whether simple or complex. In this dataset, the modal interspike interval was ~40 ms, while the minimum was 6.0 ms, and the mean spike rate was 6.2 ± 0.9 spikes/s. For each Pkj, we constructed simulated spike trains by repeatedly sampling (10^5 times) from interspike intervals measured from that cell, then constructed probability histograms of the interspike intervals. This procedure created distributions that well matched the distribution from actual Pkj recordings. To quantify the goodness of fit, we measured the overlap between the distributions of actual and simulated interspike intervals. The distribution from individual Pkj overlapped 57.1 ± 2.2 % with the average distribution of all Pkjs, providing a relative value for evaluating the goodness of fit for IPSC intervals.

Next, to test convergence, we constructed distributions that resulted from two separate simulations. In a manner similar to Pkj spike trains, one distribution was constructed by repeatedly sampling inter-IPSC intervals measured from individual ENs (Figure 3.4C, red). The second was constructed by combining simulated Pkj spike trains to various degrees. Each iteration of the simulation selected a Pkj at random and constructed a spike train with the intervals measured from that cell. In simulations which assumed convergence of *n* Pkj per EN, *n* spike trains were constructed in this manner. We then combined spike times from all Pkj simulations, constructed an interspike interval histogram (Figure 3.4C, black), and measured the overlap between the IPSC and Pkj spike distributions (Figure 3.4C, pink). This analysis assumes

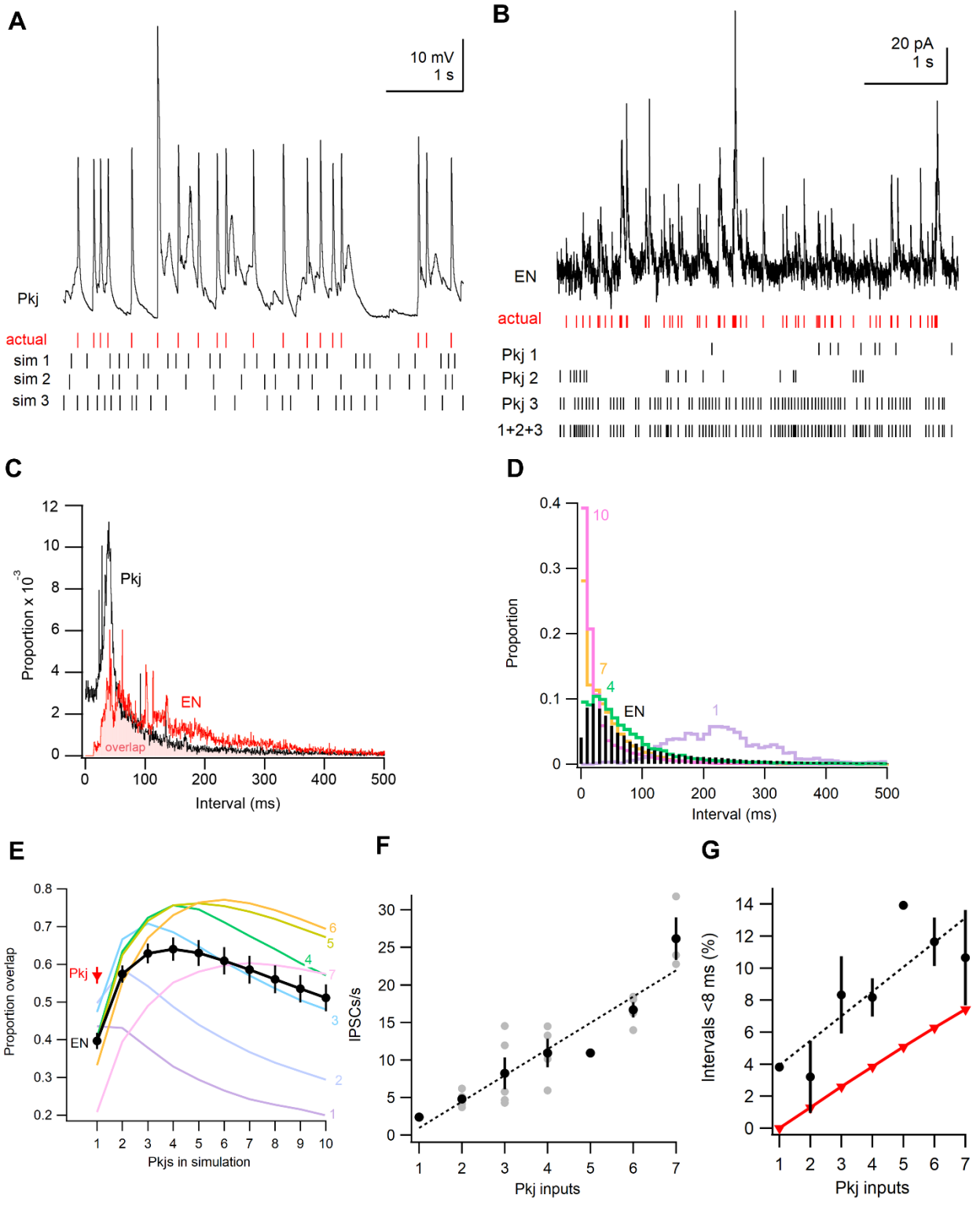
A
10 mV
1 s
Pkj
actual
sim 1
sim 2
sim 3
B
20 pA
1 s
EN
actual
Pkj 1
Pkj 2
Pkj 3
1+2+3
C
Proportion x 10^-3
Pkj
EN
overlap
Interval (ms)
D
Proportion
10
7
4
1
EN
Interval (ms)
E
Proportion overlap
Pkj
EN
Pkjs in simulation
F
IPSCs/s
Pkj inputs
G
Intervals <8 ms (%)
Pkj inputs

Figure 3.4. Simulations of IPSCs from converging Pkjs. (**A**) Example current-clamp recording and raster of spikes from a Pkj. One large-amplitude complex spike is included, remaining events are simple spikes. Red: spike times from actual recording. Black: simulated spike times for same cell. (**B**) Example voltage-clamp recording and raster of IPSCs from an EN. Red: IPSC times from actual recording. Black: simulated spike times for three different Pkjs, then all spike times combined (1+2+3). (**C**) Probability histogram of inter-event intervals constructed from single simulation for cells in (**B**). Red: EN IPSCs. Black: combined simulated Pkj spikes. Pink: overlapping region. Bin=0.5 ms. (**D**) Average probability distribution of IPSC intervals (black) and simulated distributions that included 1 Pkj (no convergence condition, purple), 4 Pkjs (maximum overlap for all ENs, green), 7 Pkjs (maximum ratio for individual ENs, orange) and 10 (maximum ratio attempted, pink). Average Pkj distribution calculated across 10^3 at eat convergence level. Average EN distribution calculated across cells in data set. Bin=10 ms. (**D**) Overlap between simulated Pkj distributions and either single Pkjs (red), all ENs in dataset(black), or ENs sorted by maximum overlap (colored lines). Number next to colored line corresponds to the number of Pkjs that produced maximum overlap. (**E**) Spontaneous IPSC rate of ENs sorted by estimated convergence ratio, or the convergence ratio that produces that largest overlap. Only one cell included in 1 and 5 Pkj groups. Slope of line= 3.49 IPSC/s/input. (**F**) Percent of inter-event intervals that were <8 ms. Black: IPSCs recorded from ENs sorted by estimated convergence ratio. Red: simulated Pkj spikes. There are small error bars on the Pkj data. Slope of the fit line = 1.53 % / input.

that Pkj spikes invariably evoke an IPSC (i.e. there are no failures) and that spiking of converging Pkjs is independent while the fish is at rest. We repeated this entire procedure 10^3 times and measured the average overlap for each cell. The average distributions for ENs (black) and different degrees of Pkjs (colored lines) are plotted in Figure 3.4D.

Simulations which assumed no convergence showed the least overlap and significantly less overlap compared to distributions from single Pkjs (*p=0.001 unpaired ttest*). Across all ENs, the overlap ordinally increased as Pkjs were added and peaked for simulations which assumed 4 Pkjs (Figure 3.4E, black). Higher degrees of convergence lead to less overlap. Thus, our results suggest that the most common degree of convergence that can explain the temporal pattern of

IPSCs is 4 cells, although convergence to greater or lesser degrees is not disqualified. In fact, a cell-by-cell analysis revealed variation in the degree of convergence with the greatest overlap (Figure 3.4E, colored lines). For example, some cells showed the greatest overlap with simulations that included 2 Pkjs (N=4/22 cells; Figure 3.4E, lavender), while others with 7 Pkjs (N=3/22 cells; Figure 3.4E, pink). Using the simulation that yielded the greatest overlap to assign the degree of convergence for each cell, the mean degree of convergence is 4.1 ± 0.4 Pkj inputs. Furthermore, we found that basal IPSC rates increased with degrees of convergence (Figure 3.4F), providing additional validation of the estimated convergence ratio for each cell. These results indicate that while the mean degree of convergence is ~4 Pkj/EN, the number of Pkjs inputs ENs receive ranges between 1-7. This variation may be attributable to the development of this synaptic connection (see Discussion).

Our cell-by-cell analysis also revealed that simulations of independent Pkj spiking invariably underestimated the proportion of brief IPSC intervals. Across all ENs, 8.3 ± 1.0% of IPSC intervals were <8 ms (i.e. the decay constant of Pkj IPSCs). Categorizing ENs by the estimated convergence showed that this proportion increased with the convergence ratio (Figure 3.4G, black). The same analysis of simulated Pkj trains revealed a proportion of 3.8 ± 1.0%, with a smaller proportion of intervals <8 ms at every level of convergence (Figure 3.4G, red). These results indicate that convergence by itself cannot account for brief IPSC intervals and suggest instead that, when compared to Pkjs selected at random, converging Pkjs are more likely to produce spikes in close succession that summate in the postsynaptic cell, even while the animal is at rest.

3.3.5 Synaptic responses and spiking to visual stimulation

To assess whether ENs receive synaptic drive in response to visual sensory stimuli, we recorded pf EPSCs and Pkj IPSCs in voltage clamp, as well as spikes in current clamp, while presenting the fish with a low-contrast light (blue LED, 2 s, 53 lux). Light presentations occasionally elicited bouts of fictive swimming, both during the light and following the offset. To measure the response to the visual stimulus only, we limited our analysis to those trials in which no bout of swimming was elicited during the light (EPSC: N=13 cells, 13 trials; IPSC: N=11 cells, 11 trials; Figure 3.5). Compared to the fish at rest, ENs tended to show more pf EPSCs during light presentation (19.5 ± 3.5 EPSCs/s; *p=0.07 paired ttest*). Responsiveness varied across cells, with 5/13 cells showing more EPSCs compared to baseline. Among cells that responded, EPSC rate increased from 14.5 ± 3.7 to 27.5 ± 6.2 EPSCs/s (*p=0.013 paired ttest*). In contrast, IPSC rates did not significantly change during the light (12.9 ± 3.4 prior to light, 14.6 ± 3.3 IPSCs/s during the light; *p=0.25 paired ttest*), with 3/11 cells showing increase IPSC rates (from 7.9 ± 4.0 to 13.7 ± 7.9 IPSC/s, *p=0.27 paired ttest*; *p=0.87 unpaired ttest compared to nonresponders*; Figure 3.6B). These results indicate that visual stimuli evoke a greater synaptic response from pf inputs than from Pkj inputs.

We next tested whether these synaptic inputs significantly modulated EN firing. Across all cells in the dataset (N=14 cells, 20 trials), light presentation induced little to no change in spike rate (from 6.0 ± 1.5 to 6.6 ± 1.9 spikes/s; *p=0.5 paired ttest*; Figure 3.5C). Generally, spikes were evenly distributed throughout the light, though we measured a significant increase in spike probability 100-200 ms after light onset (*p=0.025 paired ttest*; Figure 3.5D). EPSC rates

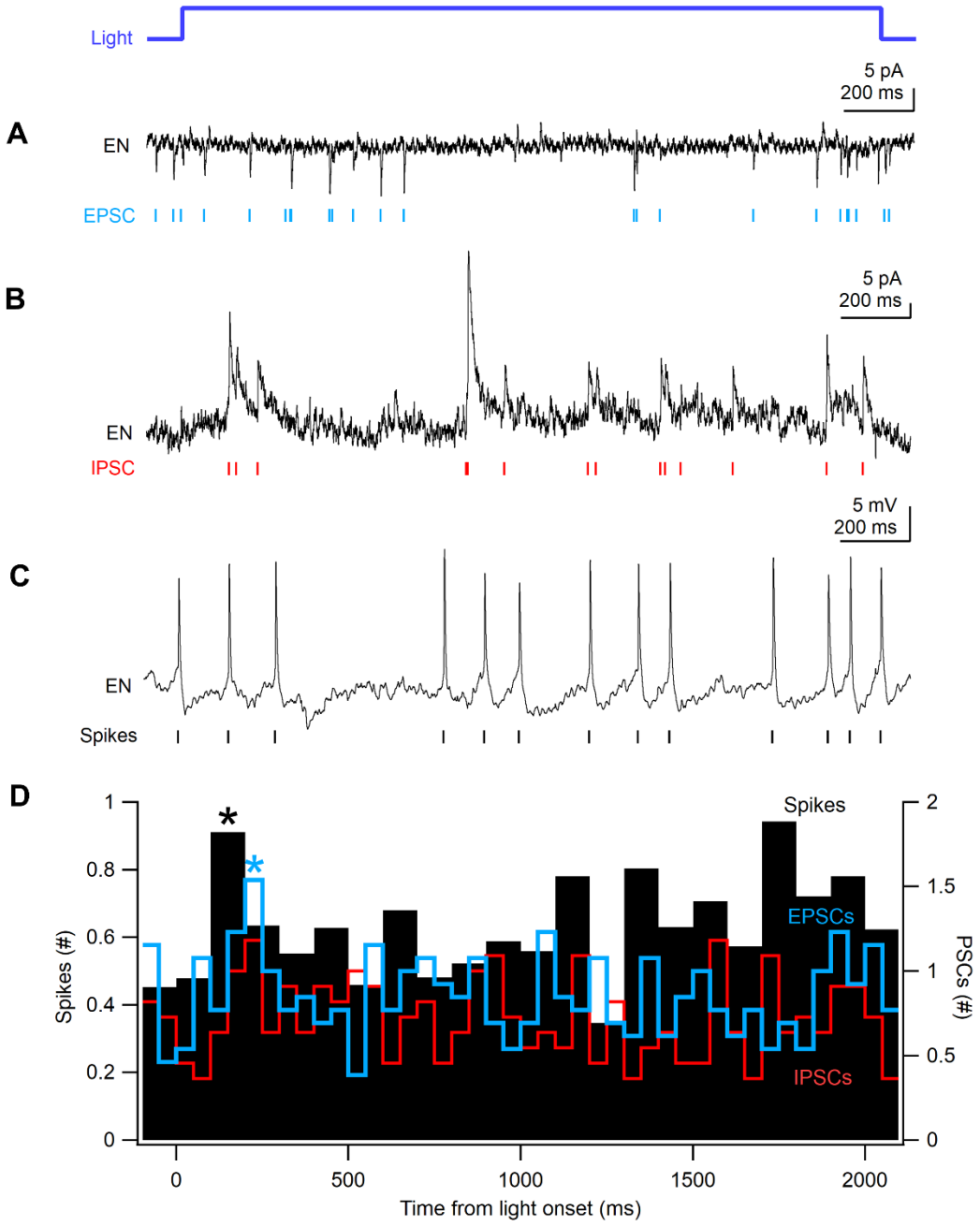

Figure 3.5. Synaptic and spiking responses to a visual stimulus. (**A**) Time course of 2 s flash from blue LED (top) and voltage-clamp recording (bottom) and raster (blue marks) of parallel fiber EPSCs during light presentation. (**B**) Example voltage-clamp recording and raster (red marks) of Pkj IPSCs during light presentation. Recording same neuron as in Figure 5A and 5B. Legend continued on next page.

Figure 3.5 continued. (**C)** Example current-clamp recording and raster (black marks) of spikes during light presentation. (**D**) Peri-event triggered histogram of spikes (black), EPSCs (blue line), and IPSCs (red line). Time 0 = light onset. Bin: spikes=100 ms, EPSCs and IPSCs=50 ms. (*) indicates significance value of $p<0.05$. All unmarked bins were not significantly different from rate measured prior to light onset (paired t-test).

increased at a similar time, surpassing the resting rate 200-250 ms after light onset (*p=0.046*; Figure 3.5D). To examine if differences in excitatory drive predicted differences in spike rate, we compared the change of rate for EPSC responsive neurons (N=3 cells with spike recordings) to nonresponsive cells (N=4 cells). Individual cells from both groups showed increases in spiking, and there was no difference in spike rate between EPSC responsive and nonresponsive cells (responsive= 5.4 ± 1.7 spikes/s; nonresponsive= 10.1 ± 5.8 spikes/s; *p=0.5*). Furthermore, we found no correlation between the change in EPSC rate and the change in spike rate ($r^2=0.03$, slope=-0.04). These data indicate that ENs receive synaptic input related to visual sensory stimuli to varying degrees and that while those inputs modulate firing rates only weakly, they may combine to produce specifically-timed action potentials.

3.3.6 Spiking and synaptic drive during spontaneous and evoked fictive swimming

To assess the neuronal response to swimming, we made recordings of spiking as well as EPSCs and IPSCs from ENs while simultaneously recording fictive swimming from the ventral root in the fish's tail (Figure 3.6A-C). Most fish generated multiple episodes of spontaneous swimming (spikes: N= 73 bouts, 12 fish). On average, spontaneous bouts lasted 428 ± 153 ms and featured mean swimming speeds of 31.9 ± 1.0 Hz. To test whether modulation of EN activity was similar

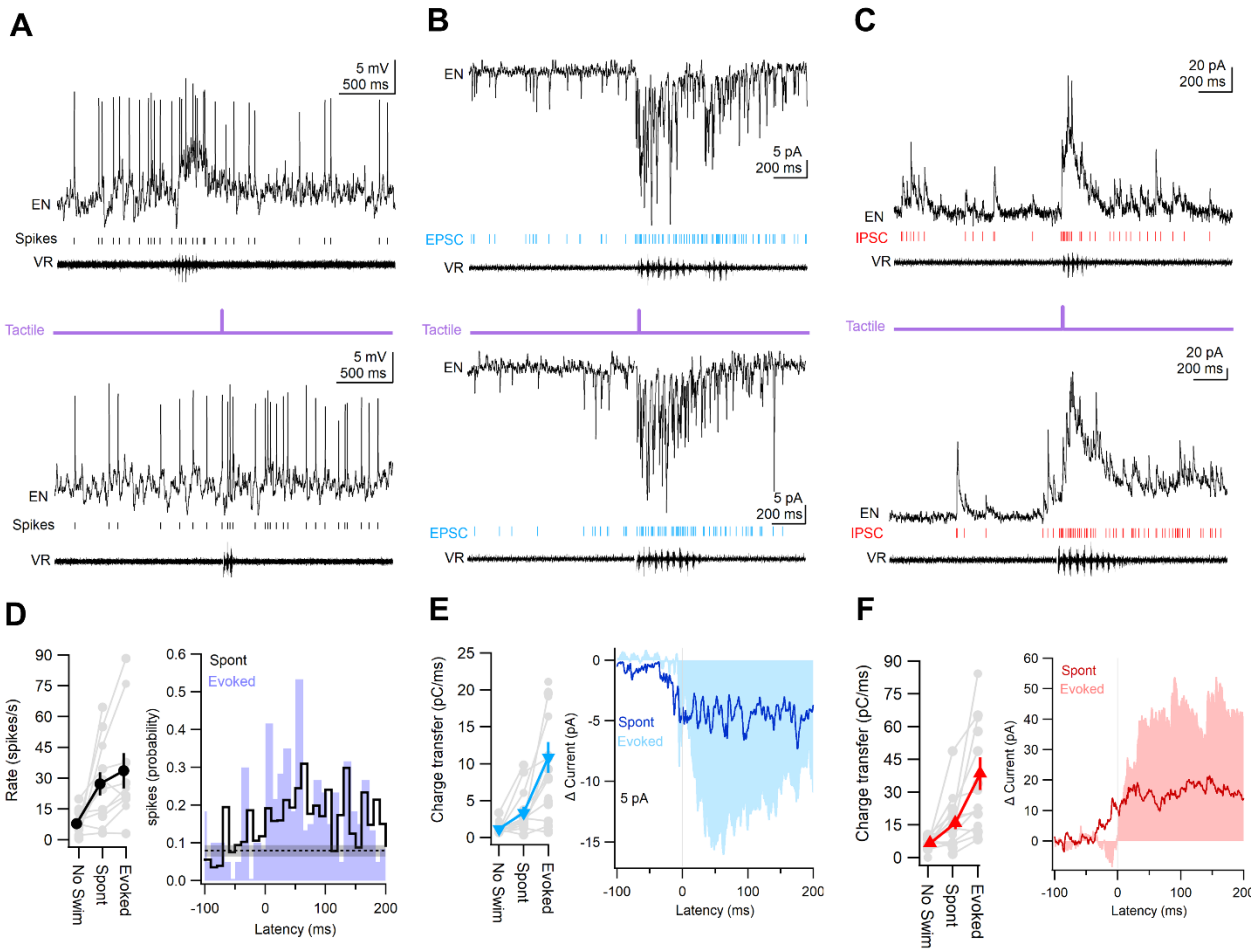

Figure 3.6. Spiking and synaptic responses to spontaneous and evoked swimming. (**A**) Example current-clamp recording and raster (black marks) of EN spikes during spontaneous (top) and evoked (bottom) swimming. Recordings from the same cell. Purple: timecourse of tactile stimulus delivered to tail (5 ms). (**B**) Example voltage-clamp recording and raster (blue marks) of parallel fiber EPSCs during spontaneous (top) and evoked (bottom) swimming. Recordings from the same cell. (**C**) Example voltage-clamp recording and raster (red marks) of Pkj IPSCs during spontaneous (top) and evoked (bottom) swimming. Recordings from the same cell. (**D**) Left, spike rate while the fish is at rest and during spontaneous and evoked swimming. Right, peri-swim triggered histogram of spikes during spontaneous (black) and evoked (purple), and the mean ± SEM baseline spike probability (dotted line). Bin=10 ms. Legend continued on next page.

Figure 3.6 continued. (**E**) Left, EPSC charge transfer during rest, spontaneous and evoked swimming. Swimming-related measurements normalized for bout length. Measurements at rest were calculated by measuring 0.01x cumulative charge transfer per 100 ms of rest. Right, voltage-clamp recordings of EPSCs collected during spontaneous (dark blue) and evoked (light blue) swimming. Recordings were zeroed to the average holding current 1s prior to swimming, each recording bout was averaged together for each cell, then the mean of all cells was calculated. Onset of swimming marked with grey line. (**F**) Left, IPSC charge transfer during rest, spontaneous and evoked swimming. Right, voltage-clamp recordings of IPSCs collected during spontaneous (dark red) and evoked (pink) swimming. Measurements made as described in 6E.

during reflexive swimming, we also evoked swimming with a brief tactile stimulus to the tip of the tail (spikes: N= 18 bouts, 10 fish). Consistent with recruitment of reflexive brainstem pathways responsible for evasive swimming maneuvers in larval zebrafish (Bhatt et al., 2007; Lacoste et al., 2015; Koyama et al., 2016), evoked swim bouts occurred with 100% reliability at a latency of 21.3 ± 2.1 ms from the stimulus, had mean swim speeds of 33.1 ± 1.6 Hz and lasted for 256 ± 42 ms.

Cells varied in how extensively their activity was modulated during swimming, but almost all cells showed increased spiking (Figure 3.6D, left). During spontaneous swimming, 11/12 cells generated more spikes during swimming, with rates increasing from 7.9 ± 1.5 spikes/s to 27.3 ± 5.7 spikes/s (*p=0.01 paired ttest*). Similarly, evoked swimming corresponded with more spikes in 10/10 cells, with rates increasing to 33.6 ± 8.6 spikes/s (*p=0.03 paired ttest*; *p=0.53* vs. spontaneous). Spike rates were elevated for ~100-150 ms during spontaneous an evoked swimming, lasting for a proportion of the entire swim bout (Figure 3.6D, right).

To examine changes in synaptic drive that may explain increased spike rates, we made voltage clamp recordings of pf EPSCs (spont: 89 bouts, 14 fish; evoked: 18 bouts, 18 fish; Figure 3.6B)

and Pkj IPSCs (spont: 70 bouts, 17 fish; evoked: 16 bouts, 14 fish; Figure 3.6C) during fictive swimming, and made measurements of charge transfer. EPSCs and IPSCs increased during both spontaneous and evoked swimming, leading to summation. For excitatory currents, the charge transfer was 2.82 ± 0.71 pC, or 3.32 ± 0.84 fC/ms when normalized for bout length (Figure 3.6E, left). In contrast, inhibitory currents summed to 7.68 ± 1.37 pC, or 15.7 ± 2.8 fC/ms (Figure 3.6F, left). During evoked swimming, EPSCs and IPSCs increased as well, and when compared to spontaneous swimming, the cumulative synaptic drive was greater. The charge transfer excitatory currents was 4.01 ± 0.78 pC or 10.8 ± 0.2 fC/ms (*p=0.009 paired ttest*; Figure 3.6E). For inhibitory currents, the charge transfer was 12.2 ± 2.4 pC, or 38.4 ± 7.5 fC/ms (*p=0.02 paired ttest*; Figure 3.6F). Thus, the amount of inhibitory drive exceeds excitatory drive during fictive swimming, and paradoxically corresponds to higher rates of spiking.

This observation raises the possibility that the timing of synaptic drive helps explain elevated spiking. We therefore examined the timing of spikes and synaptic drive, first in relation to the onset of spontaneous and evoked swimming. Of 12 cells in the dataset, 6 produced spikes that lead the swim onset, and the mean latency across all cells coincided with onset (1.0 ± 8.6 ms). In contrast, 2/10 cells spiked prior to the onset (latency=43 ± 29 ms; *p=0.15 vs spont, unpaired ttest*). An analysis of the latency of synaptic currents, measured from when currents began to summate to swim onset, revealed a similar trend. During spontaneous swimming, excitatory drive preceded inhibition in 4/8 cells in which both recordings were made. Summating EPSCs began -25.1 ± 11.3 ms prior to onset, while inhibition occurred -9.2 ± 14.5 ms prior to onset (*p=0.88*). During evoked swimming, synaptic drive lags the onset of swimming, with excitation

preceding inhibition in 7/9 cells in which both recordings were made. EPSCs were evident 6.2 ± 3.7 ms after onset (*p=0.005 vs spont, unpaired ttest*), while IPSCs occurred at 27.1 ± 8.0 ms (*p=0.004 vs spont, unpaired ttest*). These results indicate that, along with different amounts, the timing of synaptic drive differs between spontaneous and evoked swimming.

A possible explanation for spikes near the onset of spontaneous swimming is that excitation drives spikes in the window before the arrival of inhibition. However, we found that spike latencies did not fall into this window, with only one cell showing spiking after excitation but before inhibition. We also examined the relative timing of excitation and inhibition for cells that spiked prior to the onset of spontaneous swimming (N=4 cells). Contrary to our prediction, we found that 3/4 cells showed inhibitory drive *prior to* excitatory drive. These results suggest that spiking prior to swim onset is not due to escaping excitation. Rather, inhibition from Pkjs plays a role in the timing of these spikes.

3.3.7 Activity related to the motor burst cycle during spontaneous and evoked swimming

Next, we addressed the possibility that ENs generate action potentials that align with the motor burst cycle (i.e. the period between onsets of consecutive motor bursts; Figure 3.7A). Each episode of fictive swimming consists of many motor bursts (14.0 ± 4.0 bursts/episode). During spontaneous swimming, the mean burst cycle duration was 30.9 ± 3.1 ms, while the motor burst lasted 16.1 ± 4.5 ms. Similar values were measured for evoked swimming (burst cycle: 31.8 ± 1.1 ms, burst: 14.1 ± 0.7 ms). Thus, approximately half the motor burst cycle consisted of the motor burst itself, though the exact duration of each motor burst and cycle varied somewhat.

During spontaneous swimming, spikes occurred during 55.1 ± 7.3% of all burst cycles. The spike latency relative to the nearest burst onset was short (3.1 ± 0.8 ms), though spikes could be generated prior to or after the burst onset and the variation of their timing was high (CV=0.90 ± 0.06). During evoked swimming, ENs produced spikes during 57.7 ± 8.9% of cycles with a mean latency of 2.7 ± 1.9 ms (CV=0.81 ± 0.07). Thus, the firing of individual ENs often coincided with the motor burst, but the precise timing was variable and the rate too low to match the absolute timing of motor bursts.

We next investigated whether synaptic responses correlated with the burst cycle. In general, synaptic events observed from most cells did not obviously match the cycle, and instead summed to produce an envelope of tonic current that roughly matched the length of the swim bout (i.e. Figure 3.6B, 3.6C. 3.7A). However, examination of the recordings suggested that some cells showed phasic synaptic currents that rode on top of underlying tonic drive. To test whether these phasic synaptic events were entrained with the burst cycle and related to action potential timing, we calculated the timing of each synaptic event and spike relative to the motor burst cycle. For both spontaneous and evoked swimming, we first compared the timing of spikes, EPSCs, and IPSCs on a cell-by-cell basis. We then combined events across all cells and examined timing relative to the burst cycle to test how the population of ENs signaled.

Examination of events for individual cells did not reveal entrainment to the burst cycle. Furthermore, we observed no clear entrainment of all ENs to the burst cycle during spontaneous swimming when we considered the timing regardless of when in the episode the burst was generated (Figure 3.7B). However, when we combined spikes, EPSCs, and IPSCs across all

cells, while also considering the position of the burst cycle within the swim bout, we observed rhythmic synaptic drive and firing (Figure 3.7C). EPSCs were detected throughout and showed no tendency to occur at a precise time in the cycle. In contrast, IPSCs occurred more sparsely and were most likely to occur during the motor burst ("on-cycle"; Figure 3.7C). Spiking was also entrained to the burst cycle, with spikes frequently occurring late in the motor burst or just after the end of the motor burst. When we combined events from cells based on whether a given cell spiked prior to or after swim onset, we found that neither action potentials nor IPSCs were entrained to the burst cycle for either leading or lagging cells. Categorizing cells by their position in the cerebellar hemisphere also disrupted the entrainment apparent among all cells in the population.

During evoked swimming, we also observed no clear entrainment of individual cells, nor entrainment across all cells to the burst cycle alone (Figure 3.7D). Moreover, we observed less evidence of cyclical spiking and synaptic drive to the burst cycle within the structure of the swim bout (Figure 3.7E). EPSCs were uniformly distributed throughout the motor bout, whereas IPSCs occurred more sparsely. Though neither aligned to the burst cycle, IPSCs and spikes were anticorrelated, as indicated by alternating peaks evident in the histogram. Alteration was clearest during the first motor burst cycle, when the likelihood of IPSCs and spikes alternated three times, with minimal overlap. This observation raises the possibility that IPSCs and spikes are organized in part by the tactile stimulus used to evoke swimming.

Evoked swimming corresponds with a large increase in excitatory and inhibitory synaptic drive, which combines to elevate spiking in individual cells. Exact spike times are influenced by

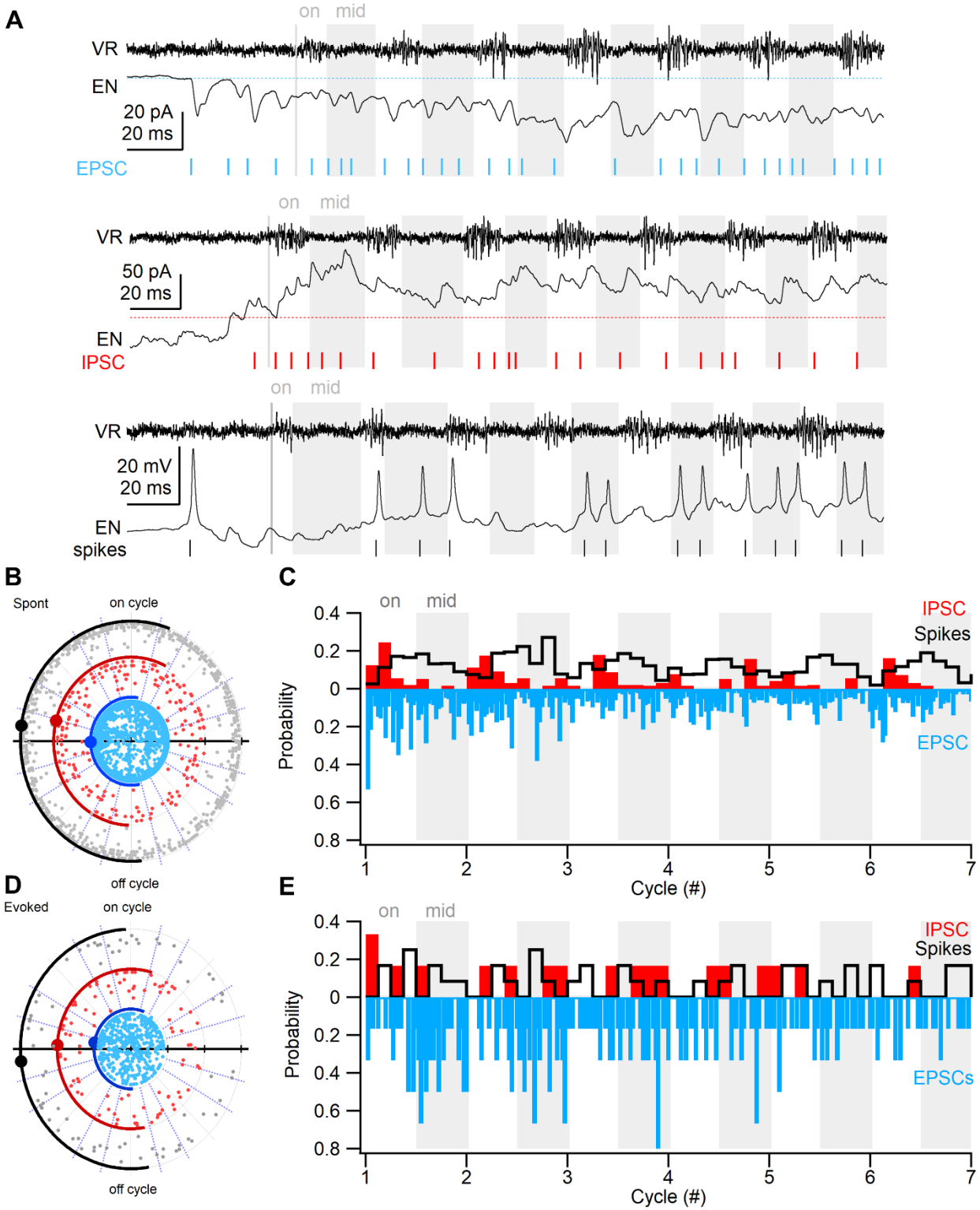
A
on
mid
VR
EN
20 pA
20 ms
EPSC
on
mid
VR
50 pA
20 ms
EN
IPSC
on
mid
VR
20 mV
20 ms
EN
spikes
B
Spont
on cycle
off cycle
C
on
mid
IPSC
Spikes
EPSC
Probability
0.4
0.2
0
0.2
0.4
0.6
0.8
1
2
3
4
5
6
7
Cycle (#)
D
Evoked
on cycle
off cycle
E
on
mid
IPSC
Spikes
EPSCs
Probability
0.4
0.2
0
0.2
0.4
0.6
0.8
1
2
3
4
5
6
7
Cycle (#)

Figure 3.7. Synaptic and spiking activity in relation to the burst cycle. (**A**) Example ventral root recordings during spontaneous fictive swimming, along with recordings and rasters of EPSCs (top, blue), IPSCs (middle, red), and spikes (bottom, black) made from the same EN. Dotted line: threshold for tonic excitatory (blue) or inhibitory (red) current, set to mean + SD of baseline current. Burst cycle marked with alternating white (on-cycle) and grey (mid-cycle) vertical bars. (**B**) Polar raster of EPSCs (blue), IPSCs (red), and spikes (black) during spontaneous swimming. Small circles are individual events, large circle with error bar is mean ± standard deviation for all events. Radius value corresponds to individual cell, ordered by number of events per recording. Top of graph (0-179º) corresponds to the the motor burst (on-cycle), with 0º=burst onset. Bottom of graph (180-359º) corresponds to the interburst period (mid-cycle), where 180º just follows burst offset and 359º is just before the onset of the subsequent burst. (**C**) Histogram of EPSCs (blue), IPSCs (red), and spikes (black) during spontaneous swimming. Histogram is average of the average histogram for each cell. Timing of the event = relative to the burst cycle + burst cycle number. EPSC probabilities plotted as negative values. Bin for EPSCs = 0.025 of cycle. Bin for IPSCs, spikes = 0.1 of cycle. Unshaded area=during motor burst (on-cycle). Gray shaded area= interburst period (off-cycle). Only first 7 burst cylcye included to ensure equal weighing of short- and long-duration swim episodes. (**D**) Same as B, but for evoked swimming. Fewer overall events are plotted because there were fewer episodes of evoked swimming in the dataset. (**E**) Same as C, but for evoked swimming.

inhibitory currents, but not entrained to the burst cycle. Furthermore, spike times and IPSCs occur with reliable timing such that their inverse relationship can be detected even when they are recorded from separate swim bouts. In contrast to evoked swimming, spike timing is entrained to the motor burst cycle at the population level during spontaneous swimming. This entrainment is not evident when all burst cycles are considered together, indicating that entrainment is not uniformly distributed across the swim bout. The precise timing of action potentials is likely influenced by Pkj IPSCs, which themselves are entrained to the burst cycle.

3.4 Discussion

In this study, we have characterized the basal synaptic and spiking activity of olig2^{+} ENs in the larval zebrafish cerebellum. ENs receive significant excitatory and inhibitory drive both at rest and during swimming. In general, inhibitory drive exceeds excitatory drive, though ENs still fire action potentials spontaneously and increase their firing during swimming. Examination of activity during sensory stimulation and fictive swimming revealed multiple modes of synaptic integration in ENs. Single, specifically-timed spikes were elicited by acute excitation in response to a visual sensory stimulus in a subset of cells. During spontaneous swimming, spiking occurred upon relief of rhythmically-modulated IPSCs. Similar anticorrelated activity was observed during evoked swimming, though inhibition was not aligned to the swim cycle, but instead seemed acutely influenced by the tactile stimulus. Thus, our data demonstrate that ENs are capable of responding to multiple kinds of input, integrating varying excitation and inhibition to produce different patterns of spikes.

3.4.1 Possible ontogeny of EN firing

We conducted our experiments soon after initial differentiation of olig2^{+} ENs (McFarland et al., 2008). The precise age likely varied across recordings and may relate to variation in the basal physiological properties of ENs. We observed that a subset of ENs were depolarized and silent for reasons not including differences in inhibitory drive or passive membrane properties. Another biological explanation for the absence of spikes is development of active membrane properties. In mammalian cerebellar nuclear cells, spontaneous spiking is supported by voltage-sensitive

conductances through $K_v3.1$ and $Na_v1.6$ channels (Afshari et al., 2004; Hurlock et al., 2009). In the zebrafish cerebellum, expression of both channel types gradually increases from 3-6 dpf in Pkj and non-Pkj types (Hsieh et al., 2014) though expression specifically in ENs has not been explored. Additional voltage-sensitive conductances are carried through P-type calcium channels, whose currents interact with calcium-dependent potassium channels to enhance repolarization (Raman et al., 2000). While expression of calcium channels in ENs has not been examined, zebrafish Pkjs show heterogeneous calcium-dependent spiking within the same time window (Sengupta and Thirumalai, 2015; unpublished observations), possibly reflecting differential development across cells. More broadly, development of the zebrafish cerebellum has most often focused on molecular phenotype (e.g. Bae et al., 2009; Takeuchi et al., 2017). As functional and behavioral experiments with these animals proceed, the physiological development of cells should be addressed more directly.

3.4.2 Features of parallel fiber inputs

ENs differ from mammalian cerebellar output neurons in that they receive excitatory inputs from pf rather than mfs (Meek et al., 1992; Bae et al., 2009). In mammals, these synaptic connections are not equivalent. Pf synapses are more numerous than mf synapses (~150,000 vs 800, respectfully; Isope and Barbour, 2002; De Zeeuw et al., 2011; Wu and Raman, 2017). Short- and long-term plasticity at these synapses proceeds through different mechanisms as well (reviewed by Mapelli et al., 2015). Indeed, it is possible that pf-EN synapses show multiple kinds of previously identified forms of plasticity, some of which are intrinsic to pfs and some of which

are intrinsic to cerebellar output neurons. In mammals, dynamic tuning of pf-Pkj synapses is likely essential for cerebellar learning and memory (Marr, 1969; Albus, 1971; Ito, 1984). Although some forms of plasticity are not anatomically possible in ENs, such as cf-dependent long-term depression, it is possible that ENs receive a similar number pf inputs as Pkjs, and that these inputs are similarly widely tuned.

In addition, interconnected Pkjs and ENs may receive synaptic input from the same pfs. In such an arrangement, inhibition would slightly lag excitation. Our analysis of synaptic drive during swimming revealed that excitation preceded inhibition for half of the cells, but followed it for the remaining. Preceding excitation could be explained by shared inputs or separate inputs that are simultaneously recruited. Additionally, such an arrangement would be predicted to promote spiking in the window between excitation and before inhibition. By analogy, nuclear cells show this form of spiking in response to cf stimulation, which leads to cf collaterals transiently promote spiking before Pkj complex spikes arrive and suppress it (Hoebeek et al., 2010; Biekenkemp and Lang, 2011; Tang et al., 2016). However, we did not find that spike timing fell within the excitation-inhibition window. An additional consequence is that these inputs may be particularly well-suited to undergo plasticity. For instance, a barrage of pf transmission could activate certain pf-EN synapses, followed by inhibition from Pkjs in response to the same pf volley. A similar pattern of sequential excitation and inhibition induces LTP at mf-nuclear cell synapses (Pugh and Raman, 2006). However, this plasticity mechanism relies on rebound firing upon relief of inhibition (Person and Raman, 2010), and it is unclear if ENs display rebound firing.

3.4.3 Inhibition from complex spikes

When simple spikes were suppressed, we observed a lower frequency of IPSCs and an overall reduction in IPSC amplitude. Based on their amplitude and frequency, these IPSCs are attributable to individual presynaptic complex spikes, and are the first of such recordings to be reported. Previous work has found that complex spikes can dramatically attenuate spiking of cerebellar nuclear cells particularly when multiple Pkjs fire simultaneously (Hoebeek et al., 2010; Blenkinsop and Lang, 2011; Tang et al., 2016). Simultaneous complex spiking by neighboring Pkjs has been observed during a variety of behaviors (e.g. Lou and Bloedel, 1992; De Gruijl et al., 2014; Bengtsson and Jörntell, 2014; Tsutsumi et al., 2015), and complex spike-dependent depression of nuclear cell firing is likely as well. Complex spiking can be monitored across all Pkjs in the larval zebrafish through calcium imaging. However, previous experiments that have used this approach (e.g. Aizenburg and Schuman, 2011; Ahrens et al., 2012; Matsui et al., 2014a) have not reported synchrony of calcium transients during cerebellar behaviors.

Changes in spiking in response to single complex spikes are less dramatic (Bengtsson et al., 2011). In addition, the complex spike waveform form most larval zebrafish Pkjs display does not include spikelets (Sengupta and Thirumalai, 2015; Scalise et al., 2016; Harmon et al., 2017). In mammalian Pkjs, these secondary, axonally-sourced spikes propagate down the axon with moderate reliability and likely prolong the inhibitory effect of complex spikes (Khaliq and Raman, 2005; Davie et al., 2008). The absence of spikelets could be related to the Pkj axon in larval zebrafish, which is short (2-8 μm; Matsui et al., 2014a) and likely does not have a high

density of sodium channels. Overall, these results demonstrate that in the zebrafish cerebellum, Pkj complex spikes exert similar levels of inhibition as simple spikes.

3.4.4 Purkinje-eurydendroid convergence

The pattern of spontaneous IPSCs was consistent with convergence of multiple Pkjs onto individual ENs. Basal IPSC rates suggested convergence of 2-5 inputs/EN, while analysis of the intervals between IPSCs suggested convergence of as many as 7 Pkjs. In addition, by comparing IPSC intervals with those constructed from randomly selected Pkjs, we determined that converging Pkjs are more likely to produce IPSCs closely in time such that they summate. This suggests that, even when the fish is at rest, firing of converging Pkjs is not independently timed, but instead organized so that Pkjs fire together. This organization is likely achieved by shared synaptic input, a feature of neighboring Pkjs that has consequences for cerebellar computations (Oscarsson 1979; Sugihara and Shinoda, 2004; De Zeeuw et al., 2011; Valera et al., 2016). Furthermore, IPSCs became spread out in time and were not particularly large when simple spikes were suppressed, indicating that shared cf drive could not explain short IPSC intervals, nor were simultaneous complex spikes generating indistinguishable IPSCs that summated. Instead, these results implicate shared pf drive in the generation of similarly-timed Pkj spikes.

Shared synaptic input is likely crucial for synchronization of Pkjs, a phenomenon observed during many cerebellar behaviors (Bell and Grimm, 1969; Heck et al., 2007; de Solages et al., 2008; Wise et al., 2010; Brown and Raman, 2018) and that likely regulates the timing of nuclear cell spikes (Gauck and Jaeger, 2000; Person and Raman, 2011; Wu and Raman, 2017). We are

uncertain of the precision of IPSC timing during fictive swimming because IPSCs could not be separated if they occurred in short succession. However, we observed significant summation of inhibitory currents, suggesting that multiple presynaptic Pkjs were recruited in concert.

Based on previous estimates of Pkj number and axon morphology, the convergence ratio we report here would not have been predicted. Previous estimates of Pkj number reported ~150 parvalbumin^{+} Pkjs per hemisphere in 6-day-old fish (Hamling et al., 2015), while we counted ~200 olig^{+} ENs. With the addition of olig2^{-} ENs (of which no counts have been reported), these results would suggest that ENs significantly outnumber Pkjs. Convergence is still possible if Pkjs innervate multiple ENs. However, Pkj axons do not show clear branching (Matsui et al., 2014a) and are too short to form serial synaptic connections with multiple ENs along the same axon. Thus, anatomical evidence does not support divergence at this synapse. Incongruent cell counts are likely attributable to differences in methodology. Pkjs were visualized by immunohistochemically staining for parvalbumin, whereas we visualized olig2^{+} ENs using conditional expression of fluorescent proteins in transgenic animals. Parvalbumin is likely expressed in all zebrafish Pkjs (Bae et al., 2009; Takeuchi et al., 2015), though it is unclear whether expression occurs immediately after Pkj differentiation or if there is a lag. Expression of olig2 in ENs seems to occur soon after differentiation (McFarland et al., 2008). In fact, olig2 expression precedes parvalbumin expression by ~16 hrs. Therefore, our cell counts may have included a greater number of newly differentiated cells. Another difference is that our fish were housed without phenylthiourea, a compound that is commonly added to prevent pigmentation, though it has various off-target effects (e.g. Elsalini and Rohr, 2003; Li et al., 2012; Parker et al.,

2013). Additional counts in which methodology is matched between cell types could resolve this discrepancy.

3.4.5 Spiking to visual sensory stimulation

Presentation of a visual stimulus elicited an excitatory synaptic response and acutely increased the likelihood of an action potential 100-200 ms after light onset in a subset of cells. The peak likelihood of EPSCs slightly lagged that for spikes. Though some variation in the timing of synaptic events is expected between recordings, it is possible that the connection between the two is coincidental. However, the latencies of synaptic responses and spike modulation match those recorded from Pkjs in response to the same stimulus (Harmon et al., 2017). Thus, even if the timing of spikes and EPSCs does not perfectly align, the timing of each event separately agrees with previous data.

A plausible interpretation for our data is that phasic excitatory synaptic drive can acutely increase the likelihood of EN spikes. Cerebellar nuclear cells show similar modes of firing. For example, spiking of these neurons is elicited with moderate reliability by acute mf input in anesthetized rats (Yarden-Rabinowitz and Yarom, 2017). Under these conditions, spikes occurred less reliably upon relief of inhibition. Our results agree with these previous findings and suggest that specifically-timed action potentials can be elicited by a mode of synaptic input in which acute excitation promotes spiking during mild, disorganized inhibition from Pkj. This mode of firing is observed in a subset of ENs in response to sensory stimuli.

3.4.6 Spiking during spontaneous swimming

While we found that individual ENs did not produce spikes that were clearly aligned to the burst cycle during spontaneous swimming, spiking was entrained when the activity of all ENs was combined. Specifically, we observed that population firing peaked at the transition between on-cycle and mid-cycle (i.e. the end of the motor burst recorded from the ipsilateral side of the tail). Furthermore, the onset of swimming coincided with EN spikes (with some variability) and was preceded by excitatory and inhibitory synaptic drive. These findings raise the possibility that ENs actively participate in executing volitional swimming.

Our findings are consistent with previous reports of cerebellar nuclear cell firing during locomotion in decerebrated and awake cats and mice (Orlovsky, 1972a; Armstrong and Edgley, 1984a; Sanaik and Raman, 2018). In each of these studies, spiking during the step cycle varied on a cell-by-cell basis, but the average response across all cells showed clear entrainment to the step cycle. Stimulation of the cerebellar nuclei elicits movements, while lesions decrease muscle tone (Orlovsky, 1972b). These findings support the hypothesis that cerebellar nuclear cells are contributing to locomotion, specifically movement of the ipsilateral fore and hind limbs.

Rhythmic firing during fictive swimming could reflect alternative modes of cerebellar processing. Firstly, ENs could be actively involved in initiating and executing volitional swimming. If this were the case, we would expect EN firing and synaptic drive to precede the onset of swimming. While average EN spike times did not lead but instead coincided with swim onset, we observed variability in spike timing such that some cells (i.e. leading neurons) preceded while others lagged swim onset, raising the possibility that not all ENs contribute to

initiation of swimming. Limiting our analysis to leading neurons disrupted entrainment of spiking to the burst cycle, however. This raises the possibility that ENs contribute differentially to swimming, with leading cells participating in initiation and a larger group of cells contributing to swim execution. Causal relationships between EN firing and swim execution could be tested with experiments in which EN firing is manipulated during swimming.

Instead of actively driving movement, it is possible that ENs simply respond to movement. In this configuration, synaptic drive reports that a swim movement is underway, and spike patterns that result from this input are permissive for, rather than controllers of, ongoing movement. While passive cerebellar output may be optimal during execution of certain well-established movements, motor command synaptic drive may become useful for plasticity that supports movement adaptation. The observation that spikes tended to occur near motor burst offset is consistent with this mode of processing, since these spikes would be ill-suited for initiating motor bursts.

Spikes are timed well for controlling other aspects of tail movement during swimming, however. For instance, ENs spikes could initiate cessation of contraction of ipsilateral tail muscles, the site of the ventral root recording. Alternatively, ENs might initiate contraction of the contralateral tail muscles, since the ipsilateral mid-cycle period corresponds to the on-cycle period on the contralateral side of the tail. In support of this possibility, unilateral optogenetic excitation of Pkjs reduces contractions of the tail to the contralateral side, possibly through suppression of EN firing (Matsui et al., 2014a). Other evidence for lateralized cerebellar contributions to movement is mixed. EN axons generally remain ipsilateral (Heap et al., 2013; Matsui et al., 2014a), with the

notable exception of projections to the red nucleus (Matsui et al., 2014b). Projections of putative target neurons in the nMLF terminate bilaterally in the spinal cord (Wang and McLean, 2014), though unilateral ablations and stimulations suggest that nMLF cells drive ipsilateral contraction (Thiele et al., 2014). In contrast, axons of red nucleus neurons terminate contralaterally (i.e. ipsilateral to upstream EN neurons; Matsui et al., 2014b). Therefore, an important step in determining whether ENs actively drive swimming will be to test which upstream neurons act as an intermediary between the cerebellum and spinal circuits that control swimming.

In walking mammals, individual cerebellar nuclear cells show stereotyped responses across cycles. We observed less stereotyped responses for individual cells, likely because fewer episodes went into our dataset, spike rates were lower compared to nuclear cells (~27 vs. ~80 spikes/s), and the burst cycle was shorter in duration (~30 ms vs ~200-300 ms). Thus, spiking rates of individual cells were too low to keep up with motor bursts. A possible explanation for this finding is the absence of reafferent sensory drive in the fictive swim preparation. In walking mammals, proprioceptive feedback communicated to the cerebellum provides rhythmic mf drive that is aligned to the step cycle (Arshvasky et al., 1972; Orlovsky, 1972a). While zebrafish lack the sensory organs for proprioception, somatosensory systems that detect mechanical stress induced by swimming may provide analogous input during normal tail movements (Lee and Bulluck, 1984; Williams et al., 2013; Requarth et al., 2014; Knafo et al., 2017). Additional synaptic drive would likely elevate spike rates further, though Pkj spiking would also likely increase. Furthermore, more rhythmic input could alter entrainment to the burst cycle and

produce more stereotyped responses of individual ENs. Experiments in which the tail can move freely could address these possibilities.

3.4.7 Synaptic contributions to spontaneous swimming

Elevated firing during spontaneous and evoked swimming corresponds to increased synaptic drive from pf and Pkj inputs. Inhibitory currents are larger than excitatory currents, more readily summate, and correspond to a higher conductance. Thus, paradoxically, inhibitory synaptic drive predominates over excitation while spiking is elevated during fictive swimming. IPSC amplitudes may have been larger than EPSC amplitudes because Pkj-EN synapses are somatic, whereas pf-EN synapses are dendritic (Alonso et al., 1992; Meek et al., 1992; Bae et al., 2009; Matsui et al., 2014a). Thus, EPSC amplitudes could have been attenuated by filtering, and recordings from the dendrite may have revealed larger EPSC amplitudes. In addition, voltage sensitive channels in the dendrite may be activated when the membrane potential is unclamped, acting as a signal boost for excitatory synaptic drive. This phenomenon has been reported in cerebellar nuclear cells which have dendritic voltage-gated calcium conductances that are activated by excitatory synaptic drive as well as disinhibitory spiking (Gauck et al., 2001; Zheng and Raman, 2009; Schneider et al., 2013). Homologous conductances in ENs could act to enhance pf drive and promote spiking.

Inhibitory and excitatory synaptic currents contribute differentially to spiking during spontaneous and evoked swimming. EPSCs were uniformly distributed across the burst cycle, suggesting that they provide a tonic tone of excitation that promotes spiking generally. In

contrast, we found evidence that ENs spike following IPSCs, with IPSCs entrained to the burst cycle of spontaneous swimming but not evoked swimming. Detection of patterns after data has been combined across cells and episodes of swimming requires that IPSC and spike timing is reproduced across episodes. Control of spike timing by Pkj inhibition has been demonstrated before in cerebellar nuclear cells through modeling and *in vitro* experiments (Gauck and Jaeger, 2000; Person and Raman, 2011; Sudhakar et al., 2015). Furthermore, asynchronous excitatory drive can integrate with structured inhibition to facilitate temporally-precise spiking (Wu and Raman, 2017). In agreement with these findings, our data provide *in vivo* evidence for the control of spike timing by Pkj inhibition.

3.4.8 Purkinje drive during evoked swimming

Although Pkj IPSCs show entrainment occurs at the population level during spontaneous swimming, individual Pkjs do not entrain to the burst cycle, though most show significantly elevated simple and/or complex spiking (Sengupta and Thirumalai, 2015; Scalise et al., 2016; Harmon et al., 2017). Many Pkj spikes likely contribute to tonic IPSC drive that coincides with phasic, rhythmic inhibition. Evoked swimming featured greater inhibitory drive overall and no entrainment to the burst cycle. Thus, during reflexive swimming, tonic inhibitory drive predominated over rhythmic drive. Compared to spontaneous swimming, Pkjs respond to evoked swimming by producing more complex spikes at short latencies (Harmon et al., 2017), raising the possibility that cf drive disorganizes simple spiking that has been elevated and likely organized by pf drive. Complex spiking may reflect responses of olivary neurons to the tactile

stimulus, rather than to swimming, which could in turn explain the alternating IPSC-spike pattern evident during the first burst cycle. Thus, spiking and synaptic drive could appear less organized because sensory and motor signals are mixed.

Putatively disorganized spiking seems to have little effect on the execution of evoked swimming, which was comparable to spontaneous swimming in many respects. These kinds of swimming rely on separate motor circuits, raising the possibility that ENs exert less influence over neurons involved in reflexive swimming. Elevated (though disorganized) spiking may instead be important for inducing plasticity in ENs. In cerebellar nuclear cells, elevated spiking, particularly during post-inhibitory rebound, activates calcium currents necessary for induction of potentiation of mf EPSCs (Person and Raman, 2010). Furthermore, in previous work from our lab (Harmon et al., 2017), the tactile stimulus used to evoke swimming was used as an unconditional stimulus in an associative learning task that is predicted to rely on potentiation of pf-EN synapses. Examination of EN spiking and excitatory drive during associative learning could provide important insights into the role of potentiation of excitatory inputs to output neurons during cerebellar learning, and address the possibility that reflexive, involuntary movements induce a "teaching signal" that supports plasticity within the cerebellar circuit.

3.5 Materials and Methods

3.5.1 Zebrafish

All procedures conformed to NIH guidelines and were approved by the Northwestern University Institutional Animal Care and Use Committee, protocol IS00000242 (IMR). Wildtype zebrafish (*Danio rerio*) were obtained from an in-house facility (Aquatic Habitats, Beverly, MA). Olig2:GFP fish were kindly provided by Dr. Bruce Appel (University of Colorado, Denver; McFarland et al., 2018). Tg(Arch-tagRFP-T:car8:GCamp5) fish ("Arch^{+}" fish), were kindly provided by Dr. Reinhard Köster (Technical University Braunschweig, Germany; Matsui et al., 2014a). vGlut2A:RG fish were kindly provided by Dr. Shin-ichi Higashijima (Okazaki Institute for Integrated Biology, Japan; Miyashi et al., 2009). Transgenic fish were screened for GFP and/or RFP fluorescence at 5 days postfertilization (dpf). Fish were housed in system water (28.5°C, pH=7.3, conductivity = 550 μS) and maintained on a 14-hour light:10-hour dark cycle. Experiments were done between 10 am and 7 pm at room temperature (~22°C) on larval fish (6-8 dpf, before sexual differentiation).

3.5.2 Electrophysiology

Recordings were conducted as previously described (Drapeau et al., 1999; Masino and Fetcho, 2005; Wang and McLean, 2014; Harmon et al., 2017). Each fish was immobilized by 3-minute immersion in α-bungarotoxin (1 mg/ml, Tocris, Bristol, United Kingdom) in system water followed by 5 minutes in "extracellular solution" containing (mM): 134 NaCl, 2.9 KCl, 2 MgCl2, 10 HEPES, 10 glucose, and 2.1 CaCl2, buffered to pH 7.8 with NaOH, with final osmolarity 290 mOsm. The immobilized fish was transferred to a Sylgard-lined plastic recording

chamber containing extracellular solution, with 0.01% MS-222 anesthetic added for experiments involving dissection for neuronal recordings. The fish was secured to the Sylgard surface with pins so the dorsal side of the head and the left side of the tail faced up. A midline incision was made and the skin was pinned to expose the brain. For recordings from peripheral motor nerves (ventral roots) along the tail, the skin was removed on the left side, from the rostral edge of the swim bladder to 3-5 segments rostral to the tail tip.

The brain was visualized with IR-DIC microscopy on a FS2 Axioskop (Zeiss, Oberkochen, Germany). The locations of electrophysiologically characterized Purkinje cells were captured with a SensiCam camera (PCO.Imaging, Kelheim, Germany) and/or from the coordinates of the Sutter MP-385 manipulator. Borosilicate patch pipettes were pulled to tip resistances of 8-12 MΩ and filled with intracellular solution containing (mM): 120 K-gluconate, 12 Na-gluconate, 3.2 NaCl, 2 MgCl2, 0.025 CaCl2, 1 EGTA, 0.3 mM Tris-GTP, 1 MgATP, 14 creatine phosphate, 10 HEPES, and 3 Alexa Fluor 594 hydroxide, buffered to pH to 7.4 with KOH. Whole-cell recordings were made with a Multiclamp 700B and Digidata 1322A with pClamp software (Molecular Devices, Sunnyvale, California) from Purkinje neurons left hemisphere of the cerebellum. Data were acquired at 50 kHz and filtered at 10 kHz. Command voltages were adjusted for the junction potential (-12 mV). Voltage clamp recordings were made at -63 mV (E_{Cl} =-75 mV) for EPSCs and at +12 mV for IPSCs. No series resistance compensation was applied. In current clamp, bridge balance and capacitance neutralization were also applied.

For ventral root recordings, patch pipettes were cut to a 20-50 μm tip diameter, heat-polished, and bent to ~20° to improve contact with the body wall. The pipette was filled with extracellular

solution and placed on the intermyotomal cleft at the 8-10 segment of the tail. Recordings from the ventral root were made with an Axopatch 200B (Molecular Devices) amplifier in current clamp mode with low and high frequency cutoffs of 300 and 4000 Hz.

Visual stimulation was delivered through illumination of a blue LED (470 nm, 53 lux, 2 s) that was surrounded by a 3 cm aluminum foil disk, positioned ~5 cm above and ~30° to the left of the fish's head. Evoked swimming was elicited with a brief electrical current (1 mA, 5 ms) applied to the tail tip by a concentric bipolar stimulating electrode (WPI, Sarasota, Florida). Experiments were conducted with the microscope light on (1100–4500 lux) and the objective placed directly above the fish.

3.5.3 Targeting fluorescent cells

GFP was made to fluoresce with a blue LED directed through the objective (488 nm; Thor Labs, Newton, New Jersey). Archaerhodopsin-3 (Arch) was activated by a green LED directed through the objective (565 nm; 5400 lux; Thor Labs, Newton, New Jersey). The size of the illuminated area was adjusted with an iris diaphragm to limit illumination to the minimum diameter necessary to illuminate the whole cerebellum. Deliver of both GFP and Arch light was controlled with a Master-9 Pulse Stimulator (A.M.P.I, Jerusalem, Israel).

Initial recordings of ENs in fish that expressed Arch in Pkjs revealed that the rates of IPSCs were depressed compared to recordings from wildtype fish (6.6 ± 1.7 IPSC/s vs 14.1 ± 1.5 IPSCs/s; *p=0.003 unpaired ttest*). Decreased IPSC rates may be attributable to diminished simple spiking in a subset of $Arch^{+}$ fish. To test whether exposure to high-intensity blue light (488 nm) used to visualize GFP lead to diminished simple spiking, we recorded from Pkjs in $Arch^{+}$ fish (N=2 cells

per group) while illuminating Pkjs with blue light in a constant or strobed (light on for 30 ms, off for 30 ms) manner for 5 minutes. Constant and strobed blue light acutely decreased spike rates (20.1 ± 6.4 spikes/s vs 6.9 ± 3.4 spikes/s during light; *p=0.03 paired ttest*). Also, simple spiking remained depressed after light was removed (4.1 ± 0.9 spikes/s; *p=0.08*). Spiking recovered to a greater extent in strobed cells, returning to 41% of the initial rate, while constantly illuminated cells recovered to 16% of the initial rate. From these results, we decided to limit our analysis to cells in which GFP^+ cells were strobe-targeted and took care to minimize exposure to high intensity light. Fish were screened at least 1 day prior to experiments, and light exposure was limited to brief flashes delivered focally through the screening scope objective. For simple spike suppression experiments, IPSCs recorded prior to Arch activation were used as control IPSCs. Arch activation was limited to 30-60 s and no data collected after sustained Arch activation was used.

3.5.4 Analysis of electrophysiological events

Electrophysiological data were analyzed in IGOR-Pro (Wavemetrics, Lake Oswego, Oregon). The electrophysiological recordings from ENs were smoothed with a 1 ms moving box average then differentiated. Rate of rise (dI/dt for voltage clamp, dV/dt for current clamp) was used to find putative synaptic current or action potentials.

Action potentials could be unambiguously detected in current clamp recordings by extracting events that cross 5 mV/ms in the dV/dt record. Voltage clamp recordings of EPSCs and IPSCs were analyzed in similar fashion. For IPSCs, positive dI/dt values were extracted from the differentiated record. In addition, the current values matching the timepoints of positive

deflections extracted from the dI/dt record were extracted and analyzed separately. Positive dI/dt values represent all positive deflections made in the voltage clamp recording, including IPSCs and electrical noise. The mean and SD of these values was measured and used to set a threshold value. Putative IPSCs were then distinguished as timepoints in the voltage clamp record that corresponded to when the differentiated record crossed the threshold value (mean + 3*SD of all positive noise). Next, the mean and SD of extracted current values was measured and used to set a threshold current value. Putative IPSCs were retained if they crossed the mean + 2*SD above the current threshold. Thus, rate of rise was used primarily to detect events, while current was used to secondarily confirm putative events. In addition, because events could not be reliably detected if their rising phases overlapped, putative events were discarded if they occurred <1 ms after the previous event. A similar procedure was used to extract EPSCs, except that negative noise. dI/dt threshold was set to mean - 3*SD of the negative noise, and current threshold was set to the mean - 2*SD.

The electrophysiological recordings from the ventral root were rectified and smoothed with a 2 ms moving box average. Examination of the smoothed and original record revealed no change in the onsets of motor bursts. Motor bouts were discrete and easily distinguished from background by examination of the original record. Individual motor bursts were detected by applying a threshold to the smoothed record, which was set at the mean + 5*SD of the noise in the smoothed record. Upward deflections were counted as motor burst onsets, whereas downward deflections were offsets.

3.5.5 IPSC simulations

Recordings from 27 Pkjs were used to construct simulated patterns of IPSCs. Cells for which spiking was recorded at the beginning of training for at least 30 s without spontaneous swimming were used. Interspike intervals between previously identified simple and complex spikes (Harmon et al., 2017) were measured and exported into a lookup table. To construct simulated spike trains, a Pkj was first chosen at random from the data set. Interspike intervals were then sampled randomly and sequentially added to the spike train such that the "spike time" was equal to the previous spike time plus the sampled interspike interval. The first spike time in the train was equal to the first interval sampled. Random sampling was repeated for each individual spike time until 10^5 spike times had been simulated.

For simulations that assumed convergence, additional Pkjs were chosen at random and separate trains of spike times were constructed. Pkjs were chosen with replacement, and simulations were independent of one another. Once the number of constructed trained equaled a specified convergence ratio (1-10 Pkjs), spike times across all simulations were aggregated and sorted, thereby mixing spike times. Because trains were independent, simultaneous simulated spikes were possible. Intervals between aggregated and sorted spike times were calculated. A probability histogram (bin=1 ms) was then constructed for the simulated intervals, and the proportion of intervals <8 ms was calculated.

For each EN, the distribution of simulated IPSC intervals was constructed by randomly sampling intervals measured form recorded IPSCs. The number of samples was equaled the number of samples in the aggregation of Pkj spike trains. A probability histogram was constructed from

these intervals and plotted against the simulated intervals histogram. The overlap was defined as the summed bin-by-bin minimums between the two distributions. Complete overlap would have a value “1”, no overlap would have a value of “0”.

After the overlap values were measured, the simulation restarted by sampling a new set of Pkjs. All previously use simulated spike trains were discarded. This process was repeated 10^3 times. Each simulation was likely to be constructed from a new combination of Pkjs. For instance, simulations that assumed a convergence of 3 Pkjs/EN could be constructed from $27^3 = 19683$ different combinations of Pkjs, meaning the chance of particular combination being selected twice in 1000 simulations was 0.26%.

3.5.6 Statistical analysis

Statistical tests are listed in the text. Paired or unpaired t-test and Pearson correlation was used. Paired t-tests were used when comparing measurements made from the same cell.

Chapter 4: Discussion and future directions

My research has contributed to a body of evidence that demonstrates shared features between mammalian and teleost cerebella. Given the immaturity of larval fish and the phylogenic distance between fish and mammals, commonalities likely reflect essential features of cerebella across all vertebrate species, including humans. In my thesis project, I have made some of the first intracellular recordings from neurons in the larval zebrafish cerebellum. My experiments have revealed the basal properties of synaptic drive made onto Pkjs and ENs. For Pkjs, I have described heterogeneous responses to sensory stimuli, spontaneous swimming, and evoked swimming. These synaptic responses, along with the position of the cell, partially predicted how each cell responded during learned swimming. Plasticity during training also proceeded differently, with different Pkj cell types responding to different aspects of the task. Manipulation of Pkj simple spiking revealed a transient instructive role during learning, where Pkjs promote plasticity elsewhere in the cerebellar circuit. ENs receive substantial inhibitory input from Pkjs. I found that inhibition from individual complex spikes is as strong as that from simple spikes, and that between 2-7 Pkjs synapse onto each EN. Although excitatory drive more consistently contributes to EN responses to a visual stimulus, inhibition induces patterned spiking in ENs during fictive swimming.

In this final chapter, I will address findings from my project more broadly, focusing on similarities and differences between fish and mammal while emphasizing directions for future experiments.

4.1 Comparison of learning and expression of conditional responses

Our associative learning experiments share much in common with other forms of cerebellum-dependent learning, such as eyelid conditioning. However, there are some notable differences worthy of further examination. In this section, I contrast features of the CR in the task we have employed to that of eyelid conditioning. I address individual differences in the ability to learn observed among fish, features of CR (specifically, timing and rate of acquisition) and offer a mechanism that allows for its acquisition and expression. Lastly, I speculate about motor circuits downstream of ENs that execute the CR.

4.1.1 Individual differences in learning ability

Our results indicate that only a proportion (~ 40%) of larval zebrafish acquire the CR. This finding has several possible explanations that are not mutually exclusive. Firstly, compared to other learning paradigms, the task we designed was rather difficult. To qualify as a fish that learned, CRs must have emerged after 10s of pairings. This was done to ensure that CRs emerged quickly enough that neuronal recordings could be made from the beginning of training to the end. However, it is likely that more pairings would lead to CRs in more fish.

Secondly, the health of individual fish likely affected acquisition. The dissection needed for these experiments was invasive, as it resulted in exposure of the brain, rotation of the tail, and removal of the skin from the tail. Although we monitored signs of health such as the heart beat and blood flow, it is possible that the physical stress of the dissection precluded learning in some fish. Anecdotally, in pilot experiments in which we did not rotate the tail or expose the brain, fish

learned more reliably, indicating that adapting this paradigm for freely-swimming fish may result in fewer failures.

Separate from the dissection, it is also possible that some fish were unhealthy or otherwise developmentally delayed at the time of the experiment. One sign of health that we monitored was the state of the swim bladder. We observed that fish with small or absent swim bladder invariably failed to learn. Other signs of poor health that we noted were enlarged eyeballs, which suggests osmotic stress, and blotchy skin. Developmental delays are more difficult to assay. Arguably, it is conceivable that, in clutches of 100s of fish, some proportion of fish are developmentally delayed and may even fail to thrive long-term. Delays corresponding to a couple hours in developmental time could produce noticeable changes in behavior among animals that are 120-168 hours old. Notably, using a less invasive preparation and older fish (20 dpf), a separate group reported cerebellum-dependent associatively learned bradycardia in ~ 40% of larval zebrafish in their study (Matsuda et al., 2017). Thus, failure to learn may be a persistent phenotype for certain fish, and whether it predicts features of adult fish remains to be determined.

4.1.2 Possible mechanism for CR acquisition and expression

The associative learning task we have employed leads to CRs much faster than eyelid conditioning. In our task, CRs emerge within 10s of trials, with fish reaching asymptotic learning levels in 40-50 trials. Eyelid conditioning, by comparison, requires 100s of pairings delivered across multiple sessions, with the period between sessions providing an opportunity for memory consolidation as well. Another difference is the timing of the CR during the CS. In our task, the

initial CR occurs late in the CS, but subsequently is executed near the CS onset as the fish receives more training. The opposite pattern occurs in eyelid conditioning, where the well-learned CR occurs just before the delivery of the US. Behaviorally, these responses are intuitive. Conditioned swimming would lead to avoidance of the tail shock if the fish could move freely, regardless of when the CR occurred during the cue. Conditioned eyelid closure, on the other hand, is only advantageous if the eyelid is closed when the airpuff US is delivered.

Differences in CR timing reflect differences in the state of the cerebellar circuit following plasticity that occurs during training. The slow learning rate of the eyelid closure CRs may reflect additional trials needed to induce plasticity at multiple sites. For eyelid conditioning, long-lasting changes likely occur at Pkjs and nuclear cells (reviewed by Freeman and Steinmetz, 2011). LTP at mf-nuclear cell synapses is promoted by coincidental activity from Pkjs that may be learned during conditioning (Pugh and Raman, 2006). In contrast, plasticity likely occurs at pf-Pkj synapses and at pf-interneuron synapses to generate Pkj simple spike pauses associated with CRs (Jirenhed et al., 2007; Wetmore et al., 2014). Therefore, a possible explanation for short latency CRs (which are observed early in training or induced by lesions to the cerebellar cortex; Ohyama et al., 2006) is that CS-related mf drive to nuclear cells leads to increased nuclear cell firing rate immediately after CS onset and execution of the CR. Well-timed CRs are only executed after Pkj spiking has been altered by additional plasticity in the cerebellar cortex.

In contrast, pf-EN LTP may be the most essential long-term change to the cerebellar circuit for producing the fictive swim CR. In ENs, inhibition by ZCS and MCS Pkjs likely overlaps with CS-related pf drive. While it is unknown if ENs display post-inhibitory rebound firing, they

would display elevated spiking during the UR. It is possible that UR-related spiking leads to a calcium influx typically associated with rebound spiking in the LTP induction protocol for mf synapses. After plasticity is complete, ENs may convert CS-related phasic excitatory drive from pfs into a burst of action potentials that feeds forward into upstream motor circuits. This "go signal" mechanism assumes that the pattern of Pkj spiking during the CS is permissive for increased EN spiking. Multiple spike patterns could fulfill this requirement.

One possibility is that Pkj firing in response to the CS could decrease as the fish reaches asymptotic CR expression. Decreased spiking could be achieved by an increase in inhibition from molecular layer interneurons. This possibility assumes that increased CS-related interneuron recruitment lags behind increased Pkj simple spiking, such that simple spikes can promote plasticity in ENs only until interneurons begin responding to the CS. To address this possibility experimentally, recordings of Pkjs from when the CR is first executed to when CR is performed at asymptotic levels would be useful, as simple spiking during the CS would be predicted to diminish. Additionally, optogenetic manipulations of interneurons may be predicted to disrupt late CR expression or extend the period when simple spikes are promoting plasticity.

Another possibility is that plasticity that proceeds late in training leads to a realignment of Pkj simple spikes, such that converging Pkjs produce synchronous action potentials. Under this hypothesis, plasticity that takes place (possibly at pf-Pkj or pf-interneuron synapses) between the initial CR and asymptotic CR expression leads to synchronization. In ENs, the phase in which potentiation of pfs occurs may correspond to asynchronous Pkj drive. Later, potentiated excitatory drive combines with the same amount of inhibition, though because inhibition is

synchronized more action potentials are permitted. Recordings of IPSCs from ENs, as well as dual recordings from converging and non-converging Pkjs during learning could reveal such a transition.

4.1.3 Divergent signals and targets of ENs

EN axons terminate in various parts of the brain, including to the tectum, pretectal nuclei in the diencephalon, inferior olive, and multiple nuclei in the brainstem (Ikenaga et al., 2006; Heap et al., 2013; Matsui et al., 2014a). During associative learning, it is likely that differentially projecting ENs contribute to different aspects of the task. For example, feedback to circuits which communicate CS and US information to the cerebellum plays an important role in regulating plasticity and maintaining flexibility in case the contingency between CS and US changes (Medina et al., 2002; Halverson et al., 2010). Such feedback may be provided by medially-located ENs which project to pretectal nuclei as well as ENs that project to the inferior olive. Neither pathway is directly inhibitory, indicating that negative feedback is likely mediated by local inhibitory interneurons.

Execution of the CR is likely dependent of EN projections to motor areas in the brainstem. Two candidate nuclei have been identified: the red nucleus and the nMLF. Both nuclei project directly to the spinal cord and are therefore well suited for driving cerebellum-dependent movements. While additional afferents to the red nucleus have not been identified, neurons in the nMLF receive visual sensory signals and support a variety of visually-guided movements (Gahtan et al., 2005; Orger et al., 2008; Wang and McLean, 2014). This raises the possibility that inputs from ENs combine with visual sensory input to initiate firing of neurons in the nMLF, which results in

the generation of the CR. ENs may also send motor-related signals to the tectum. Laterally-located ENs project into the tectal neuropil and laterally-located SCS Pkjs are preferentially responsive to motor commands.

An additional possibility is that rather than providing necessary excitatory drive for all CRs, ENs instead could provide modulatory input which increases the excitability of neurons involved in the reflexive phototaxic swim response, meaning that expression of the well-learned CR is independent of the cerebellum. This mechanism could explain why suppressing simple spikes (a manipulation which likely affects task-related EN spiking) has no effect on the well-learned CR. Under this possibility, the well-learned CR would be identical to phototaxic swimming. On the contrary, CRs late in training were generated at significantly longer latencies (~500 ms) than phototaxic episodes of swimming (~250 ms), indicating that the circuit for phototaxic swimming is not simply potentiated, nor is it likely working alone. Calcium imaging of multiple spinal-projecting neuronal populations during spontaneous, reflexive, and learned swimming may provide an agnostic means to determine which motor systems interact with the cerebellum to execute the CR.

4.2 Cerebellar involvement in volitional movement

4.2.1 Studying movement initiation

While the cerebellum is clearly involved in altering movements that have been initiated by other motor systems, it remains unclear if it is involved in initiation. Movements can be initiated

through direct or indirect stimulation of the cerebellar nuclei. Additionally, conditional responses produced after cerebellum-dependent associative learning (i.e. eyeblink conditioning; McCormick and Thompson, 1984b) are movements generated by the cerebellum in response to sensory drive. Presumably, the CR produced in the task we have employed reflects a transformation of sensory drive related to the CS into a pattern of spiking by ENs which leads to movement initiation.

Of course, many movements, broadly defined as volitional movements, are not clearly related to stimuli from the external environment. Experimentally, these movements may be executed within a task where the animal is cued to perform a certain movement and rewarded (e.g. Thach, 1968). While these movements are not independent from sensory stimuli, the critical processing of cues likely takes place is hedonic learning areas like the basal ganglia. If the cerebellum participates, cerebellar neurons are likely receiving signals from these areas in addition to sensory drive related to the cue. While zebrafish do not have a layered cerebral cortex or an identified structure which is homologous to the mammalian striatum, these animals display emotional learning that depends on the tectum, habenula, and neuromodulatory systems (Amo et al., 2014). Furthermore, similar paradigms can induce cerebellum-dependent bradycardia (Matsuda et al., 2017), suggesting that the cerebellum is involved in emotional learning and may receive inputs from these underlying learning circuits.

A minority of experiments, including those described here, study volitional movements by focusing on spontaneously generated movements, which cannot be attributed to any particular sensory stimuli. Conceptually, during these movements, signals that are necessary for initiating

movements are generated by other movement areas (i.e. motor cortex, superior colliculus, mesencephalic locomotor region, etc.), and a copy of these motor commands is provided to the cerebellum. While this efference copy likely primes the cerebellar circuit to undergo plasticity in the event of a motor error, it is also possible that this synaptic drive filters through the circuit quickly enough to contribute to movement initiation (e.g. Azim et al., 2014). In this scheme, cerebellar efference combines with descending signals from other areas within the reticulospinal system to initiate movements. A fundamental requirement for the cerebellum to contribute is that synaptic drive must arrive, and resultant spikes must occur, *prior to* the initiation of the movement. Our recordings from a subset of ENs meet these minimum requirements.

4.2.2 Possible internal forward models in larval zebrafish cerebellum

Various models have been developed to address cerebellar processing during volitional movements. Synaptic drive preceding the onset of a movement is a fundamental facet of internal forward models, in which the cerebellum integrates an anticipatory motor command signal with the momentary sensory context, filters these inputs through synaptic connections that have been specifically tuned across time, and sends a corrective signal that adjusts movements in real time before errors can occur (e.g. Miall and Wolpert, 1996; Shadmehr et al., 2010; Streng et al., 2018). Foundational experiments on internal forward models have used behavioral and neuronal data from humans and non-human primates, and focused on the cerebellum's contribution to complex, forebrain-dependent movements. Perhaps consequently, finding a tractable system to test predictions about synaptic drive, sensorimotor signaling, and plasticity derived from these models has been difficult.

Developing an approach for studying this model in larval zebrafish may provide a way forward. Several of our findings are compatible with forward models. Synaptic connections seem to undergo plasticity rapidly to support learning, consistent with dynamic tuning of synaptic connections within the cerebellum. Motor and sensory information is represented synaptically and in spiking activity. In both Pkjs and ENs, synaptic drive precedes the onset of spontaneous swimming. For Pkjs, this synaptic drive leads to simple and complex spiking that can also precede swimming onset, whereas for ENs, this synaptic drive leads to spiking that corresponds with the onset of swimming. Furthermore, most ENs that spiked prior to movement onset received swimming-related inhibition prior to spiking, indicating that potentially corrective signals from ENs can be shaped by Pkj inhibition without introducing significant lags. Thus, the larval zebrafish cerebellum shows many of the features necessary for using internal forward models to initiate and adapt movements.

While simple sensory representation can be studied in associative learning tasks, more complex representations require alternative approaches. Forward models predict that the cerebellum receives multimodal sensory stimuli that allow it to represent pertinent environmental information as well as the status of the body. For a free-swimming larval zebrafish, such information might include vestibular input about the whole-body pitch angle, lateral line information about water currents, and mechanoreceptive information about the position of the fins and tail. Larval zebrafish can use sensory stimuli like this in real time, as they can display cerebellum-dependent rapid adaptation of the speed and strength of optomotor swimming (Ahrens et al., 2012). This form of swimming correlates with activity in many other brain areas,

such as the tectum, forebrain and reticulospinal system (Orger et al., 2008; Naumann et al., 2016), and it is likely that the cerebellum is integrating sensory and motor signals from these areas to adapt swim commands. What remains to be studied is how optic flow information is synaptically represented in the cerebellum; how neuronal subtypes respond to the task; and, most critically, the precise temporal relationship between synaptic and spiking activity of cerebellar neurons and swimming.

4.3 Interspecies differences in the mossy fiber-parallel fiber pathway

Mammalian and teleost cerebellar output neurons receive excitatory input from different presynaptic sources – mfs and pfs, respectively. Furthermore, mfs come from more distributed sources in the fish, suggesting that presynaptic properties of mf may be more diverse. These differences may have consequences for the computations performed by the cerebellum.

4.3.1 Feedforward excitation and integration at pf-granule cell synapse

An issue not addressed by my experiments but pertinent to cerebellar processing is possible divergence of mf and granule cell properties between fish and mammals. In mammals, individual neurons that supply mfs integrate input from various presynaptic sources and make divergent inputs to several hundred granule cells (Fox et al., 1967). Individual granule cells receive convergent input from 3-7 different mfs, as inferred from the number of synaptic glomeruli per cell (Eccles 1967). This anatomical arrangement leads to varied multimodal processing at the single cell level, with individual granule cells responding to stimuli from a single sensory

modality, multiple sensory modalities, motor commands, or a combination of sensory and motor inputs (Azizi and Woodward, 1990; Chabrol et al., 2015; Ishikawa et al., 2015; Knogler et al., 2017; Sylevester et al., 2017). Sensory stimulation within a mf's preferred modality will lead to bursts of EPSPs in granule cells, leading to a matching burst of action potentials at a ratio of ~ 3 EPSPs : 1 pf spike (Chadderton et al., 2004; Rancz et al., 2007). Thus, while excitation from mfs is passed forward to Pkjs through granule cells with reasonably high fidelity, granule cells can also combine signals across multiple sensory and movement modalities, depending on the properties of their presynaptic partners.

Some of these features are also found in larval zebrafish, where granule cells have 1-4 "dendritic claws", which may form glomeruli with mf connections. These neurons display responses to sensory stimuli or motor commands, with some responding to multiple modalities (Knogler et al., 2017). However, granule cell spiking seems to require a greater number of mf EPSPs, though a precise input-output relationship has not been measured. Thus, granule cells may be better suited to integrate across multiple mf transmission events in the fish. Speculatively, in the mammal, this integrative step may take place instead in neurons that supply mfs. These neurons are primarily found in the pontine nucleus, a structure that seems to be lacking in fish (Finger, 1978). If this hypothesis were true, it would be predicted that individual granule cells receive mf input from disparate sources and that the ratio of mf EPSPs to granule cell spikes is >3:1.

4.3.2 Sparse coding at the pf-Pkj synapse in larval zebrafish

The Marr-Albus-Ito (MAI) theory of cerebellar information storage (Marr, 1969; Albus, 1971; Ito, 1984) has been highly influential in the study of cerebellar learning and processing. This

theory emphasizes the computational power of pf-Pkj synapses. Because they are numerous (~150,000 synapses/cell; Isope and Barbour, 2002) and modestly strong and plastic, these connections are well-suited for providing a specific combinatorial signal. Furthermore, inhibitory interneurons also receive pf input and limit both granule cell spiking and net excitation provided to Pkjs. Together, these features allow pfs to provide a discrete, graded, combinatorial signal which acutely modulates Pkj firing. Specific firing patterns of Pkj feeds forward to cerebellar nuclear cells, where they modulate firing with precision.

Plasticity at pf-Pkj synapses likely follows a similar mechanism as in mammals, since LTP and LTD can be induced with similar protocols at these synapses in mormyrid fish (Han et al., 2007). It is unclear whether pfs are suited to supply a sparse, combinatorial signal to Pkjs in larval zebrafish. While the number of pf-Pkj synapses has not been estimated, granule cells outnumber Pkjs 20:1 in larval zebrafish (Knogler et al., 2017), compared to ~20000:1 in cat (Mayhew, 1991). Our recordings of individual pf EPSCs had small amplitudes of 5-10 pA, though EPSCs summated substantially to promote spiking, indicating that they can provide a combinatorial signal. A prediction based on the MAI theory is that the combination of pf synapses active during different behaviors should be different. Consistent with this prediction, we observe that pf drive to visual stimuli is generally weaker the pf drive during swimming, indicating different combinations of pf drive. ZCS cells show differences between pf drive in response to a visual stimulus when the animal is naïve and when the animal is trained, suggesting plasticity in the combinatorial code based on the behavioral relevance of the stimulus. Of interest is whether pf drive differs between types of swimming. Visual comparison of activity during different types of

swimming reveal no clear differences in motor command synaptic drive supplied by pfs. Nevertheless, it is possible that some motor command synaptic input related to volitional, cued, and reflexive swimming is carried by separate pfs.

4.4 Synaptic plasticity that supports cerebellar learning

Results from our associative learning task reveal changes in Pkj activity that could be explained through multiple mechanisms. Also, Pkj simple spiking likely promotes plasticity in ENs. In this section, I address differences in cf input that complicate generalization of certain types of plasticity from the mammal to the fish. Then I discuss forms of synaptic plasticity that likely occur during cerebellar learning.

4.4.1 Divergent complex spike properties

The waveform of complex spikes recorded in larval zebrafish differs from those recorded from mammalian Pkjs. In mammalian cells, synaptic currents trigger the initial sodium-mediated rise and peak and contribute to a period of depolarization after the peak that lasts for 5-10 ms. Before the cell completely repolarizes, secondary events call spikelets are frequently observed. Approximately 2-5 spikelets are observed per complex spike, with 60% of these events propagating down the axon (Khaliq and Raman, 2005). Depolarization related to cf transmission activates voltage-sensitive channels in the Pkj soma, axon, and dendrite. While activation of axonal currents underlies spikelets, activation in the dendrite contributes to pauses in ongoing

simple spike that frequently follow a complex spike (Davie et al., 2008). Depolarization in the dendrite is also essential for cf-dependent synaptic plasticity.

The secondary axonal and dendritic spikes that distinguish complex spikes from simple spikes are missing from most zebrafish complex spikes. Rather, complex spikes were larger in amplitude, due to synaptic current which overwhelms voltage-dependent sodium influx. Furthermore, secondary spikes in the axon and dendrite would not necessarily be predicted based on the anatomy of zebrafish Pkjs. In mammals, cfs wrap around the Pkj dendrite, making hundreds of synapses. In contrast, zebrafish cfs terminate in the somatic layer of the cerebellar cortex, suggesting that they make somatic synapses only (Takeuchi et al., 2014). Therefore, complex spike-related dendritic depolarization would rely on somatic conductances. Additionally, the Pkj axon is short (2-8 μm; Matsui et al., 2014a) and it is unclear how essential axonally-sourced currents are for propagation and transmission when the soma is nearby. The axon is short enough that passive spread of synaptic currents from the soma might be sufficient to trigger multiple release events. However, this possibility leads to the prediction that complex spikes may evoke larger IPSCs or IPSCs very close in time, though we made neither observation while recording complex spike IPSCs. Subsequent studies should address sources of calcium influx in Pkj dendrites in larval zebrafish. Calcium imaging of sparsely-labeled Pkjs could be used to test whether Pkj dendrites show increased calcium during cerebellum-dependent behaviors or simply in response to direct stimulation of the inferior olive (e.g. Hsieh et al., 2014).

4.4.2 Parallel fiber-Purkinje cell plasticity during associative learning

Our results demonstrate an increase in pf drive to a subset of Pkjs (ZCS cells) over the course of associative learning. The observation can be explained through multiple mechanisms. Firstly, several of these neurons showed responses to the CS prior to training, and potentiation of these inputs could explain increased pf drive and simple spiking observed late in training. In fact, potentiation may be favored by the learning task that we employed because the CS and US were separated considerably in time (2 s; Jörntell and Hansel, 2006; Suvrathan et al., 2016), and paired pf-cf transmission induces pf LTP at long latencies. Additionally, we observed that ZCS cells occasionally produced complex spikes during spontaneous swimming, suggesting that, rather than simply not being recruited, complex spiking was suppressed during learned swimming. Such a mechanism would be useful for maintaining the relative distance between CS-related pf transmission and US-related cf transmission, ultimately sustaining pf inputs in a potentiated state.

Even in light-responsive neurons, however, initial synaptic drive was low and modulation of simple spike rate was weak. It is possible that many of these weakly responsive neurons may have been subjected to substantial pf transmission, but synapses that detected this signal were initially silent. The unveiling of transmission events through the potentiation of silent pf synapses could explain increased excitation to the CS as well. This possibility is reinforced by the fact that a substantial proportion of pf synapses are silent (Isope and Barbour, 2002; Liu and Regehr, 2014; Valera et al., 2016) and silent synapses are common early in development (Durand et al., 1996; Wu et al., 1996).

An additional possibility is that more granule cells are being recruited in response to the visual stimulus as the fish progresses through training. Such plasticity has been observed during eyelid conditioning, where imaging of granule cells across training revealed an increase in the number of active neurons during the training stimulus on trials in which the CR was performed (Giovannucci et al., 2017). These results cannot be explained by plasticity of signals that communicate sensory stimuli, and instead indicate that, in well-trained animals, pfs show anticipatory motor command information. These results are remarkable because the eyelid closure CR is thought to be a sensory-evoked movement that depends completely on the cerebellum. Thus, synaptic drive related to a motor command generated elsewhere in the brain would not be expected. If this mechanism explains pf-Pkj plasticity observed in our experiments, we may expect to see a change in pf drive during spontaneous swimming, with greater drive after training than at the beginning of training. To test whether increased drive is attributable to granule cell recruitment or unveiling of silent synapses, imaging of GCaMP fluorescence in granule cells across learning could be performed (e.g. Knogler et al., 2017; Giovannucci et al., 2017).

4.4.3 Possible plasticity at pf-EN synapses

Mammalian nuclear cells receive excitation from mfs, whereas teleost ENs make synapses with pfs. The significance of this difference is unclear, and it is possible that pf-EN synapses prove to be more similar to pf-Pkj synapses. Plasticity at mf and pf synapses manifests differently. For instance, pfs reliably show short-term facilitation whereas mfs show either potentiation or depression (Sims and Hartell, 2005; Pugh and Raman, 2006; Wu and Raman, 2017). Pre- and

postsynaptic long-term plasticity at pfs occurs through a variety of mechanisms, some of which (i.e., climbing-fiber dependent postsynaptic depression) seem unlikely in ENs. Postsynaptic pf plasticity is yoked to intracellular calcium levels. Moderate calcium levels promote homosynaptic potentiation (Lev-Ram et al., 2002) whereas high calcium levels promote depression (Coesmans et al., 2004). In Pkjs, high calcium concentrations are induced by cf transmission, and it is unknown if an equivalent calcium influx occurs in ENs. Pfs also show presynaptic plasticity, where low rates of transmission induce potentiation and high rates induce depression via endocannabinoid signaling (Sakurai, 1987; Shibuki and Okada, 1992; van Beugen et al., 2006; Qiu and Knöpfel, 2007). Presumably, some forms of presynaptic plasticity are intrinsic to granule cells and independent of postsynaptic identity, meaning they would be found at pf-EN synapses as well.

Alternatively, potentiation of mf synapses proceeds through heterosynaptic interactions with Pkjs (Aizenman et al., 1998; Pugh and Raman, 2006; McElvain et al., 2010; Pugh and Raman, 2008). Postsynaptic potentiation of mf synapses relies on sequential waves of calcium, with the first wave related to mf transmission and the second wave related to rebound firing following inhibition from Pkjs (Person and Raman, 2010).

Results from our associative learning experiments indicate that sequential excitatory-inhibitory drive to ENs likely takes place during training. A subset of ENs in naïve fish show EPSCs at short latencies in response to visual stimulation. When the same stimulus was used for associative learning, many Pkjs showed increased firing in response to the light, with MCS cells showing greater complex spiking and ZCS showing greater simple spiking. Thus, the

physiological pattern of signals arriving at ENs during learning more closely matches the pattern which induces potentiation at mf-nuclear cell synapses. Moreover, the effect of suppressing simple spikes, a manipulation which disproportionately affects ZCS cells, suggests that Pkjs promote learning by promoting plasticity at pf-EN synapses.

It is possible that pf-EN synapses show multiple forms of plasticity, some intrinsic to pfs and others to cerebellar output neurons, generally. Plasticity mechanisms shared between pfs in mammals and fish or between ENs and cerebellar nuclear cells are likely essential for cerebellum-dependent learning and memory, and their identification is a worthy research goal.

References

Ahrens MB, Li JM, Orger MB, Robson DN, Schier AF, Engert F, and Portugues R. 2012. Brain-wide neuronal dynamics during motor adaptation in zebrafish. *Nature* **485**(7399):471-77.

Afshari FS, Ptak K, Khaliq ZM, Grieco TM, Slater NT, McCrimmon DR, and Raman IM. 2004. Resurgent Na currents in four classes of neurons of the cerebellum. *Journal of Neurophysiology* **92**(5):2831-43.

Ahn AH, Dziennis S, Hawkes R, and Herrup K. 1994. The cloning of zebrin II reveals its identity with aldolase C. *Development* **120**(8):2081-90.

Aizenberg M, and Schuman EM. 2011. Cerebellar-dependent learning in larval zebrafish. *Journal of Neuroscience* **31**(24):8708-12.

Aizenman CD, and Linden DJ. 2000. Rapid, synaptically driven increases in the intrinsic excitability of cerebellar deep nuclear neurons. *Nature Neuroscience* **3**(2):109-11.

Aizenman CD, Manis PB, and Linden DJ. 1998. Polarity of long-term synaptic gain change is related to postsynaptic spike firing at a cerebellar inhibitory synapse. *Neuron* **21**(4):827-35.

Albus JS. 1971. A theory of cerebellar function. *Mathematical Biosciences* **10**:25-61

Alonso JR, Arevalo R, Briñon, Lara J, Weruaga E, and Aijon J. 1992. "Paravalbumin immunoreactive neurons and fibres in the teleost cerebellum." *Anatomy and Embryology (Berlin)* **185**(4): 355-61.

Amo R, Kinoshita M, Aoki R, Aizawa H, Agetsuma M, Aoki T, Shiraki T, Kakinuma H, Matsuda M, Yamazaki M, Takahoko M, Tsuboi T, Higashijima S, Miyasaka N, Koide T, Yabuki Y, Yoshihara Y, Fukai T, and Okamoto H. 2014. The habenulo-raphe serotonergic circuit encodes an aversive expectation value essential for adaptive active avoidance of danger. *Neuron* **84**(5):1034-48.

Anchisi D, Scelfo B, and Tempia F. 2001. Posynaptic currents in deep cerebellar nuclei. *Journal of Neurophysiology* **85**(1):323-31.

Ansorge K, and Grüsser-Cornehls U. 1977. Visual and visual-vestibulat responses of frog cerebellar neurons. *Exploratory Brain Research* **29**:445-65.

Arenz A, Silver RA, Schaefer AT, and Margrie TW. (2008). The contribution of single synapses to sensory representation in vivo. *Science* **321**(5891):977-80. DOI: 10.1126/science.1158391.

Armstrong DM. 1986. Supraspinal contributions to the initiation and control of locomotion in the cat. *Progress in Neurobiology* **26**:273-361.

Armstrong DM. 1988. The supraspinal control of mammalian locomotion. *Journal of Physiology* **405**:1-37.

Armstrong DM, and Edgley SA. 1984a. Discharges of nucleus interpositus neurones during locomotion in the cat. *Journal of Physiology* **351**:411-32.

Armstrong DM, and Edgley SA. 1984b. Discharges of Purkinje cells in the paravermal part of the cerebellar anterior lobe during locomotion in the cat. *Journal of Physiology* **352**:403-424.

Armstrong DM, Edgley SA, and Libierth M. (1988). Complex spikes in Purkinje cells of the paravermal part of the anterior lobe of the cat cerebellum during locomotion. *Journal of Physiology* **400**:405-14.

Arrenberg AB, Del Bene F, and Baier H. 2009. Optical control of zebrafish behavior with halorhodopsin. *Procedures of the National Academy of Science* **106**(42):17968-73.

Arshavsky YI, Berkenblit MB, Fukson OI, Gelfand IM, and Orlovsky GN. 1972. Recordings of neurones of the dorsal spinocerebellar tract during evoked locomotion. *Brain Research* **43**:272-75.

Arshavsky YI, Gelfand IM, Orlovsky GN, and Pavlova GA. 1978. Messages conveyed by spinocerebellar pathways during scratching in the cat. I. Activity of neurons of the lateral reticular nucleus. *Brain Research* **151**:479-91.

Azim E, Jiang J, Alstermark B,and Jessell TM. 2014. Skilled reaching relies on a V2a propriospinal internal copy circuit. *Nature* **508**(7496):357-63.

Azizi SA, and Woodward DJ. 1990. Interactions of visual and auditory mossy fiber inputs in the paraflocculus of the rat: a gating action of multimodal inputs. *Brain Research* **533**(2):255-262.

Bae YK, Kani S, Simizu T, Tanabe K, Nojima H, Kimura Y, Higashijima S, and Hibi M. 2009. Anatomy of zebrafish cerebellum and screen for mutations affecting its development. *Developmental Biology* **330**(2):406-426.

Babinski, J. 1899. De l'asynergie cérébelleuse. *Reviews Neurology* 7:806-816.

Barbour B. 1993. Synaptic currents evoked in Purkinje cells by stimulating individual granule cells. *Neuron* **11**(4):759-69.

Bauswein E, Kolb FP, Leimbeck B, and Rubia FJ. 1983. Simple and complex spike activity of cerebellar Purkinje cells during active and passive movements in the awake monkey. *Journal of Physiology* **339**:379-394.

Bell CC, and Grimm RJ. 1969. Discharge properties of Purkinje cells recorded on single and double microelectrodes. *Journal of Neurophysiology* **32**(6):1044-55.

Bengtsson F, and Jorntell H. 2014. Specific relationship between excitatory inputs and climbing fiber receptive fields in deep cerebellar nuclear neurons. *PLoS One* **9**(1):e84616.

Bengtsson F, Ekerot CF, and Jorntell H. 2011. In vivo analysis of inhibitory synaptic inputs and rebounds in deep cerebellar nuclear neurons. *PLoS ONE* **6**:e18822.

Berthier NE, and Moore JW. 1990. Activity of deep cerebellar nuclear cells during classical conditioning of nictitating membrane extension in rabbits. *Experimental Brain Research* **83**(1):44-54.

Bhatt DH, McLean DL, Hale ME, and Fetcho JR. 2007. Grading movement strength by changes in firing intensity versus recruitment of spinal interneurons. *Neuron* **53**(1):91-102.

Blazquez PM, Hirata Y, Heiney SA, Green AM, and Highstein SM. 2003. Cerebellar signatures of vestibulo-ocular reflex motor learning. *Journal of Neuroscience* **23**(30):9742-51.

Blenkinsop TA, and Lang EJ. 2011. Synaptic action of the olivocerebellar system on cerebellar nuclear spike activity. *Journal of Neuroscience* **31**(41):14708-20.

Blot A, and Barbour B. 2014. Ultra-rapid axon-axon ephaptic inhibition of cerebellar Purkinje cells by the pinceau. *Nature Neuroscience* **17**(2):289-95.

Bosco G, and Poppele RE. 1993. Broad directional tuning in spinal projections to the cerebellum. *Journal of Neurophysiology* **70**(2):863-6.

Bosman LW, Koekkoek SK, Shapiro J, Rijken BF, Zandstra F, van der Ende B, Owens CB, Potters JW, de Gruijl JR, Ruigrok TJ, and De Zeeuw CI. 2010. Encoding of whisker input by cerebellar Purkinje cells. *Journal of Physiology* **588**(19):3757-83.

Bower JM, Beermann DH, Gibson JM, Shambes GM, and Welker W. 1981. Principles of organization of a cerebro-cerebellar circuit. Micromapping the projections from cerebral (SI) to cerebellar (granule cell layer) tactile areas of rats. *Brain Behavior and Evolution* **18**(1-2):1-18.

Bower JM and Woolston DC. 1983. Congruence of spatial organization of tactile projections to granule cell and Purkinje cell layers of cerebellar hemispheres of the albino rat: vertical organization of cerebellar cortex. *Journal of Neurophysiology* **49**(3):745-66.

Boyle R, and Pompeiano O. 1979. Sensitivity of interpositus neurons to neck afferent stimulation. *Brain Research* **168**(1):180-5.

Brocard F and Dubuc R. 2003. Differential contribution of reticulospinal cells to the control of locomotion induced by the mesencephalic locomotor region. *Journal of Neurophysiology* **90**(3): 1714-27.

Brockerhoff SE, Hurley JB, Janssen-Bienhold U, Neuhauss SC, Driever W and Dowling JE. 1995. A behavioral screen for isolating zebrafish mutants with visual system defects. *Proceedings of the National Academy of Sciences.* **92**(23):10545-9.

Brochu G, Maler L, and Hawkes R. 1990. Zebrin II: a polypeptide antigen expressed selectively by Purkinje cells reveals compartments in rat and fish cerebellum. *Journal of Comparative Neurology* **291**(4):538-52.

Brown ST, and Raman IM. 2018. Sensorimotor integration and amplification of reflexive hisking by well-timed spiking in the cerebellar corticonuclear circuit. *Neuron* **99**:1-12.

Burgess HA, and Granato M. 2007. Sensorimotor gating in larval zebrafish. *Journal of Neuroscience* **27**:4984-94.

Caddy KW, and Biscoe TJ. 1979. Structural and quantitative studies on the normal C3H and Lurcher mutant mouse. *Philosophical Transactions of the Royal Society of London, Series B, Biological Sciences* **287**:167-201.

Campbell NC, and Hesslow G. 1986. The secondary spikes of climbing fibre responses recorded from Purkinje cell somata in cat cerebellum. *Journal of Physiology* **377**:207-24.

Capelli P, Pivetta C, Esposito MS, and Arber S. 2017. Locomotor speed control circuits in the caudal brainstem. *Nature* **551**:373-77.

Castro A, Becerra M, Manso MJ, and Anadón MJ. 2006. Calretinin immnoreativity in the brain of the zebrafish, Danio rerio: Distribution and comparision with some neuropetides and neurotransmitter-synthesizing enzymes. II. Midbrain, Hindbrain, and rostral spinal cord. *Journal of Comparative Neurology* **494**:792-814.

Cerminara NL and Apps R. 2011. Behavioural significance of cerebellar modules. *Cerebellum* **10**(3):484-94.

Cerminara NL, Lang EJ, Sillitoe RV, and Apps R. 2015. Redefining the cerebellar cortex as an assembly of non-uniform Purkinje cell microcircuits. *Nature Reviews Neuroscience* **16**(2):79-93.

Chadderton P, Margrie TW, and Häusser M. 2004. Integration of quanta in cerebellar granule cells during sensory processing. *Nature* **428**(6985):856-60.

Chan-Palay V. 1977. *Cerebellar Dentate Nucleus: Organization, Cytology and Transmitters*. Spring-Verlag, Berlin.

Charbrol FP, Arenz A, Wiechert MT, Margrie TW, and DiGregorio DA. 2015. Synaptic diversity enables temporal coding of coincident multisensory inputs in single neurons. *Nature Neuroscience* **18**(5):718-727.

Chen C, and Thompson RF. 1995. Temporal specificity of long-term depression in parallel fiber-Purkinje synapses in rat cerebellar slice. *Learning and Memory* **2**:185-98.

Clark RE, Zhang AA, and Lavond DG. 1992. Reversible lesions of the cerebellar interpositus nucleus during acquisition and retention of a classically conditioned behavior. *Behavioral Neuroscience* **106**(6):879-88.

Coesmans M, Weber JT, De Zeeuw CI, and Hansel C. 2004. Bidirectional parallel fiber plasticity in the cerebellum under climbing fiber control. *Neuron* **44**(4):691-700.

D'Angelo E, De Filippi G, Rossi P, and Taglietti V. 1998. Ionic mechanism of electroresponsiveness in cerebellar granule cells implicates the action of a persistent sodium current. *Journal of Neurophysiology* **80**(2):493-503.

Davie JT, Clark BA, and Häusser M. 2008. The origin of the complex spike in cerebellar Purkinje cells. *Journal of Neuroscience* **28**(30):7599-609.

de Gruijl JR, Hoogland TM, and De Zeeuw CI. 2014. Behavioral correlates of complex spike synchrony in cerebellar microzones. *Journal of Neuroscience* **34**(27): 8937-47.

de Ruiter MM, De Zeeuw CI, and Hansel C. 2006. Voltage-gated sodium channels in cerebellar Purkinje cells of mormyrid fish. *Journal of Neurophysiology* **96**(1):378-90.

de Solages C, Szapiro G, Brunel N, Hakim V, Isope P, Buisseret P, Rousseau C, Barbour B, and Léna C. 2008. High-frequency organization and synchrony of activity in the purkinje cell layer of the cerebellum. *Neuron* **58**(5):775-88.

de Schutter E, and Bower JM. 1994. An active membrane model of the cerebellar Purkinje cell II. Simulation of synaptic responses. *Journal of Neurophysiology* **71**(1):401-19.

De Zeeuw CI, Hoebeek FE, Bosman LW, Schonewille M, Witter L, and Koekkoek SK. 2011. Spatiotemporal firing patterns in the cerebellum. *Nature Reviews Neuroscience* **12**:327-44.

Drapeau P, Ali DW, Buss RR, and Saint-Amant L. 1999. In vivo recording from identifiable neurons of the locomotor network in the developing zebrafish. *Journal of Neuroscience Methods* **88**(1):1-13.

Durand GM, Kovalchuk Y, and Konnerth A. 1996. Long-term potentiation and functional synapse induction in developing hippocampus. *Nature* **381**:71-75.

Eccles JC, Ito M, and Szentagothai J. 1967. *The Cerebellum as a Neuronal Machine*. Springer, New York.

Eccles JC, Llinás R, and Sasaki K. 1965. Intracellularly recorded responses of the cerebellar Purkinje cells. *Experimental Brain Research* **1**(2):161-83.

Eccles JC, Llinás R, and Sasaki K. 1966. The excitatory synaptic action of climbing fibres on the Purkinje cells of the cerebellum. *Journal of Physiology* **182**(2):268-96.

Eccles JC, Sabah NH, Schmidt RF, and Táboříková H. 1972. Cutaneous mechanoreceptors influencing impulse discharges in cerebellar cortex. II. In Purkyně cells by mossy fiber input. *Experimental Brain Research* **15**(3):261-77.

Edgerton JR, and Reinhart PH. 2003. Distinct contributions of small and large conductance Ca2+-activated K+ channels to rat Purkinje neuron function. *Journal of Physiology* **548**(1):53-69.

Esposito MS, Capelli P, and Arber S. 2014. Brainstem nucleus MdV mediates skilled forelimb motor tasks. *Nature* **508**(7496):351-6. DOI: 10.1038/nature13023.

Elsalini OA, and Rohr KB. 2003. Phenylthiourea disrupts thyroid function in developing zebrafish. *Development Genes and Evolution* **212**(12):593-8.

Favilla M, Ghelarducci B, Magherini PC. 1978. Sensitivity of lateral cerebellar nucleus to macular stimulation in the rabbit. *Experimental Brain Research* **33**(1): 41-50.

Finger T. 1978. Cerebellar Afferents in Teleost Catfish (Ictaluridae). *Journal of Comparative Neurology* **181**:173-182.

Folgueira M, Anadón R, and Yáñez J. 2006. Afferent and efferent connections of the cerebellum of a salmonid, the rainbow trout (Oncorhynchus mykiss): a tract-tracing study. *Journal of Comparative Neurology* **497**(4):542-65.

Foster KA, and Regehr WG. 2004. Variance-mean analysis in the presence of a rapid antagonist indicates vesicle depletion underlies depression at the climbing fiber synapse. *Neuron* **43**(1):119-31.

Fox CA, Hillman DE, Siegesmund KA, and Dutta CR. 1967. The primate cerebellar cortex: a Golgi and electron microscopic study. *Progress in Brain Research* **25**:174-225.

Freeman JA. 1970. Responses of cat cerebellar Purkinje cells to convergent inputs from cerebral cortex and peripheral sensory systems. *Journal of Neurophysiology* **33**(6):697-712.

Freeman JH, and Steinmetz AB. 2011. Neural circuitry and plasticity mechanisms underlying delay eyeblink conditioning. *Learning and Memory* **18**(10):666-77.

Gahtan E, Tanger P, and Baier H. 2005. Visual prey capture in larval zebrafish is controlled by identified reticulospinal neurons downstream of the tectum. *Journal of Neuroscience* **25**(40):9294-303.

Gähwiler BH, and Llano I. 1989. Sodium and potassium conductances in somatic membranes of rat Purkinje cells from organotypic cerebellar cultures. *Journal of Physiology* **417**:105-22.

Garwicz M, Jorntell H, and Ekerot CF. 1998. Cutaneous receptive fields and topography of mossy fibres and climbing fibres projecting to cat cerebellar C3 zone. *Journal of Physiology* **512**(Pt 1):277-93.

Gauck V, and Jaeger D. 2000. The control of rate and timing of spikes in the deep cerebellar nuclei by inhibition. *Journal of Neuroscience* **20**(8):3006-16.

Gauck V, Thomann M, Jaeger D, and Borst A. 2001. Spatial distribution of low- and high-voltage-activated calcium currents in neurons of the deep cerebellar nuclei. *Journal of Neuroscience* **21**(15):RC158.

Gellman R, Houk JC, and Gibson AR. 1983. Somatosensory properties of the inferior olive of the cat. *Journal of Comparative Neurology* **215**(2):228-243.

Gerrits NM, Epema AH, and Voogd J. 1984. The mossy fiber projection of the nucleus reticularis tegmenti pontis to the flocculus and adjacent ventral paraflocculus in the cat. *Neuroscience* **11**(3):627-44.

Gilbert PF, and Thach WT. 1977. Purkinje cell activity during motor learning. *Brain Research* **128**(2):309-28.

Giovannucci A, Badura A, Deverett B, Najafi F, Pereira TD, Gao Z, Ozden I, Kloth AD, Pnevmatikakis E, Paninski L, De Zeeuw CI, Medina JF, and Wang SS. 2017. Cerebellar granule cells acquire a widespread predictive feedback signal during motor learning. *Natura Neuroscience* **20**(5):727-34.

Goodkin HP, and Thach WT. 2003. Cerebellar control of constrained and unconstrained movements. I. Nuclear inactivation. *Journal of Neurophysiology* **89**(2):884-95.

Guo CC, Ke MC, and Raymond JL. 2014. Cerebellar Encoding of Multiple Candidate Error Cues in the Service of Motor Learning. *Journal of Neuroscience* **34**(30):9880-90.

Halverson HE, Lee I, and Freeman JH. 2010. Associative plasticity in the medial auditory thalamus and cerebellar interpositus nucleus during eyeblink conditioning. *Journal of Neuroscience* **30**(26):8787-96.

Halverson HE, Khilkevich A, and Mauk MD. 2015. Relating cerebellar purkinje cell activity to the timing and amplitude of conditioned eyelid responses. *Journal of Neuroscience* **35**(20):7813-32.

Hamling KR, Tobias ZJ, and Weissman TA. 2015. Mapping the development of cerebellar Purkinje cells in zebrafish. *Developmental Neurobiology* **75**(11):1174-1188.

Han VZ, and Bell CC. 2003. Physiology of cells in the central lobes of the mormyrid cerebellum. *Journal of Neuroscience* **23**(35):11147-57.

Han VZ, Zhang Y, Bell CC, and Hansel C. 2007. Synaptic plasticity and calcium signaling in Purkinje cells of the central cerebellar lobes of mormyrid fish. *Journal of Neuroscience* **27**(49):13499-512.

Hansel C, Linden DJ, and D'Angelo E. 2001. Beyond parallel fiber LTD: the diversity of synaptic and non-synaptic plasticity in the cerebellum. *Nature Neuroscience* **4**(5):467-75.

Harmon TC, Magaram U, McLean DL, and Raman IM. 2017. Distinct responses of Purkinje neurons and roles of simple spikes during associative motor learning in larval zebrafish. *eLife*, 6:e22537.

Hashimoto K, and Kano M. 1998. Presynaptic origin of paired-pulse depression at climbing fibre–Purkinje cell synapses in the rat cerebellum. *Journal of Physiology* **506**(2):391-405.

Häusser M, and Clark BA. 1997. Tonic synaptic inhibition modulates neuronal output pattern and spatiotemporal synaptic integration. *Neuron* **19**(3):665-78.

Heap LA, Goh CC, Kassahn KS, and Scott EK. 2013. Cerebellar output in zebrafish: an analysis of spatial patterns and topography in eurydendroid cell projections. *Frontiers in Neural Circuits* **7**:53.

Heck DH, Thach WT, and Keating JG. 2007. On-beam synchrony in the cerebellum as the mechanism for the timing and coordination of movement. *Procedures of the National Academy of Sciences* **104**(18):7658-63.

Heiney SA, Kim J, Augustine GJ, and Medina JF. 2014. Precise Control of Movement Kinematics by Optogenetic Inhibition of Purkinje Cell Activity. *Journal of Neuroscience* **34**(6):2321-30.

Hesslow G and Ivarsson M. 1996. Inhibition of the inferior olive during conditioned responses in the decerebrate ferret. *Experimental Brain Research* **110**:36-46.

Hirano T, and Ohmori H. 1986. Voltage-gated and synaptic currents in rat Purkinje cells in dissociated cell cultures. *Procedures of the National Academy of Science* **83**(6):1945-9.

Hirata Y and Highstein SM. 2001. Acute adaptation of the vestibuloocular reflex: signal processing by floccular and ventral parafloccular Purkinje cells. *Journal of Neurophysiology* **85**(5):2267-88.

Hodos W and Butler AB. 1997. Evolution of sensory pathways in vertebrates. *Brain Behavior and Evolution* **50**(4):189-97.

Hoebeek FE, Witter L, Ruigrok TJH, and De Zeeuw CI. 2010. Differential olivo-cerebellar cortical control of rebound activity in the cerebellar nuclei. *Procedures of the National Academy of Science* **107**(18):8410-5.

Holdefer RN, Houk JC, and Miller LE. 2005. Movement-Related Discharge in the Cerebellar Nuclei Persists After Local Injections of GABAA Antagonists. *Journal of Physiology* **93**(1):35-43.

Hsieh JY, Ulrich B, Issa FA, Wan J, and Papazian DM. 2014. Rapid development of Purkinje cell excitability, functional cerebellar circuit, and afferent sensory input to cerebellum in zebrafish. *Frontiers in Neural Circuits* **8**:147.

Hurlock EC, Bose M, Pierce G, and Joho RH. 2009. Rescue of motor coordination by Purkinje cell-targeted restoration of Kv3.3 channels in Kcnc3-null mice requires Kcnc1. *Journal of Neuroscience* **29**(50):15735-44.

Husson Z, Rousseau CV, Broll I, Zeilhofer HU, and Dieudonné S. 2014. Differential GABAergic and glycinergic inputs of inhibitory interneurons and Purkinje cells to principal cells of the cerebellar nuclei. *Journal of Neuroscience* **34**(28):9418-31.

Ikenaga T, Yoshida M, and Uematsu K. 2006. Cerebellar efferent neurons in teleost fish. *Cerebellum* **5**(4):268-74.

Ishikawa T, Shimuta M, and Häusser M. 2015. Multimodal sensory integration in single cerebellar granule cells in vivo. *eLife* **4**:e12916.

Isope P, and Barbour B. 2002. Properties of unitary granule cell-->Purkinje cell synapses in adult rat cerebellar slices. *Journal of Neuroscience* **22**(22):9668-78.

Ito M. 1984. *The Cerebellum and Neural Control*. New York: Raven Press.

Ito M, and Kano, M. 1982. Long-lasting depression of parallel fiber-Purkinje cell transmission induced by conjunctive stimulation of parallel fibers and climbing fibers in the cerebellar cortex. *Neuroscience Letters* **33**(3):253-8.

Ito M, Yamaguchi K, Nagao S, Yamazaki T. 2014. Long-term depression as a model of cerebellar plasticity. *Progress in Brain Research* **210**:1-30.

Jahnsen H. 1986. Electrophysiological characteristics of neurones in the guinea-pig deep cerebellar nuclei in vitro. *Journal of Physiology* **372**:129-47.

Jirenhed DA, Bengtsson F, and Hesslow G. 2007. Acquisition, extinction, and reacquisition of a cerebellar cortical memory trace. *Journal of Neuroscience* **27**(10):2493-502.

Johansson F, Jirenhed DA, Rasmussen A, Zucca R, and Hesslow G. 2014. Memory trace and timing mechanism localized to cerebellar Purkinje cells. *Procedures of the National Academy of Science* **111**(41), 14930-34.

Jörntell H and Hansel C. 2006. Synaptic memories upside down: bidirectional plasticity at cerebellar parallel fiber-Purkinje cell synapses. *Neuron* **52**(2):227-38.

Joseph, J.W., Shambes, G.M., Gibson, J.M., and Welker, W. 1978. Tactile projections to granule cells in caudal vermis of the rat's cerebellum. *Brain Behavior and Evolution* **15**:141-149.

Juvin L, Gratsch S, Trillaud-Doppia E, Gariepy JF, Buschges A, and Dubuc R. 2016. A specific population of reticulospinal neurons controls the termination of locomotion. *Cell Reports* **15**(11): 2377-86.

Kahn JA and Roberts A. 1982. The central nervous origin of the swimming motor pattern in embryos of Xenopus laevis. *Journal of Experimental Biology* **99**:185-196.

Kandel ER, Schwartz JH, Jessell TM, Siegelbaum SA, and Hudspeth AJ. 2013. *Principles of Neuroscience, 5th Edition.* McGraw-Hill, United States.

Kenyon GT, Medina JF, and Mauk MD. 1998. A mathematical model of the cerebellar-olivary system I: self-regulating equilibrium of climbing fiber activity. *Journal of Computational Neuroscience* **5**(1):17-33.

Khaliq ZM, Gouwens NW, and Raman IM. 2003. The contribution of resurgent sodium current to high-frequency firing in Purkinje neurons: an experimental and modeling study. *Journal of Neuroscience* **23**(12):4899-912.

Khaliq ZM, and Raman IM. 2005. Axonal propagation of simple and complex spikes in cerebellar Purkinje neurons. *Journal of Neuroscience* **25**(2):454-63.

Kim CH, Oh SH, Lee JH, Chang SO, Kim J, and Kim SJ. 2012. Lobule-specific membrane excitability of cerebellar Purkinje cells. *Journal of Physiology* **590**(2):273-88.

Kim JH, Wang JJ, and Ebner TJ. 1987. Climbing fiber afferent modulation during treadmill locomotion in the cat. *Journal of Neurophysiology* **57**(3):787-802.

Kimura Y, Satou C, Fujioka S, Shoji W, Umeda K, Ishizuka T, Yawo H, and Higashijima S. 2013. Hindbrain V2a neurons in the excitation of spinal locomotor circuits during zebrafish swimming. *Current Biology* **23**(10):843-9.

Knafo S, Fidelin K, Prendergast A, Tseng PB, Parrin A, Dickey C, Böhm UL, Figueiredo SN, Thouvenin O, Pascal-Moussellard H, and Wyart C. 2017. Mechanosensory neurons control the timing of spinal microcircuit selection during locomotion. *eLife* **6**:e25260.

Knogler LD, and Drapeau P. 2014. Sensory gating of an embryonic zebrafish interneuron during spontaneous motor behaviors. *Frontiers of Neural Circuits* **8**:121.

Knogler LD, Markov DA, Dragomir EI, Štih V, and Portugues R. 2017. Sensorimotor Representations in Cerebellar Granule Cells in Larval Zebrafish Are Dense, Spatially Organized, and Non-temporally Patterned. *Current Biology*. **27**(9):1288-1302.

Koyama M, Minale F, Shum J, Nishimura N, Schaffer CB, and Fetcho JR. 2016. A circuit motif in the zebrafish hindbrain for a two alternative behavioral choice to turn left or right. *eLife* **9**;5. pii: e16808.

Lacoste AM, Schoppik D, Robson DN, Haesemeyer M, Portugues R, Li JM, Randlett O, Wee CL, Engert F, and Schier AF. 2015. A convergent and essential interneuron pathway for Mauthner-cell-mediated escapes. *Current Biology* **25**(11):1526-34.

Lambert TD, Li WC, Soffe SR, and Roberts A. 2004. Brainstem control of activity and responsiveness in resting frog tadpoles: tonic inhibition. *Journal of Comparative Physiology A* **190**(4): 331-42.

Lefler Y, Yarom Y, Uusisaari MY. 2014. Cerebellar inhibitory input to the inferior olive decreases electrical coupling and blocks subthreshold oscillations. *Neuron* **81**(6):1389-400.

Lee KH, Mathews PJ, Reeves AMB, Choe KY, Jami SA, Serrano RE, and Otis TS. 2015. Circuit Mechanisms Underlying Motor Memory Formation in the Cerebellum. *Neuron* 86(2):529-40.

Lee LT, and Bulluck TH. 1984. Sensory Representation in the Cerebellum of the Catfish. *Neuroscience* **13**(1): 157-69.

Lev-Ram V, Wong ST, Storm DR, and Tsien RY. 2002. A new form of cerebellar long-term potentiation is postsynaptic and depends on nitric oxide but not cAMP. *Procedures of the National Academy of Science* **99**: 8389–93.

Li Z, Ptak D, Zhang L, Walls EK, Zhong W, and Leung YF. 2012. Phenylthiourea specifically reduces zebrafish eye size. *PLoS One* **7**(6):e40132.

Lisberger SG. 2010. Visual guidance of smooth-pursuit eye movements: sensation, action, and what happens in between. *Neuron* **66**(4):477-91.

Llinás R, and Sugimori M. 1980. Electrophysiological properties of in vitro Purkinje cell somata in mammalian cerebellar slices. *Journal of Physiology* **305**:171-95.

Llinas R, Baker R, and Sotelo C. 1974. Electrotonic coupling between neurons in cat inferior olive. *Journal of Neurophysiology* **37**(3):560-71.

Lewis AH, and Raman IM. 2014. Resurgent current of voltage-gated Na(+) channels. *Journal of Physiology* **592**(22):4825-38.

Liu KS, and Fetcho JR. 1999. Laser ablations reveal functional relationships of segmental hindbrain neurons in zebrafish. *Neuron* **23**:325-35.

Liu A, and Regehr WG. 2014. Normalization of input patterns in an associative network. *Journal of Neurophysiology* **111**(3):544-51.

Lou JS, and Bloedel JR. 1992. Responses of sagittally aligned Purkinje cells during perturbed locomotion: synchronous activation of climbing fiber inputs. *Journal of Neurophysiology* **68**(2):570-80.

Luan H, Gdowski MJ, Newlands SD, Gdowski GT. 2013. Convergence of vestibular and neck proprioceptive sensory signals in the cerebellar interpositus. *Journal of Neuroscience* **33**(3):1198-210.

Mapelli L, Pagai M, Garrido JA, and D'Angelo E. 2015. Integrated plasticity at inhibitory and excitatory synapses in the cerebellar circuit. *Frontiers of Cellular Neuroscience* **5**.

Marr D. 1969. A theory of cerebellar cortex. *Journal of Physiology* **202**:437-70.

Masino MA and Fetcho JR. 2005. Fictive swimming motor patterns in wild type and mutant larval zebrafish. *Journal of Neurophysiology* **93**(6):3177-3188.

Mason CR, Miller LE, Baker JF, and Houk JC. 1998. Organization of reaching and grasping movements in the primate cerebellar nuclei as revealed by focal muscimol inactivations. *Journal of Neurophysiology* **79**(2):537-54.

Mathy A, Clark BA, and Häusser M. 2014. Synaptically induced long-term modulation of electrical coupling in the inferior olive. *Neuron* **81**(6):1290-6.

Mathy A, Ho SS, Davie JT, Duguid IC, Clark BA, and Häusser M. 2009. Encoding of oscillations by axonal bursts in inferior olive neurons. *Neuron* **62**(3):388-99.

Matsuda K, Yoshida M, Kawakami K, Hibi M, and Shimizu T. 2017. Granule cells control recovery from classical conditioned fear responses in the zebrafish cerebellum. *Scientific Reports* **7**(1):11865.

Matsui H, Namikawa K, Babaryka A, and Koster RW. 2014a. Functional regionalization of the teleost cerebellum analyzed in vivo. *Procedures of the National Academy of Science* **111**(32):11846-11851.

Matsui H, Namikawa K, and Koster RW. 2014b. Identification of the zebrafish red nucleus using Wheat Germ Agglutinin transneuronal tracing. *Communicative and Integrative Biology* **7**(6): e994383.

Mauk MD, Steinmetz JE, and Thompson RF. 1986. Classical conditioning using stimulation of the inferior olive as the unconditioned stimulus. *Procedures of the National Academy of Science* **83**(14):5349-5353.

Mauk MD, Li W, Khilkevich A, and Halverson H. 2014. Cerebellar mechanisms of learning and plasticity revealed by delay eyelid conditioning. *International Review of Neurobiology* **117**:21-37.

Mayhew TM. 1991. Accurate prediction of Purkinje cell number from cerebellar weight can be achieved with the fractionator. *Journal of Comparative Neurology* **308**(2):162-8.

McCormick DA, Clark GA, Lavond DG, and Thompson RF. 1982. Initial localization of the memory trace for a basic form of learning. *Procedures of the National Academy of Science* **79**(8):2731-5.

McCormick DA, and Thompson RF. 1984a. Neuronal responses of the rabbit cerebellum during acquisition and performance of a classically conditioned nictitating membrane-eyelid response. *Journal of Neuroscience* **4**(11):2811-22.

McCormick DA and Thompson RF. 1984. Cerebellum: essential involvement in the classically conditioned eyelid response. *Science* **223**(4633):296-9.

McDevitt CJ, Ebner TJ, and Bloedel JR. 1987. Relationships between simultaneously recorded Purkinje cells and nuclear neurons. *Brain Research* **425**(1):1-13.

McElvain LE, Bagnall MW, Sakatos A, and du Lac S. 2007. Bidirectional plasticity gated by hyperpolarization controls the gain of postsynaptic firing responses at central vestibular nerve synapses. *Neuron* **68**:763-775.

McFarland KA, Topczewska JM, Weidinger G, Dorsky RI, and Appel B. 2008. Hh and Wnt signaling regulate formation of olig2+ neurons in the zebrafish cerebellum. *Developmental Biology* **318**(1):162-71.

McLean DL, and Fetcho JR. 2004. Ontogeny and innervation patterns of dopaminergic, noradrenergic, and serotonergic neurons in larval zebrafish. *Journal of Comparative Neurology* **480**(1):38-56.

Medina JF and Mauk MD. 1999. Simulations of cerebellar motor learning: computational analysis of plasticity at the mossy fiber to deep nucleus synapse. *Journal of Neuroscience* **19**(16):7140-51.

Medina JF, Nores WL, and Mauk MD. 2002. Inhibition of climbing fibres is a signal for the extinction of conditioned eyelid responses. *Nature* **416**(6878):330-333.

Medina JF, Nores WL, Ohyama T, and Mauk MD. 2000. Mechanisms of cerebellar learning suggested by eyelid conditioning. *Current Opinion in Neurobiology* **10**(6):717-24.

Meek J, Hafmans TGM, Maler L, and Hawkes R. 1992. Distribution of zebrin II in the gigantocerebellum of the mormyrid fish Gnathonemus petersii compared with other teleosts. *Journal of Comparative Neurology* **316**:17-31.

Miles FA and Lisberger SG. 1981. Plasticity in the vestibulo-ocular reflex: a new hypothesis. *Annual Review Neuroscience* **4**:273-99.

Momiyama A, and Takahashi T. 1994. Calcium channels responsible for potassium-induced transmitter release at rat cerebellar synapses. *Journal of Physiology* **476**(2):197-202.

Monsivais P, Clark BA, Roth A, and Häusser M. 2005. Determinants of action potential propagation in cerebellar Purkinje cell axons. *Journal of Neuroscience* **25**(2):464-72.

Mu Y, Li XQ, Zhang B, and Du JL. 2012. Visual input modulates audiomotor function via hypothalamic dopaminergic neurons through a cooperative mechanism. *Neuron* **75**(4):688-99.

Miyasaka N, Morimoto K, Tsubokawa T, Higashijima S, Okaoto H, and Yoshihara Y. 2009. From the olfactory bulb to higher brain centers: genetic visualization of secondary olfactory pathways in zebrafish. *Journal of Neuroscience* **29**(15):4756-67.

Muller U, and Heinsen H. 1984. Regional differences in the ultrastructure of purkinje cells of the rat. *Cell Tissue Research* **235**(1):91-8.

Najac M, and Raman IM. 2017. Synaptic excitation by climbing fibre collaterals in the cerebellar nuclei of juvenile and adult mice. *Journal of Physiology* **595**(21):6703-18.

Naumann EA, Fitzgerald JE, Dunn TW, Rihel J, Sompolinsky H, and Engert F. 2016. From whole-brain data to functional circuit models: the zebrafish optomotor response. *Cell* **167**(4): 947-60.

Naumann EV, Fitzgerald JE, Dunn TW, Rihel J, Sompolinsky H, and Engert F. 2016. From Whole-Brain Data to Functional Circuit Models: The Zebrafish Optomotor Response. *Cell* 947-60.

Nedelescu H, and Abdelhack M. 2013. Comparative morphology of dendritic arbors in populations of Purkinje cells in mouse sulcus and apex. *Neural Plasticity* **2013**:948587.

Nguyen-Vu TD, Kimpo RR, Rinaldi JM, Kohli A, Zeng H, Deisseroth K, and Raymond JL. 2013. Cerebellar Purkinje cell activity drives motor learning. *Nature Neuroscience* **16**(12):1734-36.

Noda H. 1981. Visual Mossy Fiber Inputs to the Flocculus of the Monkey. *Annals of the New York Academy of Sciences* **374**(1):465-75.

Ohmae S, and Medina JF. 2015. Climbing fibers encode a temporal-difference prediction error during cerebellar learning in mice. *Nature Neuroscience* **18**(12):1798-803.

Ohmae S, Uematsu A, and Tanaka M. 2013. Temporally Specific Sensory Signals for the Detection of Stimulus Omission in the Primate Deep Cerebellar Nuclei. *Journal of Neuroscience* **33**(39):15432-41.

Ohyama T, Nores WL, Medina JF, Riusech FA, and Mauk MD. 2006. Learning-induced plasticity in deep cerebellar nucleus. *Journal of Neuroscience* **26**(49):12656-63.

Orger MB, Kampff AB, Severi KE, Bollmann JH, and Engert F. 2008. Control of visually guided behavior by distinct populations of spinal projection neurons. *Nature Neuroscience* **11**(3):327-33.

Oscarsson O. 1979. Functional units of the cerebellum-sagittal zones and microzones. *Trends in Neuroscience* **2**:143-5.

Ozden I, Dombeck DA, Hoogland TM, Tank DW, and Wang SS. 2012. Widespread state-dependent shifts in cerebellar activity in locomoting mice. *PLoS One* **7**(8):e42650.

Orlovsky GN. 1970. Work of the reticulospinal neurons during locomotion. *Biophysics* **15**:178-86.

Orlovsky GN. 1972a. Work of the neurons of the cerebellar nuclei during locomotion. *Biophysics* **17**:1177-85.

Orlovsky GN. 1972b. The effect of different descending systems on flexor and extensor activity during locomotion. *Brain Research* **40**:359-71.

Palkovits M, Mezey E, Hamori J, and Szentagothai J. 1977. Quantitative histological analysis of the cerebellar nuclei in the cat. I. Numerical data on cells and on synapses. *Experimental Brain Research* **28**:189-209.

Pantoja C, Hoagland A, Carroll EC, Karalis V, Conner A, and Isacoff EY. 2016. Neuromodulatory regulation of behavior individuality in zebrafish. *Neuron* **91**(3):587-601.

Parker MO, Brock AJ, Millington ME, and Brennan CH. 2013. Behavioural phenotyping of casper mutant and 1-pheny-2-thiourea treated adult zebrafish. *Zebrafish* **10**(4):466-71.

Perrett SP, Ruiz BP, and Mauk MD. 1993. Cerebellar cortex lesions disrupt learning-dependent timing of conditioned eyelid responses. *Journal of Neuroscience* **13**(4):1708-18.

Person AL and Raman IM. 2010. Deactivation of L-type Ca current by inhibition controls LTP at excitatory synapses in the cerebellar nuclei. *Neuron* 66(4):550-59.

Person AL, and Raman IM. 2011. Purkinje neuron synchrony elicits time-locked spiking in the cerebellar nuclei. *Nature*, **481**(7382):502-5.

Portugues R and Engert F. 2011. Adaptive locomotor behavior in larval zebrafish. *Frontiers in Systems Neuroscience* **5**(30):1-11.

Portugues R, Haesemeyer M, Blum ML, and Engert F. 2015. Whole-field visual motion drives swimming in larval zebrafish via a stochastic process. *Journal of Experimental Biology* **218**(Pt 9):1433-43.

Powell K, Mathy A, Dugid I, and Häusser M. 2015. Synaptic representation of locomotion in single cerebellar granule cells. *eLife* **4**: e07290.

Proville RD, Spolidoro M, Guyon N, Dugué GP, Selimi F, Isope P, Popa D, and Léna C. 2014. Cerebellum involvement in cortical sensorimotor circuits for the control of voluntary movements. *Nature Neuroscience* **17**(9): 1233-9.

Pugh JR and Raman IM. 2006. Potentiation of mossy fiber EPSCs in the cerebellar nuclei by NMDA receptor activation followed by postinhibitory rebound current. *Neuron* **51**(1):113-23.

Pugh JR and Raman IM. 2008. Mechanisms of potentiation of mossy fiber EPSCs in the cerebellar nuclei by coincident synaptic excitation and inhibition. *Journal of Neuroscience*, **28**(42):10549-60.

Qiu DL, and Knöpfel T. 2007. An NMDA receptor/nitric oxide cascade in presynaptic parallel fiber-Purkinje neuron long-term potentiation. *Journal of Neuroscience* **27**:3408–15.

Raman IM and Bean BP. 1997a. Resurgent sodium current and action potential formation in dissociated cerebellar Purkinje neurons. *Journal of Neuroscience* **17**(12):4517-26.

Raman IM and Bean BP. 1997b. Altered subthreshold sodium currents and disrupted firing patterns in Purkinje neurons of Scn8a mutant mice. *Neuron* **19**(4):881-91.

Raman IM, and Bean BP. 2001. Inactivation and recovery of sodium currents in cerebellar Purkinje neurons: evidence for two mechanisms. *Biophysical Journal* **80**:729-37.

Raman IM, Gustafson AE, and Padgett D. 2000. Ionic currents and spontaneous firing in neurons isolated from the cerebellar nuclei. *Journal of Neuroscience* **20**(24):9004-16.

Rancz EA, Ishikawa T, Duguid IC, Chadderton P, Mahon S, and Hausser M. 2007. High-fidelity transmission of sensory information by single cerebellar mossy fibre boutons. *Nature* **450**:1245-48.

Rasmussen A, Jirenhed DA, Wetmore DZ, and Hesslow G. 2014. Changes in complex spike activity during classical conditioning. *Frontiers in Neural Circuits* **8**:90.

Raymond, JL, Lisberger SG, and Mauk, MD. 1996. The cerebellum: A neuronal learning machine? *Science* **272**:1126-31.

Requarth T, Kaifosh P, Sawtell NB. 2014. A role for mixed corollary discharge and proprioceptive signals in predicting the sensory consequences of movements. *Journal of Neuroscience* **34**(48):16103-16.

Ruigrok TJ. 2011. Ins and outs of cerebellar modules. *Cerebellum* **10**(3):464-74.

Safo P, and Regehr WG. 2008. Timing dependence of the induction of cerebellar LTD. *Neuropharmacology* **54**:213-18.

Sakurai M. 1987. Synaptic modification of parallel fibre-Purkinje cell transmission in in vitro guinea-pig cerebellar slices. *Journal of Physiology* **394:**463–80.

Sarnaik R, and Raman IM. 2018. Control of voluntary and optogenetically perturbed locomotion by spike rate and timing of neurons of the mouse cerebellar nuclei. *eLife* **7**: e29546.

Sauerbrei BA, Lubenov EV, and Siapas AG. 2015. Structured Variability in Purkinje Cell Activity during Locomotion. *Neuron* **87**(4):840-52.

Scalise K, Shimizu T, Hibi M, and Sawtell NB. 2016. Responses of cerebellar Purkinje cells during fictive optomotor behavior in larval zebrafish. *Journal of Neurophysiology* 116(5):2067-80.

Schneider ER, Civillico EF, and Wang SS. 2013. Calcium-based dendritic excitability and its regulation in the deep cerebellar nuclei. *Journal of Physiology* **109**(9):2282-92.

Schultz W, Montgomery EB Jr, and Marini R. 1979. Proximal limb movements in response to microstimulation of primate dentate and interpositus nuclei mediated by brain-stem structures. *Brain* **102**(1):127-46.

Sears LL and Steinmetz JE. 1991. Dorsal accessory inferior olive activity diminishes during acquisition of the rabbit classically conditioned eyelid response. *Brain Research* **545**(1-2):114-22.

Sengupta M and Thirumalai V. 2015. AMPA receptor mediated synaptic excitation drives state-dependent bursting in Purkinje neurons of zebrafish larvae. *eLife* **4**:e09158.

Severi KE, Portugues R, Marques JC, O'Malley DM, Orger MB, and Engert F. 2014. Neural control and modulation of swimming speed in the larval zebrafish. *Neuron* **83**(3): 692-707.

Shadmehr R, Smith MA, and Krakauer JW. 2010. Error correction, sensory prediction, and adaptation in motor control. *Annual Review Neuroscience* **33**:89-108.

Shibuki K, and Okada D. 1992. Cerebellar long-term potentiation under suppressed postsynaptic Ca2+ activity. *Neuroreport* **3**:231–234.

Shik ML, and Orlovsky GN. 1976. Neurophysiology of locomotor automatism. *Physiological Review* **56**(3):465-501.

Silver RA, Momiyama A, and Cull-Candy SG. 1998. Locus of frequency-dependent depression identified with multiple-probability fluctuation analysis at rat climbing fibre-Purkinje cell synapses. *Journal of Physiology* **510**(3):881-902.

Sims RE, and Hartell NA. 2005. Differences in transmission properties and susceptibility to long-term depression reveal functional specialization of ascending axon and parallel fiber synapses to Purkinje cells. *Journal of Neuroscience* **25**(12):3246-57.

Smetana R, Juvin L, Dubuc R, and Alford S. 2010. A parallel cholinergic brainstem pathway for enhancing locomotor drive. *Nature Neuroscience* **13**(6): 731-8.

Soffe SR, Roberts A, and Li WC. 2009. Defining the excitatory neurons that drive the locomotor rhythm in a simple vertebrate: insights into the origin of reticulospinal control. *Journal of Physiology* **587**(20): 4829-44.

Streng ML, Popa LS, and Ebner TJ. 2018. Modulation of sensory prediction error in Purkinje cells during visual feedback manipulations. *Nature Communications* **9**(1):1099.

Sudhakar SK, Torben-Nielsen B, and De Schutter E. 2015. Cerebellar Nuclear Neurons Use Time and Rate Coding to Transmit Purkinje Neuron Pauses. *PLoS Computational Biology* **11**(12):e1004641.

Sugihara I and Shinoda Y. 2004. Molecular, topographic, and functional organization of the cerebellar cortex: a study with combined aldolase C and olivocerebellar labeling. *Journal of Neuroscience* **24**(40):8771-85.

Sugihara I and Shinoda Y. 2007. Molecular, Topographic, and Functional Organization of the Cerebellar Nuclei: Analysis by Three-Dimensional Mapping of the Olivonuclear Projection and Aldolase C Labeling. *Journal of Neuroscience* **27**(36):9696-710.

Suvrathan A, Payne HL, and Raymond JL. 2016. Timing Rules for Synaptic Plasticity Matched to Behavioral Function. *Neuron* **92**(5):959-67. *Journal of Neuroscience* **27**(36):9696-710.

Sylvester SJG, Lee MM, Ramirez AD, Lim S, Goldman MS, Aksay ERF. 2017. Population-scale organization of cerebellar granule neuron signaling during a visuomotor behavior. *Scientific Report* **7**(1):16240.

Takeuchi M, Matsuda K, Yamaguchi S, Asakawa K, Miyasaka N, Lal P, Yoshihara Y, Koga A, Kawakami K, Shimizu T, and Hibi M. 2015. Establishment of Gal4 transgenic zebrafish lines for analysis of development of cerebellar neural circuitry. *Developmental Biology* **397**(1):1-17.

Takeuchi M, Yamaguchi S, Sakakibara Y, Hayashi T, Matsuda K, Hara Y, Tanegashima C, Shimizu T, Kuraku S, and Hibi M. 2017. Gene expression profiling of granule cells and Purkinje cells in the zebrafish cerebellum. *Journal of Comparative Neurology* **525**(7):1558-85.

Tanabe K, Kani S, Shimizu T, Bae YK, Abe T and Hibi M. 2010. Atypical protein kinase C regulates primary dendrite specification of cerebellar Purkinje cells by localizing Golgi apparatus. *Journal of Neuroscience* **30**(50):16983-16992.

Tang T, Suh CY, Blenkinsop TA, and Lang EJ. 2016. Synchrony is Key: Complex Spike Inhibition of the Deep Cerebellar Nuclei. *Cerebellum* **15**(1):10-13.

Tang T, Xiao J, Suh CY, Burroughs A, Cerminara NL, Jia L, Marshall SP, Wise AK, Apps R, Sugihara I, and Lang EJ. 2017. Heterogeneity of Purkinje cell simple spike-complex spike interactions: zebrin- and non-zebrin-related variations. *Journal of Physiology* **595**(15):5341-57.

Tempia F, Hoxha E, Negro G, Alshammari MA, Alshammari TK, Panova-Elektronova N, and Laezza F. 2015. Parallel fiber to Purkinje cell synaptic impairment in a mouse model of spinocerebellar ataxia type 27. *Frontiers of Cellular Neuroscience* **9**:205.

Telgkamp P, and Raman IM. 2002. Depression of inhibitory synaptic transmission between Purkinje cells and neurons of the cerebellar nuclei. *Journal of Neuroscience* **22**(19):8447-57.

ten Brinke MM, Boele HJ, Spanke JK, Potters JW, Kornysheva K, Wulff P, IJpelaar AC, Koekkoek SK, and De Zeeuw CI. 2015. Evolving Models of Pavlovian Conditioning: Cerebellar Cortical Dynamics in Awake Behaving Mice. *Cell Reports* **13**(9):1977-88.

ten Brinke MM, Heiney SA, Wang X, Proietti-Onori M, Boele H, Bakermans J, Medina JF, Gao Z, De Zeeuw CI. 2017. Dynamic modulation of activity in cerebellar nuclei neurons during pavlovian eyeblink conditioning in mice. *eLife* **6**:e28132.

Thach WT. 1968. Discharge of Purkinje and cerebellar nuclear neurons during rapidly alternating arm movements in the monkey. *Journal of Neurophysiology* **31**:785-97.

Thach WT, Perry JG, Kane SA, and Goodkin HP. 1993. Cerebellar nuclei: rapid alternating movement, motor somatotopy, and a mechanism for the control of muscle synergy. *Revue Neurologique (Paris)* **149**(11):607-28.

Thiele TR, Donovan JC, and Baier H. 2014. Descending control of swim posture by a midbrain nucleus in zebrafish. *Neuron* **83**(3):679-91.

Tsutsumi S, Yamazaki M, Miyazaki T, Watanabe M, Sakimura K, Kano M, and Kitamura K. 2015. Structure-function relationships between aldolase C/zebrin II expression and complex spike synchrony in the cerebellum. *Journal of Neuroscience* **35**(2):843-52.

Valera AM, Binda F, Pawlowski SA, Dupont JL, Casella JF, Rothstein JD, Poulain B, and Isope P. 2016. Stereotyped spatial patterns of functional synaptic connectivity in the cerebellar cortex. *eLife* **5**: e09862.

Valera AM, Doussau F, Poulain B, Barbour B, and Isope P. 2012. Adaptation of granule cell to Purkinje cell synapses to high-frequency transmission. *Journal of Neuroscience* **32**(9):3267-80.

van Beugen, BJ, Nagaraja, RY, and Hansel C. 2006. Climbing fiber-evoked endocannabinoid signaling heterosynaptically suppresses presynaptic cerebellar long-term potentiation. *Journal of Neuroscience* **26**:8289–8294.

van Kan PLE, Gibson AR, and Houk JF. 1993. Movement-related inputs to intermediate cerebellum of the monkey. *Journal of Neurophysiology* **69**:74-94.

Vinueza Veloz MF, Zhou K, Bosman LW, Potters JW, Negrello M, Seepers RM, Strydis C, Koekkoek SK, and De Zeeuw CI. 2015. Cerebellar control of gait and interlimb coordination. *Brain Structure and Function* **220**(6):3513-36.

Volkmann K, Rieger S, Babaryka A, and Koster RW. 2008. The zebrafish cerebellar rhombic lip is spatially patterned in producing granule cell populations of different functional compartments. **313**(1):167-80.

Voogd J and Glickstein M. 1998. The anatomy of the cerebellum. *Trends in Neuroscience* **2**:305–371.

Voogd J, and Ruigrok TJ. 2004. The organization of the corticonuclear and olivocerebellar climbing fiber projections to the rat cerebellar vermis: The congruence of projection zones and the zebrin pattern. *Journal of Neurocytology* **33**(1):5-21.

Wadiche JI, and Jahr CE. 2005. Patterned expression of Purkinje cell glutamate transporters controls synaptic plasticity. *Nature Neuroscience* **8**(10):1329-34.

Wang WC and McLean, DL. 2014. Selective responses to tonic descending commands by temporal summation in a spinal motor pool. *Neuron* **83**(3):708-21. DOI: 10.1016/j.neuron.2014.06.021

Wetmore DZ, Jirenhed DA, Rasmussen A, Johansson F, Schnitzer MJ, and Hesslow G. 2014. Bidirectional plasticity of Purkinje cells matches temporal features of learning. *Journal of Neuroscience* **34**(5):1731-7.

Witter L, Canto CB, Hoogland TM, de Gruijl JR, and De Zeeuw CI. 2013. Strength and timing of motor responses mediated by rebound firing in the cerebellar nuclei after Purkinje cell activation. *Frontiers in Neural Circuits* **7**:133.

Williams R 4th, Neubarth N, and Hale ME. 2013. The function of fin rays as proprioceptive sensors in fish. *Nature Communications* **4**:1729.

Williams SR, Christensen SR, Stuart GJ, and Häusser M. 2002. Membrane potential bistability is controlled by the hyperpolarization-activated current I(H) in rat cerebellar Purkinje neurons in vitro. *Journal of Physiology* **539**(2):469-83.

Winkelman BH, Belton T, Suh M, Coesmans M, Morpurgo MM, Simpson JI. 2014. Nonvisual complex spike signals in the rabbit cerebellar flocculus. *Journal of Neuroscience* **34**(9):3218-30.

Wise AK, Cerminara NL, Marple-Horvat DE, and Apps R. 2010. Mechanisms of synchronous activity in cerebellar Purkinje cells. *Journal of Physiology* **588**(1):2373-90.

Witter L, Canto CB, Hoogland TM, de Gruijl JR, and De Zeeuw CI. 2013. Strength and timing of motor responses mediated by rebound firing in the cerebellar nuclei after Purkinje cell activation. *Frontiers in Neural Circuits* **7**(133):1-14.

Wu GY, Malinow R, and Cline HT. 1996. Maturation of a Central Glutamatergic Synapse. *Science* **274**(5289):972-76.

Wu Y, and Raman IM. 2017. Facilitation of mossy fibre-driven spiking in the cerebellarnuclei by the synchrony of inhibition. *Journal of Physiology* **595**(15):5245-64.

Wulff P, Schonewille M, Renzi M, Viltono L, Sassoè-Pognetto M, Badura A, Gao Z, Hoebeek FE, van Dorp S, Wisden W, Farrant M, and De Zeeuw CI. 2009. Synaptic inhibition of Purkinje cells mediates consolidation of vestibulo-cerebellar motor learning. *Nature Neuroscience* 12(8):1042-9

Xiao J, Cerminara NL, Kotsurovskyy Y, Aoki H, Burroughs A, Wise AK, Luo Y, Marshall SP, Sugihara I, Apps R, and Lang EJ. 2014. Systematic regional variations in Purkinje cell spiking patterns. *PLoS One* **9**(8):e105633.

Xue HG, Yang CY, Yamamoto N, and Ozawa H. 2007. Fiber connections of the periventricular pretectal nucleus in a teleost, tilapia (Oreochromis niloticus). *Neuroscience Research* **57**(2):184-93.

Yang Y and Lisberger SG. 2013. Interaction of plasticity and circuit organization during the acquisition of cerebellum-dependent motor learning. *eLife* **2**:e01574.

Yang Y and Lisberger SG. 2014. Role of plasticity at different sites across the time course of cerebellar motor learning. *Journal of Neuroscience* **34**(21):7077-90.

Yang CY, Yoshimoto M, Xue HG, Yamamoto N, Imura K, Sawai N, Ishikawa Y, and Ito H. 2004. Fiber connections of the lateral valvular nucleus in a percomorph teleost, tilapia (Oreochromis niloticus). *Journal of Comparative Neurology* **474**(2):209-26.

Yarom Y, and Cohen D. 2002. The olivocerebellar system as a generator of temporal patterns. *Annual Review New York Academy of Science* **978**:122-34.

Yarden-Rabinowitz Y, and Yarom Y. 2017. In vivo analysis of synaptic activity in cerebellar nuclei neurons unravels the efficacy of excitatory inputs. *Journal of Physiology* **595**(17):5945-63.

Zangger P, and Schultz W. 1977. The activity of cells of nucleus reticularis tegmenti pontis during spontaneous locomotion in the decorticate cat. *Neuroscience Letters* **7**:95-9.

Zhang Y, and Han VZ. 2007. Physiology of morphologically identified cells in the posterior caudal lobe of the mormyrid cerebellum. *Journal of Neurophysiology* **98**(3):1297-308.

Zhang W, Shin JH, and Linden DJ. 2004. Persistent changes in the intrinsic excitability of rat deep cerebellar nuclear neurones induced by EPSP or IPSP bursts. *Journal of Physiology* **561**(3):703-19.

Zheng N, and Raman IM. 2009. Ca currents activated by spontaneous firing and synaptic disinhibition in neurons of the cerebellar nuclei. *Journal of Neuroscience* **29**(31):9826-38.

Zheng N, and Raman IM. 2011. Prolonged postinhibitory rebound firing in the cerebellar nuclei mediated by group I metabotropic glutamate receptor potentiation of L-type calcium currents. *Journal of Neuroscience* **31**(28):10283-92.

Zhou H, Lin Z, Voges K, Ju C, Gao Z, Bosman LW, Ruigrok TJ, Hoebeek FE, De Zeeuw CI, and Schonewille M. 2014. Cerebellar modules operate at different frequencies. *eLife* **3**:e02536.

Zottoli SJ. 1977. Correlation of the startle reflex and Mauthner cell auditory responses in unrestrained goldfish. *Journal of Experimental Biology* **66**:243-54.